



**HAL**  
open science

## Fundamentals and critical appraisal of electrochemical techniques for investigating microbial corrosion

Pierangela Cristiani, Masoumeh Moradi, Régine Basséguy, Digby Macdonald, Tingyue Gu, Dawei Zhang, Julian Wharton, Dake Xu

► **To cite this version:**

Pierangela Cristiani, Masoumeh Moradi, Régine Basséguy, Digby Macdonald, Tingyue Gu, et al.. Fundamentals and critical appraisal of electrochemical techniques for investigating microbial corrosion. Corrosion Science, 2025, 246, pp.112694. 10.1016/j.corsci.2025.112694 . hal-04923049

**HAL Id: hal-04923049**

**<https://hal.science/hal-04923049v1>**

Submitted on 31 Jan 2025

**HAL** is a multi-disciplinary open access archive for the deposit and dissemination of scientific research documents, whether they are published or not. The documents may come from teaching and research institutions in France or abroad, or from public or private research centers.

L'archive ouverte pluridisciplinaire **HAL**, est destinée au dépôt et à la diffusion de documents scientifiques de niveau recherche, publiés ou non, émanant des établissements d'enseignement et de recherche français ou étrangers, des laboratoires publics ou privés.



Distributed under a Creative Commons Attribution - NonCommercial 4.0 International License



## Fundamentals and critical appraisal of electrochemical techniques for investigating microbial corrosion

Pierangela Cristiani<sup>a,\*</sup>, Masoumeh Moradi<sup>b,c</sup>, Régine Basseguy<sup>d</sup>, Digby Macdonald<sup>e</sup>, Tingyue Gu<sup>f</sup>, Dawei Zhang<sup>g,h,i</sup>, Julian Wharton<sup>j</sup>, Dake Xu<sup>b,\*</sup>

<sup>a</sup> *Ricerca sul Sistema Energetico - RSE, V. Rubattino 54, Milano 20134, Italy*

<sup>b</sup> *Corrosion and Protection Center, Northeastern University, Shenyang, 110819, PR China*

<sup>c</sup> *Virginia-Maryland College of Veterinary Medicine, Virginia Tech, Blacksburg, VA, USA*

<sup>d</sup> *Laboratoire de Génie Chimique, Université de Toulouse, CNRS, INPT, UPS, Toulouse, France*

<sup>e</sup> *Departments of Nuclear Engineering and Materials Science and Engineering, University of California at Berkeley, Berkeley, CA, 94720 USA*

<sup>f</sup> *Department of Chemical and Biomolecular Engineering, Edison Biotechnology Institute, Ohio University, Athens, OH 45701, USA*

<sup>g</sup> *Beijing Advanced Innovation Center for Materials Genome Engineering, Institute for Advanced Materials and Technology, University of Science and Technology Beijing, Beijing 100083, China*

<sup>h</sup> *National Materials Corrosion and Protection Data Center, University of Science and Technology Beijing, Beijing 100083, China*

<sup>i</sup> *BRI Southeast Asia Network for Corrosion and Protection (MOE), Shunde Innovation School of University of Science and Technology Beijing, Foshan 528399, China*

<sup>j</sup> *National Centre for Advanced Tribology at Southampton (nCATS), Faculty of Engineering and Physical Sciences, University of Southampton, Highfield, Southampton SO17 1BJ, UK*

### ARTICLE INFO

#### Keywords:

Microbial influenced corrosion MIC  
Electrochemical techniques  
Open Circuit Potential  
Linear Polarization Resistance LPR  
Electrochemical Impedance Spectroscopy EIS  
Extracellular electron transfer EET  
Biofilm

### ABSTRACT

Electrochemical (EC) techniques are crucial in detecting microbiologically-influence corrosion (MIC) in both laboratory and field settings. This review fundamentally examines the electron transfer mechanisms and microbial interactions with corroding metal surfaces, emphasizing the strengths and inherent limitations of EC in accurately assessing corrosion rates across various scales. The non-destructive and electrical stimulating techniques are discussed, highlighting their applicability for in field conditions. Emerging local techniques are assessed for their potential in laboratory MIC investigations. Despite their limitations, advanced EC methods, integrated with microelectrodes and microscopy, facilitate exploration of MIC phenomena in a multi-evidence approach.

### 1. Introduction

Microbiologically-influenced corrosion (also simplified as microbial corrosion or MIC) is corrosion driven or accelerated by microbial activity on metal surfaces, involving diverse microorganisms such as bacteria, archaea, fungi, algae, and protozoa. These microorganisms range from the most economically destructive to the most extensively studied since the phenomenon was first reported [1–5]. Recent advances in molecular tools like next-generation sequencing (NGS) [6–9], have expanded our understanding of the microbial communities involved in MIC [10–12]. It reveals a broader diversity than traditional culture methods, which could only identify less than 0.01 % of the total, mostly focusing on the well-known corrosive sulfate reducing bacteria (SRB). While the specific microorganisms involved in MIC are numerous, the key question remains: “*What is the corrosion rate of a material in an*

*environment with aggressive microbial activity?*” [13,14]. The answer, which will likely remain unchanged in the future, is “it depends”. This prompts further questions: “What material? What environmental conditions?” and importantly, “During what time period?”. Similarly, for questions concerning other types of complex issues on a large scale, such as “What is the cost of a war?” or “What is the impact of humanity on the climatic change?”, the answer about MIC cannot be separated from timing and various stochastic variable conditions that can alter the course of events at the microbial scale, especially during crucial steps. The unpredictable nature and strategies of life over time make MIC distinct from other corrosion scenarios. However, since MIC, as any corrosion, is an electrochemical (EC) phenomenon driven by redox chemical reactions on conductive materials, its rate can be measured and monitored using electrochemical techniques.

Microorganisms directly alter the chemical-physical conditions at the metal-solution interface [15,16] creating a complex environment

\* Corresponding authors.

E-mail addresses: [pierangela.cristiani@rse-web.it](mailto:pierangela.cristiani@rse-web.it) (P. Cristiani), [xudake@mail.neu.edu.cn](mailto:xudake@mail.neu.edu.cn) (D. Xu).

<https://doi.org/10.1016/j.corsci.2025.112694>

Received 9 August 2024; Received in revised form 24 November 2024; Accepted 8 January 2025

Available online 11 January 2025

0010-938X/© 2025 The Authors. Published by Elsevier Ltd. This is an open access article under the CC BY-NC license (<http://creativecommons.org/licenses/by-nc/4.0/>).

**Nomenclature***Acronyms*

AC	Alternating current
AFM	Atomic Force Microscopy
BES	Bio-Electrochemical Systems
CA	Chrono Amperometry
CV	Cyclic Voltammetry
c-cyt	Cytochrome
DEIS	Dynamic Electrochemical Impedance Spectroscopy
DET	Direct Electron Transfer
DC	Direct Current
DIA	Differential Impedance Analysis
DNA	Deoxyribonucleic Acid
EC	Electrochemical Techniques
EET	Extracellular Electron Transfer
EFM	Electrochemical Frequency Modulation
EIS	Electrochemical Impedance Spectroscopy
EN	Electrochemical Noise
EPS	Exo-Polysaccharides
FESEM	Emission Scanning Electron Microscopy
HER	Hydrogen electrochemical reduction (protons or water into hydrogen gas)
LEIS	Localized Electrochemical Impedance Spectroscopy
LOM	Local Operating Model
LPR	Linear Polarization Resistance
MIC	Microbiologically-Influenced Corrosion (or microbial corrosion)
M-S	Mott-Schottky plots
OCP	Open Circuit Potential
OER	Oxygen Electrode Reaction
PDP	Point Defect Model
PDP	Potentiodynamic Polarization
QMT	Quantum-Mechanical Tunnelling
RNA	Ribonucleic Acid
SCE	Standard Calomel Electrode
SECM	Scanning ElectroChemical Microscopy
SKP	Scanning Kelvin Probe
SVET	Scanning Vibrating electrode Technique
SRB	Sulfate Reducing Bacteria
LEIS	Localized Electrochemical Impedance Spectroscopy

*As used in the equations*

A	area (cm <sup>2</sup> )
ba	( $\beta_a = \frac{b_a}{\ln 10}$ ) anodic Tafel slopes
bc	( $\beta_c = \frac{b_c}{\ln 10}$ ) cathodic Tafel slopes
$a_{OH^-}$	activity of OH <sup>-</sup> species
$C_O$	concentration of oxygen vacancies
$C_v^L$	concentration of cation vacancies at the metal/barrier layer interface
$C_i^0$	concentration of cation interstitials at the barrier layer/outer layer interface
$C_H$	concentration of hydrogen ion at the barrier layer/outer layer interface
$C_{H^+}^0$	standard concentration of hydrogen ion (1 mol L <sup>-1</sup> )
[C]	enzyme concentration (mol L <sup>-1</sup> )
[Ox]	concentration of oxidized species
[Red]	concentration of reduced species
[S]	substrate concentration (mol L <sup>-1</sup> )

$p_{O_2}$	partial oxygen pressure
C	capacitance
e	electron charge
E <sub>FB</sub>	flat band potential
E	potential (V/Ref)
E°	standard potential (V/Ref)
E <sub>corr</sub> and E <sub>redox</sub>	corrosion and redox (Nernst) potential, respectively
$E_{1/2}$	half $j_{max}$ potential
E <sub>pit</sub>	pitting potential or breakdown potential
E <sub>prot</sub>	protection potential.
E <sub>crit</sub>	critical potential
F	Faraday constant (96,485 C mol <sup>-1</sup> )
$\Delta G^0$	standard Gibbs free energy
$H_{AD}$	overlap between D and A orbitals
$j$	current density (A m <sup>-2</sup> )
$j_{corr}$	corrosion current density
$j_{max}$	maximum current density from a reaction
$j_{SS}$	steady state current density
$j_{crit}$	critical current density for passivation
$j_{pass}$	and passive current density
k <sub>B</sub>	Boltzmann constant (1.38 × 10 <sup>-23</sup> J K <sup>-1</sup> )
k <sub>ET</sub>	electron transfer rate (ET rate)
k <sub>ET(0)</sub>	activation-free rate
$k_i$ and $k_i^0$	rate constant and standard rate constant of the ith reaction
$k_n$	hopping rate with n number of hopping steps
$K_M$	Michaelis constant (mol L <sup>-1</sup> )
$K_S$	half-saturation constant
$l$	path (cm) between anode and cathode
$L_{SS}$	steady state barrier layer thickness
n	kinetic order of the dissolution reaction of the barrier layer
ND and NA	donor and acceptor densities, respectively (cm <sup>-3</sup> )
( $r_{DA} - r_o$ )	separation distance between D and A orbitals
$R_b$	media resistance (Ω)
R <sub>e</sub>	electrolyte resistance
R <sub>p</sub>	polarisation resistance
R	gas constant (8.314 J mol <sup>-1</sup> K <sup>-1</sup> )
T	temperature (298 K for standard conditions)
V	applied potential (V/Ref)
z	number of electrons transferred in the redox reaction
Z	$Z_{real} + jZ_{imag}$ Z' + jZ'' complex impedance
$\alpha$	polarizability of the bl/ol interface
$\alpha_a$ and $\alpha_c$	anodic and cathodic transfer coefficients
$\beta$	pH dependence of the potential drop across the bl/ol interface
$\beta$	medium performance factor
$\delta$	thickness
$\delta$ and $\chi$	oxidation state of cation in outer layer and barrier layer
$\epsilon$	dielectric constant
$\epsilon_0$	permittivity of vacuum (8.85 × 10 <sup>-14</sup> Fcm <sup>-1</sup> )
$\epsilon_{bl}$ and $L_{bl}$	electric field strength and thickness of the barrier layer (bl). Same for outer layer (ol)
$\eta$	overpotential
$\lambda$	reaction energy
$\sigma_e(x)$	electronic conductivity profile in the barrier layer
$\sigma$	ionic conductivity (S cm <sup>-1</sup> )
$\phi_{bl}^m$	potential drop across the metal/barrier layer interface
$\omega = 2\pi f$	angular frequency

which evolve from a conditioning film to a mature biofilm, formed by aerobic and anaerobic layers (Fig. 1). This environment modifies both electrochemical and biological processes either accelerating or inhibiting corrosion.

It has been widely demonstrated that the primary MIC mechanism, involves the direct interaction of the microorganisms and/or their metabolites with the metal surface [17–20]. The Fig. 1 illustrates how the complex interaction between algae (phototrophic) and bacteria (heterotrophic) can in different ways led to material degradation. MIC can either occur directly, via reactive oxygen species (ROS) produced by the photosynthetic metabolic activity, or indirectly, by providing metabolic products (oxygen) to bacteria within biofilms. Also, microorganisms can compete with the surface for oxygen consumption during their aerobic metabolism, making the environment anaerobic and therefore less aggressive. They can also prevent the diffusion of certain chemical species, particularly organic matter from dead organisms, through a structured biofilm layer. In aerobic conditions, biofilms formed by microorganisms can create differential oxygen concentration cells, promoting localized corrosion like pitting [17–20]. Conversely, biofilms can also protect metals by limiting oxygen availability or fostering the formation of protective layers of corrosion products [21].

The concept of electroactive biofilms emerged at the start of the 21st century, recognizing that microorganisms could exchange electrons with non-soluble substrates such as conducting materials [221,222]. Thus, in anaerobic environments, extracellular electron transfer (EET) explains why corrosion is enhanced [3–5,22]. Therefore, since microorganisms are recognized as being able to catalyze the EC reactions involved in corrosion, MIC phenomena have been extensively investigated using EC techniques [15]. Many EC techniques have been successfully employed to study various aspects of MIC under aerobic and anaerobic conditions in complex electrolytes, such as microbiological culture media [21–30]. Electrochemistry is almost always necessary to quantify corrosion rates, investigate MIC reactions, study the mechanisms at the metal/biofilm interface, and monitor the onset of MIC and its propagation [31]. Other techniques, such as weight loss, metallographic and microscopy observations, only confirm the electrochemical information and the occurrence of MIC by post-experimental examination (after the fact!). EC techniques offer real-time monitoring with minimal disruption of the interface. However, they face challenges related to the resolution and sensitivity needed to detect subtle changes.

The unpredictable nature of biofilm formation complicates EC measurements, as biofilms evolve over time and can vary in thickness, composition, and microbial activity. Furthermore, biofilm heterogeneity, both spatially and metabolically, introduces additional complexities in interpreting EC data. Transcriptomics of producing enzymes and metabolomics are some new chemical techniques with great potential for monitoring MIC mechanisms and development. The ability to rapidly detect, identify, and determine the metabolic status of bacteria *in situ* could revolutionize microbiology [32]. However, these techniques require invasive sampling of the biofilm and complex knowledge, which is still lacking, for data interpretation [33,34]. Even, no direct correlation exists between microbial composition and corrosion rate, highlighting the complexity of MIC. It must be remarked that there are no field conditions where just a single species exists, and it is not possible to recognize by EC techniques alone the single contribution to MIC of different species living in the biofilm. Ultimately, combining EC with molecular techniques and artificial intelligence may offer deeper insights into microbial corrosion and help model its behaviour in real-world scenarios.

By sampling electrical feedback from the metallic surface, EC techniques offer the possibility of detecting and monitoring the redox reactions of the corrosion process in real time, thereby avoiding (or minimizing) invasive effects that can markedly alter the investigated phenomena. On the other hand, electrochemistry can also be severely disruptive, depending on the intensity of the electric perturbation used. Typically, an electrochemical system reversibly reacts to a temporary electrochemical stimulation of a few mV or  $\mu\text{A}$ , and it takes a few minutes to reach a new equilibrium or steady-state if such a stimulation persists. If the perturbation is much higher (*i.e.*, more than between 10 and 20 mV), the system can be irreversibly modified or take hours to return to the original condition, depending on the kinetics of the processes involved. This is particularly important in the case of MIC, as microbes can detach from the electrode due to the stimulation. Therefore, possible to acquire information about the progress of the corrosion process by monitoring the response of an electrochemical system to a controlled electric stimulation.

Considering these aspects, this review aims to screen EC techniques used to investigate MIC at laboratory level, and to monitor MIC in the field, discussing challenges in understanding MIC mechanisms.

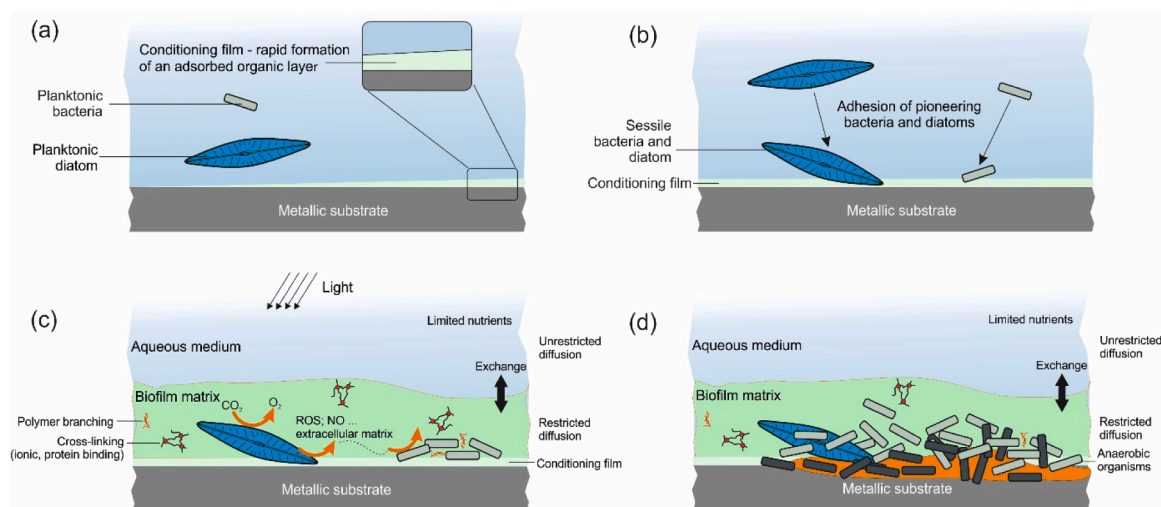


**Fig. 1.** Relevant steps of microorganism attachment and biofilm formation in aerated waters: (a) rapid and spontaneous conditioning film of adsorbed organic and/or inorganic layer formation produced by natural biological and chemical processes in the form of metabolites and decomposition products of marine life or present in the environment; (b) reversibly microbial initial attachment; (c) secretion of extracellular polymeric substances (polysaccharides, proteins and extracellular DNA that form the slimy aggregates termed biofilms) during biofilm growth with some metabolites (ROS, NO, extracellular matrix, ...) that influence physicochemical conditions at the metal/biofilm interface; and (d) mature biofilm formation with various structural components and dynamic consortia of microbial clusters including aerobic and anaerobic organisms (spatiotemporal diversity).

## 2. Macro- to nano-scale MIC

This section reviews how living biofilms create inhomogeneous conditions that can lead to localized corrosion and disrupt protective oxide layers. Microorganisms can either promote or inhibit corrosion, depending on several environmental factors, with oxygen content being the most relevant. These phenomena can be investigated at different scales using electrochemical techniques. The thermodynamics of extracellular electron transfer (EET) through biofilm and conductive networks are described, highlighting the central role that ionic species and redox mediators play in accelerating corrosion kinetics.

A biofilm is a catalytic respiring barrier growing at the metal-solution interface. The respiration of microorganisms consists of a cascade of redox reactions where electrons are delivered to a final electron acceptor (oxygen, nitrate, and sulfate) by protein electron carriers. Direct interaction with the conductive substrate (electrode) changes the chemical-physical characteristic of the interface, usually allowing microorganisms to obtain nutrients and a satisfactory environment for their community. The corrosion phenomenon also occurs at the metal-solution interface, driven by the electrochemical performance of this specific location, where the oxide passive layer develops, depending on the thermodynamics and kinetics of the system.

The oxide layer thickness is a few nanometres for a passive metals like stainless steel and titanium alloys, whereas oxide films of a hundred nanometres are reported for copper alloys (often termed protective oxide layers). The less protective oxides that develop on carbon steel are hundreds of microns thick and cannot match the performance of the thinner passive films of stainless steels. Nevertheless, stainless steels also suffer from MIC. Several laboratory studies have discussed and documented how communities of bacteria, including single-cell components, can attach and propagate to form a biofilm and then disrupt and degrade the passive layers of stainless steel in a few hours. Typically, Sulfate Reducing Bacteria (SRB) are involved in creating pitting phenomena, such as documented on 304 L stainless steel in the presence of *Geobacter sulfureducens* under an established biofilm (Fig. 2 [24]). MIC was here explained by an inhomogeneous surface energy distribution that caused bacteria colonization and pit formation, while in another study [35], the co-presence of conductive cell filaments and magnetite in the biofilm was outlined (Fig. 3).

A different example of stainless steel pitting corrosion due to aerobic *Shewanella algae* was documented by the nanomanipulation mode of Atomic Force Microscopy (AFM) which allowed for obtain the three-dimensional topography of cell/passive film under the settlement. In this case, the variation of Volta potential in the area of the microbe settlement was correlated to accelerated degradation of the passive film [36].

A uniform condition at the interface never truly exists, probably not even in the case of uniform acidic corrosion of iron, and certainly not for

alloys in any environment, especially when a biofilm is present. Typically, the oxygen concentration inside the biofilm decreases due to aerobic respiration, thus the surface area immediately adjacent to the biofilm will be subject to anaerobic conditions. In contrast, the areas of the metallic surface without a biofilm will be under aerobic conditions, thus creating a galvanic couple (driven by differential aeration). Moreover, local inhomogeneities, such as differences in medium composition, concentrations, phases, and states (gas, liquid, and solid) of the matter, are present in both the anaerobic and aerobic biofilm layers. These factors contribute to increasing the complexity of the interface and possible electron pathways.

Despite the increase of biofilm thickness promoting the anaerobic condition on the metal surface and stabilizing these conditions, there is no evidence that biofilm thickness (or the count of microorganisms) strictly correlates to the corrosion rate. Inhomogeneities conditions on the surface and electron pathways across the biofilm are more likely responsible for corrosion and corrosion inhibition than the biofilm thickness itself.

Fig. 4 illustrates the microscale distribution of aerobic bacterial cells (*Vibrio sp.*) on a carbon steel surface, observed using Field Emission Scanning Electron Microscopy (FESEM) and confocal microscopies [37]. The exopolymer matrix filling the space between bacteria agglomerates (green) is not visible. However, it is an important component of this oxygen-respiring biofilm, which has shown to provide a protective behaviour against corrosion. On abiotic samples, the higher abundance of oxygen at the surface caused more intensive corrosion of the steel, covered by a partially protective (inhomogeneous) layer of iron oxides of hundred microns in thickness.

Biofilm has a complex structure although more than 90 % of their weight is water (in a liquid phase) [38]. Various physical and electrochemical characteristics were measured by assessing the entrained water with microsensors, including local fluid flow velocities, oxygen concentration, redox potential, and local mass transfer coefficient profile within the biofilms. Examples illustrate the use of microelectrodes and microsensors in studying biofilm structure and physical-chemical characteristics.

A clearer physical description of biofilms was achieved by using redox microelectrodes in a work that investigates the stratified structure of biofilm and transport/transformation processes involved, as detailed in Ref. [39]. Dissolved oxygen and pH were measured at 100  $\mu\text{m}$  intervals through a 2.5 mm thick mixed species biofilm. Recently, a J-shaped oxygen microelectrode was used with an open flow system under microscopic examination at depth intervals of 10  $\mu\text{m}$ . The location of the electrode tip was verified using confocal laser microscopy, providing highly accurate information on the depth of the electrode within the biofilm and its position relative to pores in the biofilm matrix. Local oxygen gradients were measured within cell clusters and pores. Microsensors were also successfully used for sensing sulfide and

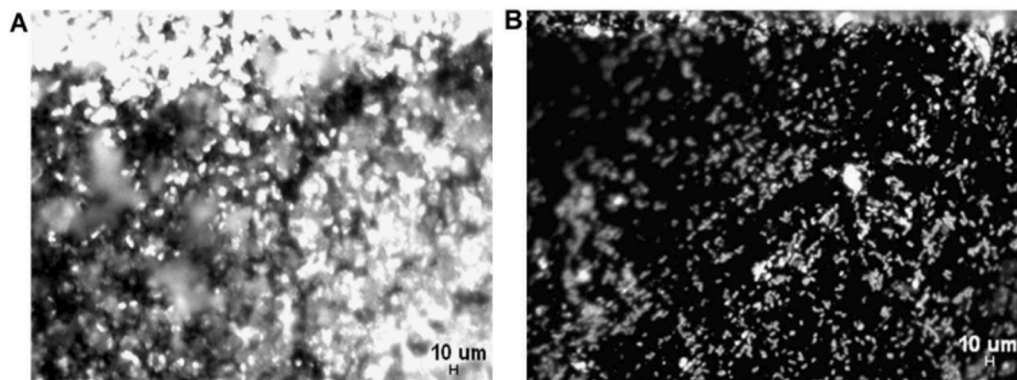
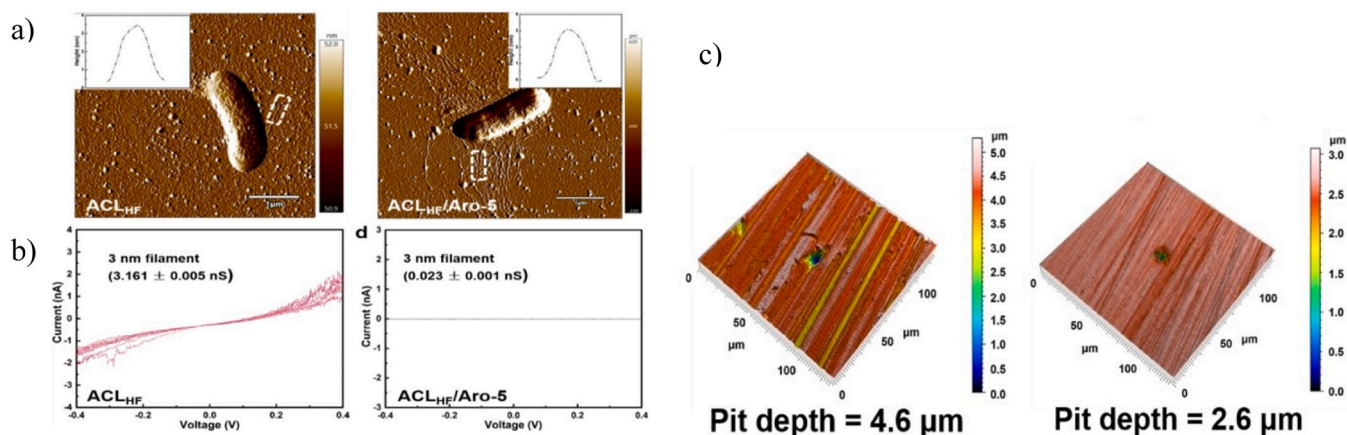
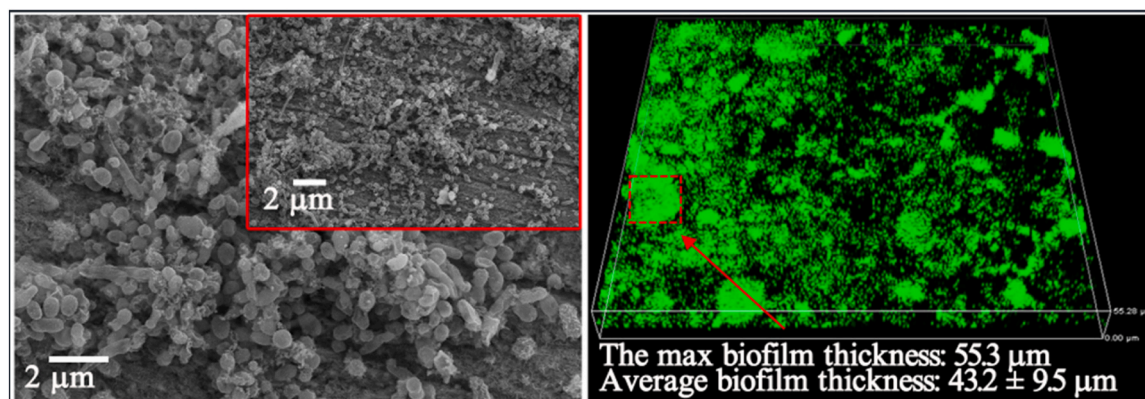


Fig. 2. Dense local settlement of *Geobacter sulfureducens* (white spots) in the vicinity of deep pits on 304 L stainless steel a) and in a region free of pitting (b) observed by an Epifluorescence microscopy (from ref. [24]).



**Fig. 3.** Atomic force microscope analysis of primary filaments emanating from genetically modified *G. sulfureducens* strain (strain named ACL<sub>HF</sub> and ACL<sub>HF</sub>/Aro-5) a) Amplitude image and filament height measurement (inset) taken at the location designated by the dashed white box for strain ACL<sub>HF</sub> (left) and strain ACL<sub>HF</sub>/Aro-5 (right) b) Current-voltage analysis of conductance filament for strain ACL<sub>HF</sub> (left) and strain ACL<sub>HF</sub>/Aro-5 (right) c) Confocal laser scanning microscopy images of the stainless steel surface after biofilms had been removed from incubations with strain ACL<sub>HF</sub> (left) or strain ACL<sub>HF</sub>/Aro-5 (right). Modified from ref. [35].



**Fig. 4.** FESEM scanning electron microscopy and confocal microscopy (CLSM) images of biofilms formed by *Vibrio* sp. on X80 carbon steel (from ref. [37]).

measuring pH to monitor the activity of sulfate-reducing microorganisms and sulfur oxidizers. Amperometric and potentiometric measurements of H<sub>2</sub>S were also successfully conducted using microelectrodes, documenting the anaerobic conditions present in biofilms interfacing with air [40]. In another study, of the use of microelectrodes combined with electrochemical impedance spectroscopy (EIS) was explored to differentiate between one- and two-electron transfer electrochemical reactions occurring within marine microbial biofilms [41]. Unlike conventional electrodes, microelectrodes are able to detect the local activities (concentrations) of various chemical species that influence either the current or potential at the metallic interface and within the biofilm. By combining microelectrodes with micro-mechanical devices and microscopy for scanning macro surfaces (of a few centimetres squared) at the microscale (as in Figs. 3 and 4), it is possible to measure and analyze data from the corrosion products and other micro-components characterizing the metallic surface.

Building on advancements in microsensors technologies, local electrochemical techniques such as the scanning electrochemical microscopy (SECM), the scanning vibrating probe technique (SVET), and the local EIS (LEIS) are now more widely used to study the interactions of chemical and microbial components at the microscale. A more detailed description of such local techniques applied to MIC studies was recent reviewed by Chang *et al.* [42] to which reference is made for further details. Hence, here they are only briefly described in the last chapter.

### 2.1. Extracellular electron transfer at the biofilm and metal interface

During the colonization of a metallic surface, bacteria excrete Extracellular Polymeric Substances (EPS), which include polysaccharides, fatty acids, proteins, and enzymes. These substances help anchor the biofilm to the surface and facilitate interactions whether cooperative or competitive, with other microorganisms. The EPS network forms the structural component of the biofilm, which can exceed more than 100 μm in thickness. Extracellular Electron Transfer (EET) within the biofilm can occur through the structural network of EPS and bacterial membranes (dielectric components), as well as through the locally conductive aqueous media that constitutes most of the biofilm's mass, due to the dissolved ions and enzymes it contains. Fig. 5 summarizes the three popular biofilm models for EET for Sulfate Reducing Bacteria (SRB), which can to varying synergically extents contribute to the progression of the corrosion process: a) direct contact or conductive cell extensions (pili) of living cells, b) a conductive EPS network within the biofilm, c) the use of electron-shuttles (*e.g.*, extracellular or self-excreted small molecules such as phenazines, flavines, quinones, and extracellular cytochromes hydrogenase). Electron shuttles actively enable clusters of microorganisms located away from the metal surface to contribute to the electrochemical process.

Research to elucidate the role of the biofilm components in EET is ongoing in several laboratories, particularly with the development of Bio-Electrochemical Systems (BES). However, the results remain controversial and do not yet provide a comprehensive explanation of

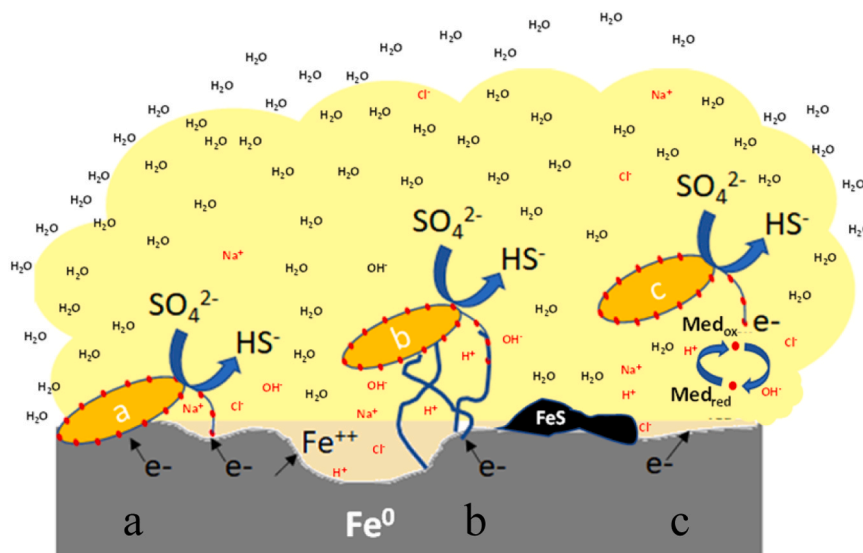


Fig. 5. Schematic of the three different possible electron-transfer mechanisms of SRB in an ionic conductive biofilm: a) EET by bacterial membrane or connected pili, b) EET by interconnected solid conductive elements (nanowire) of the EPS matrix; c) EET by mediators excreted in the liquid matrix acting as shuttle of electrons.

corrosion phenomena [43]. Among these, EET facilitated by extracellular redox mediators is the most well-documented [44]. These studies typically combine transcriptomic analyses of RNA and EC measurements.

2.1.1. Biofilm conductivity and consequence for EET

The components forming the solid polymeric network within the biofilm display semiconductor properties, characterized by their conductivity in a range between  $10^{-6}$  and  $1 \text{ mS cm}^{-1}$ . The presence of redox components can enhance conductivity, but their pseudo-capacitive characteristics are significantly lower compared to those of corrosion products, passive oxides and organic coatings [43,45] (see Fig. 6). It is important to note that EET through a network of organic polymers (dielectric), such as cell membranes or EPS in the biofilm, is several orders of magnitude lower than electron transfer in metallic materials. Additionally, ionic conductivity within the biofilm is also orders of magnitude lower than that of metals. However, natural waters and biological solutions typically exhibit ionic conductivity that is several orders of magnitude higher than the common biological polymers, and corrosion products (Fig. 6). At  $25^\circ\text{C}$ , the conductivity is less than  $10^{-6} \text{ S cm}^{-1}$  for cellulose [46], is  $7.6 \times 10^{-8} \text{ S cm}^{-1}$  for benzene,  $1.35 \times 10^{-9} \text{ S cm}^{-1}$  for ethyl alcohol and  $3 \times 10^{-7} \text{ S cm}^{-1}$  for glycol [47].

The dielectric characteristics of biofilms were primarily studied in BES, such as microbial fuel cells and microbial electrolysis cells. In these systems, microorganisms exhibit the same metabolic behaviour as in MIC, but reside on ideally-polarized (i.e., inert) anodes that do not corrode. The electrochemical process, whether spontaneous or induced by an external polarization, generates ions from water redox processes, the oxidation of organic compounds and other redox reactions occurring at the electrode/biofilm interface. In capacitive corrosion processes, ions are also supplied by metal dissolution (corrosion products), which

leads to the formation of capacitive or pseudo capacitive passive layers. In polarized systems, where electrodes are inert and highly conductive, anode dissolution does not occur. Consequently, it is possible to estimate the capacitive properties of the biofilm, unlike in the corrosion process where these properties are influenced by corrosion products. A conductivity of approximately  $250 \mu\text{S cm}^{-1}$  was observed in ‘electroactive’ (polarized) biofilms, which consisted of a diverse bacteria consortia sustaining current densities of around  $1 \text{ A m}^{-2}$  on a polarized inert anode [48]. Similar values of biofilm conductivity were reported for single strains of *Geobacter sulfureducens* by the same authors. The conductivity of biofilms formed by dual-species *Geobacter aggregates* was two orders of magnitude lower [49], and the conductivity of biofilms composed of multispecies methanogenic aggregates derived from wastewater digesters was one order of magnitude lower [50]. It was suggested that a stronger selection microorganisms occurs in biofilms with higher conductivity compared to planktonic microbial aggregates because electrons need to be transported much farther in the first case [47].

However, another explanation, not yet fully explored, involves the enrichment of ions and metabolites in the liquid fraction of biofilm under polarization. This phenomenon was documented by micro-electrodes in air-respiring cathodes of microbial fuel cells, where a thick anaerobic biofilm composed of a rich microbial community on the cathode facilitated the rapid delivery of electrons to the oxygen of the air through the production of sulfides [40].

It can be inferred that in the corrosion of carbon steel induced by *Geobacter sulfureducens*, the production of motile sulfide anions ( $\text{HS}^-$ ) likely enhances the electrical conductivity of the biofilm. Additionally, the enrichment of cations coming from metal corrosion, where diffusion is limited in the quiescent aqueous media of the biofilm, can also increase the conductivity at the interface metal-biofilm, though this is

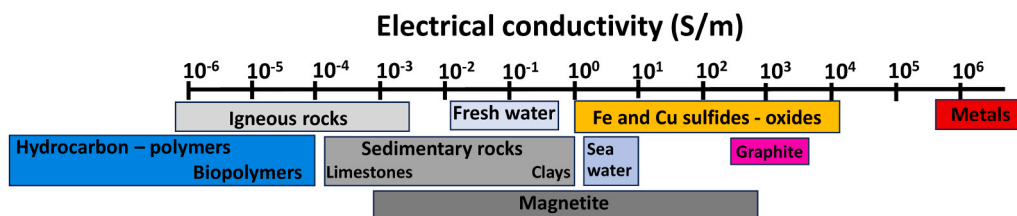


Fig. 6. Electrical conductivity approximative ranges for different materials and ionic waters.

partially offset by the precipitation of salts and oxides. Notably, the excretion of soluble redox enzymes (electron shuttles) can increase the ionic conductivity of the biofilm in both BES and MIC scenarios. These enzymes interact with the other redox species and attached to solid components.

At the macroscale, biofilm pseudo-capacitance typically cannot be distinguished from the corrosion product pseudo-capacitance and can be neglected in corrosion cases. A significant pseudo-capacitive effect induced by a biofilm (inhibiting corrosion of steel in that case [51], was convincingly detected in lab experiments only after the solid (dielectric) phase of biofilm containing EPS was artificially concentrated of about one order of magnitude, an unusual condition.

Amino acids that form proteins, enzymes, co-factors, as well as nucleic acids (*i.e.*, DNA and RNA), can conduct the electrical current in the biofilm more effectively than the EPS polysaccharides. This is because they contain active redox centres, often including metal atoms, and a complex distribution of dipoles that can be spatially adjusted to allow the electron exchange. Therefore, direct electron uptake from a metal through conductive polymers is organized similarly to conductive nanowires [52], outer membrane redox protein c-type cytochromes (c-cyts), and other redox proteins (such as multi-copper proteins OmpB and OmpC) can, to some extent, increase the biofilm's electrical conductivity. This process works synergistically with the soluble shuttle mechanisms, as described in Fig. 5.

### 2.1.2. The thermodynamic approach to EET in biofilm components

*The thermodynamic analysis is crucial for understanding how electrochemical techniques can measure the complex EET processes between biofilms and conductive surface. This chapter addresses some fundamental principles relevant to any type of bioelectrochemical system.*

From a thermodynamic standpoint, corrosion is an irreversible and spontaneous process driven by the potential difference between anodic and cathodic reactions, which correspond to different redox systems occurring in different (or the same) spatial areas on the same material. The electromotive force corresponding to the potential difference is counteracted by the ionic resistance within the system. For a single system (anodic or cathodic contribution), the electromotive force results from the concentration gradient of redox molecules, which establishes the equilibrium potential for a charge transfer reaction as described by the Nernst equation (Eq. 1). This gradient promotes the ET between reactions with different equilibrium potentials. The Nernst equation relates the electrochemical equilibrium potential to the concentration of species involved in the redox process:

$$E = E^\circ - \frac{RT}{zF} \ln \left( \frac{[\text{Red}]}{[\text{Ox}]} \right) \quad (1)$$

where  $E$  is the potential,  $E^\circ$  is the standard potential,  $R = 8.314 \text{ J mol}^{-1} \text{ K}^{-1}$  is the gas constant,  $T = 298 \text{ K}$  is the temperature,  $z$  is the number of electrons transferred in the redox reaction,  $F$  is the Faraday constant ( $96,485 \text{ C mol}^{-1}$ ),  $[\text{Ox}]$  and  $[\text{Red}]$  are the concentrations of oxidized and reduced species, respectively.

By analyzing the thermodynamic aspects of an enzymatic redox reaction [53], in the context of Marcus' theory for electron transfer [54], it becomes possible to explain how electron transfer between the orbitals of two groups of ionizable biological molecules (*e.g.*, co-factors, amino acids, DNA bases, and enzymes) can occur and determine the maximum distance over which it can take place.

The relevant concept from Marcus' theory, as reviewed by Cordes and Giese [53], is that in the thermodynamic energy balance of a redox reaction, the reorganization energy-energy that molecules can dissipate into the surrounding medium - must also be considered. This explained how enzymes and other shuttles significantly influence the energy required for a redox reaction to occur.

The ET rate ( $k_{\text{ET}}$ ) estimated from the driving force (redox reaction energy) and the reorganization energy (entropic components due to the

surrounding molecules, such as enzymes) is given according to Eq. 2

$$k_{\text{ET}} = k_{\text{ET}}(0) \exp \left[ \frac{-(\lambda + \Delta G^\circ)^2}{4\lambda RT} \right] \quad (2)$$

where  $\lambda$  is the energy required to bring the nuclei from the equilibrium position of the reactants to the equilibrium position of the products, which must be compensated for by the standard Gibbs free energy ( $-\Delta G^\circ$ ).  $k_{\text{ET}}(0)$  is the activation-free rate occurring when  $-\Delta G^\circ$  equals  $\lambda$ . The excess free energy that must be dissipated in the media can be harnessed from enzymes that allow ET to occur.

The molecular distance between distinct orbitals of electron donor and acceptor plays a significant role in ET. Therefore, an additional element  $H_{\text{AD}}$ , representing the electronic coupling matrix was later introduced into Marcus' theory, as shown in the Eq. 3.

$$k_{\text{ET}} = \left( \frac{4\pi^3}{h^2 \lambda k_B T} \right)^{1/2} H_{\text{AD}}^2 \exp \left[ \frac{-(\lambda + \Delta G^\circ)^2}{4\lambda RT} \right] \quad (3)$$

$H_{\text{AD}}^2$  represents the probability of an electron crossing a potential barrier between a Donor (D) and an Acceptor (A) when the activation energy is reached [54]. The overlap between D and A orbitals ( $H_{\text{AD}}$ ) decays exponentially with increasing D-A separation distance ( $r_{\text{DA}} - r_0$ ), as expressed in the Eq. 4 [53]. The factor  $\beta$  reflects the performance of the medium to influence the ET rate.

$$H_{\text{AD}} = H_{\text{AD}}^0 \exp(-\beta(r_{\text{DA}} - r_0)) \quad (4)$$

Relative values of  $H_{\text{AD}}$  and  $\beta$  can be derived from crystal structures of proteins and/or protein complexes. Experimental and computational calculations have shown that ET by tunnelling can occur efficiently at a maximum distance of about  $20 \text{ \AA}$  [55] with a  $\beta$ -value of  $1.4 \text{ \AA}^{-1}$  [56]. Distances that exceed  $H_{\text{AD}}$  (the limit for fast electron tunnelling reactions) can be overcome by a cascade of multistep hopping processes involving different types of molecules, typically enzymes. The rate of the hopping mechanism scales algebraically (rather than exponentially as with the tunnelling rate) with the number ( $n$ ) of hopping steps, as shown in Eq. 5, where  $k_n$  is the hopping rate and ranges between 1 and 2 [53]. The hopping mechanism enables EET to occur over an extended distance, effectively minimizing energy dispersion.

$$k_{\text{ET}} \propto k_n n^{-n} \quad (5)$$

Spectroscopic observations indicate that tunnelling is the main mechanism for rapid and direct electron transfer in simple organic molecules. For more complex or distant molecules, hopping allows faster electron transfer compared to a single-step electron tunnelling process. This mechanism explains, why amino acids of proteins, particularly triptosyne and sulfur-containing tyrosine, can undergo rapid and reversible oxidization and reduction [57]. DNA is highly effective at carrying charge, utilizing guanine or adenine bases as steps for the ET hopping mechanism.

It is important to note that chemical intermediates, such as metal complexes, can promote super exchange of electrons between proteins and other organic aggregates. Typically, the co-factors in protein complexes that enable photosynthesis and respiration aid ET across cell membranes. A sequence of organic and inorganic co-factors, with slight differences in their reduction potentials, drives electrons in a defined direction (either outside or inside membranes and cells) through a suitable cascade. This process is coupled with an inverse ionic flow to balance local charge.

In the context of corrosion, redox proteins like c-type cytochrome (c-cyt) including hydrogenase and iron-sulfur proteins, are extensively implicated in enabling EET over multiple length scales (up to tens of micrometres) in well studied bacteria models such as *Geobacter* and *Shewanella* [58]. However, for long-distance EET, the chain-to-chain hopping is the primary source of resistance in conducting polymers [59]. For example, outer membrane c-cyts, can directly exchange



electrons over a few nanometres. Consequently, flavin and other small molecules are also excreted during long-distance EET, although their exact role was not fully understood.

In a comprehensive study analyzing the thermodynamics of processes promoted by biofilms on an uncorrodible anode, Torres *et al.* concluded that a solid network of conductive polymers was the most preferred mechanism associated with EET, as described in Fig. 5 [60]. However, subsequent research, both in bioelectrochemical systems and microbial corrosion, has not detailed convincing pathways, especially for non-sulfate-reducing bacteria [43]. Most studies have not considered the possible role of variations in the ionic conductivity within the biofilm in relation to the electrochemical process, and the motility of mediators, with a few exceptions. As emphasized by Blackwood [43], any claims of high electrical conductivity in bioelectrochemical systems need to be carefully verified in light of the coupled ionic balance. This is particularly relevant for microbial corrosion, as metal dissolution increases the aqueous medium conductivity and alters pH within the biofilm. Ionizable mediators, including inorganic ions such as sulfides, and ionizable elements *i.e.* hydrogen and metal ions, although present in lower concentrations compared to other ionic salts in the biofilm, can significantly impact the ionic conductivity of the medium [40]. They can significantly influence the progression of EET both at the metal interface and through interactions with the semi-conducting components (such as membranes, pili, EPS, and nucleic chains) within the biofilm.

From a kinetics perspective, the ionic gradient's electromotive force within the biofilm (which consists of over 95 % water) can generate an electrical current, constrained by ohmic resistance. The ionic conductivity ( $\sigma$ ) is expressed in Eq. 6:

$$\sigma = \frac{l}{(R_b A)} \quad (6)$$

where  $\sigma$  is the ionic conductivity usually expressed as  $S\text{ cm}^{-1}$ ,  $l$  is the path (cm) between anode and cathode,  $A$  is the area ( $\text{cm}^2$ ) where the electrical field between anode and cathode is expressed, and  $R_b$  ( $\Omega$ ) is the media resistance. In biofilms, mass transfer phenomena can be complex due to the local interactions between ions (or ionizable molecules) and semi-conductive organic components of the biofilm and corrosion products. Consequently, local ionic conductivity can vary significantly, depending on the local production and consumption of active elements, their charge, concentration, and the thickness they need to traverse.

If an enzyme concentration is the rate-determining step (the slower one) of the EET, the current density ( $j$ ) can be expressed as a function of its concentration  $[C]$  using the Nernst-Michaelis equation [60], as expressed in Eq. 7:

$$j = \frac{j_{\max}[C]}{(K_M + [C])} \quad (7)$$

where:  $[C]$  is the enzyme concentration,  $j_{\max}$  is the maximum rate of the enzyme-catalyzed reaction, and  $K_M$  is the Michaelis constant, representing the enzyme-substrate concentration at which the reaction rate is half of  $j_{\max}$ . When a more complex microbial metabolism limits EET, we can empirically calculate the current density from the concentration of the substrates limiting microbial growth by the Nernst-Monod, Eq. 8:

$$j = \frac{zFj_{\max}[S]}{(K_S + [S])} \quad (8)$$

where  $j$  is the current density,  $j_{\max}$  is the maximum current density from the reaction,  $[S]$  is the concentration of the substrate, and  $K_S$  is the half-saturation constant.

Various phenomena contribute to limiting the electric current through the metal-biofilm interface, making it challenging to theoretically determine, *a priori*, the limiting step and components of energy losses that restrict the overall EET process to different extents.

Significant insights can be gained from measuring the electrical parameters of the electrochemical system, as the current density and electrode potential can be correlated by combining the Nernst and Michaelis-Menten equations, as in expressed in Eq. 9:

$$j = \frac{j_{\max}}{1 + \exp\left[-\frac{F}{RT}(E - E_{1/2})\right]} \quad (9)$$

where  $E$  is the Nernst potential,  $E_{1/2}$  is the potential when  $j$  is equal to half  $j_{\max}$ .

The difference between  $E$  and  $E_{1/2}$  represents all phenomena that limit EET, which can be attributed inseparably to diffusion (substrates and/or metabolites), the electron transfer rate at the electrode-electrolyte interface, and microbial kinetics. These factors are usually expressed as the overpotential  $\eta$ .

The overpotentials dissipated to transfer  $z$  electrons from the liquid solution inside the metal (considering the electrode-electrolyte interface of both anode and cathode regions), are expressed by the Butler-Volmer equation (Eq. 10):

$$j = j_o \left[ \exp\left(\frac{\alpha_a z F \eta}{RT}\right) - \exp\left(\frac{\alpha_c z F \eta}{RT}\right) \right] \quad (10)$$

where  $\alpha_a$  and  $\alpha_c$  are the anodic and cathodic transfer coefficients, respectively, and  $\eta$  is the overpotential. Note that Eq. (10) does not recognize mass-transfer effects.

All the aforementioned electric parameters can be measured using electrochemical methods which can force EET out of its equilibrium to varying extents by adding a controlled quantity of energy to the system via an external electrical source.

## 2.2. The electric behaviour of passive layers in the presence of biofilm

*This chapter examines how different layers—passive, outer, and biofilm—affect the corrosion resistance of metals like stainless steel. It highlights the Point Defect Model's role in explaining the formation and breakdown of barrier layers on stainless steel, with a particular focus on the electrical properties of these layers and their implications for charge transfer and corrosion rates.*

A schematic of the electric behaviour of different layers playing a role in the corrosion process of an active-passive alloys, such as stainless steel, is illustrated in Fig. 7. Steels with chromium contents higher than 10–12 % are termed 'stainless' due to the ability to form naturally occurring, protective, and self-repairing chromium and iron oxide layers on their surface when exposed to an oxidizing atmosphere. The passive film is thin (between 1 and 3 nm); however, it can be detected by ETs due to its high resistance to electrical current flow. Once this film has formed, the metal is 'passivated', meaning it has gained kinetic stability despite lacking thermodynamic stability. In addition to the passive oxide layer (referred to as the barrier layer, bl), other layers can form depending on the external environment. These include layers resulting from the reprecipitation of corrosion products (known as outer layer, ol) and layers associated with biological activity (*i.e.*, a biofilm). The biofilm and the porous outer layer are generally mixed within the same thickness. These layers have different electrical properties. Fig. 7 also illustrates the distribution of ionic and electronic conductive components, as well as the capacitive and diffusive components at the metal surface. The double layer serves as the interface between the ionically and the electronically conductive parts. The biofilm is considered as an ionic conductor, while the barrier layer is described by a capacitive/resistive (and in some cases diffusive [61]) mixed conductor. The outer layer also exhibits capacitive/resistive behaviour, but due to its porosity, a diffusive Warburg component should be included to represent the restricted diffusion of species (such as dissolved oxygen) through this water-saturated layer.

The electrochemical performance of materials is primarily correlated

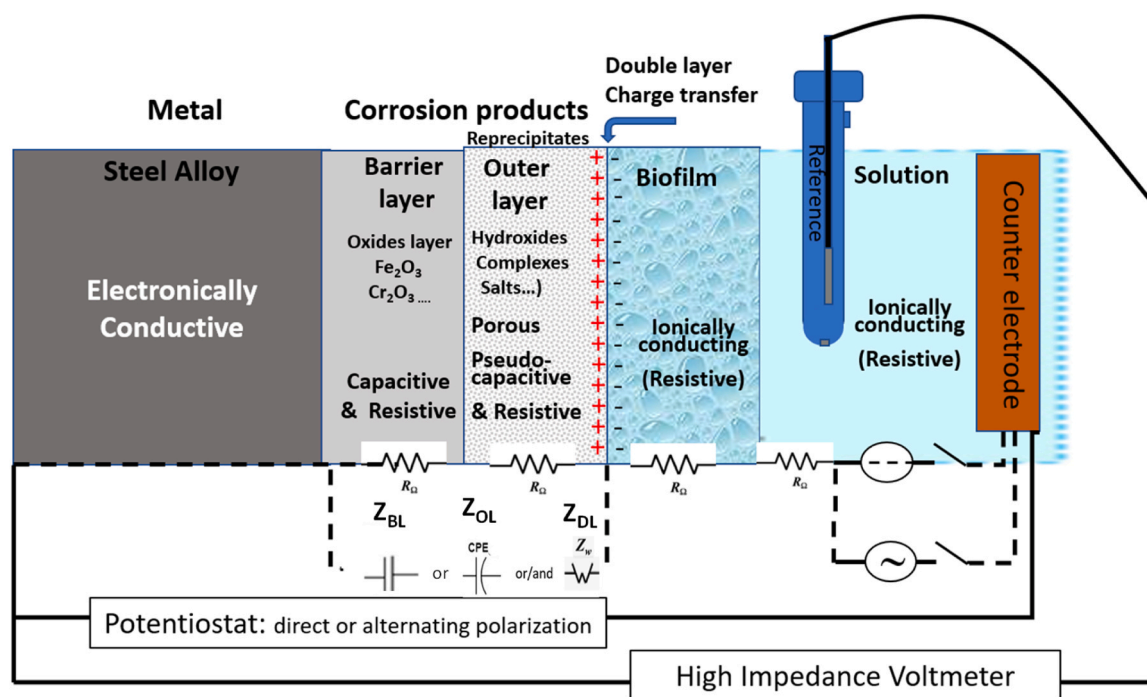


**Fig. 7.** Schematic of electric properties of different corrosion layers of stainless steel and biofilm which can be explored by EC techniques.  $Z_{BL}$ ,  $Z_{OL}$ , and  $Z_{DL}$  are the resistive and capacitive or pseudo-capacitive impedance components for the Barrier layer, Outer layer, and Double layer respectively;  $R_{\Omega}$  is the faradaic resistance of each component.

with the nature of the various layers. For stainless steels, the corrosion resistance is typically attributed to the barrier layer. However, the outer layer and biofilm can also significantly influence the interfacial impedance, either positively or negatively. For instance, if the biofilm generates metabolites that accelerate the dissolution of the barrier layer, this could lead to a decrease in the interfacial impedance and, consequently, an increase in the corrosion rate. The electrons or electron holes produced at the interface between the electrolyte (with or without the biofilm) and the solid layer (corrosion products) are transferred to the metal via electronic resistance. For a homogeneous oxide, the impedance per surface area is approximately equivalent to a resistor parallel with a capacitor. However, the corrosion products are often inhomogeneous in both composition and spatial distribution between the metal and the electrolyte interface. These can then be associated with a dielectric layer, characterized by a resistivity and a permittivity that result from the combined contributions from each component. Thus, the global impedance varies spatially. Similarly, a biofilm can be unevenly distributed on the solid interface (*i.e.*, patchy), contributing to charge transfer and ionic conductivity, much like the solution.

It is important to note that at the corrosion potential, both cathodic and anodic reactions simultaneously contribute to the net current density flowing across the interface. Different electrochemical techniques, both stationary and potentiodynamic can help identify the phenomena involved and determine the predominant or limiting phenomenon. The impedance associated with the double-layer capacitance at the interface can generally be neglected compared to the impedance of the anodic oxide layer when the metal is in a passive state. Indeed, the space charge capacitance of the barrier layer is generally much smaller than that of the double layer. Since the capacitances are in series, the phenomenon with the lower capacitance (*i.e.*, the space charge capacitance) generally dominates. For the cathodic branch, a parallel impedance with single components must be considered for modelling the global process. For example, oxygen reduction or water reduction on the passive surface generally occurs at the barrier layer/outer layer interface, where charge carriers must traverse the barrier layer to and from the metal. For a sufficiently thin barrier layer, electron/electron-hole transfer is

generally via direct, resonant quantum-mechanical tunnelling (QMT). As such, an electronic QMT impedance must be added to the cathodic charge-transfer resistance. Both these impedances (anodic and cathodic charge transfer impedance) can be strongly influenced by microorganisms' activity. The sum of the two can be determined by impedance analyses [62].

### 2.2.1. Barrier layer and outer layer

The pathway of a metal atom/ion through passive layers to solution is detailed in the schematic of Fig. 8. The figure shows a point defective oxide barrier layer that forms via the generation of oxygen vacancies at the metal/barrier later interface and a porous, outer layer that forms via the reaction of the cations that are transmitted through the barrier layer with components in the environment, including the solvent water and eventually, biofilm. The barrier layer grows rapidly reaching a thickness between 1 and 3 nm in the case of stainless steels, while the outer layer forms at a more constant rate, growing to macroscopic dimensions (> 100  $\mu\text{m}$  or more). The outer layer is the visible corrosion (rust) observed on corroded non-stainless ferrous alloys. Because the outer layer forms via the precipitation of the metal cations transmitted through the barrier layer, species present in the environment, including microorganisms, may be incorporated via co-precipitation. Thus, over extended exposure periods, the passive films on most metals and alloys, including stainless steels, becomes dominated by the outer layer.

The most highly developed theoretical model for the passive state is the Point Defect Model (PDM) [63–65]. The PDM is recognized for providing an accurate account of the growth and breakdown of passive films at the atomistic level, as well as accurately describing passive dissolution and the formation of the precipitated outer layer. The point defect model offers valuable insight into the microbial interactions with metal surfaces at the atomic level, helping to explain key aspects of MIC, such as the initial stages of biofilm formation, localized corrosion, and the role of microbial metabolites in modifying surface reactivity. While the model itself focuses on atomic defects, integrating it with microbial behaviour allows for a deeper understanding of how microbial communities contribute to corrosion, both by accelerating it through

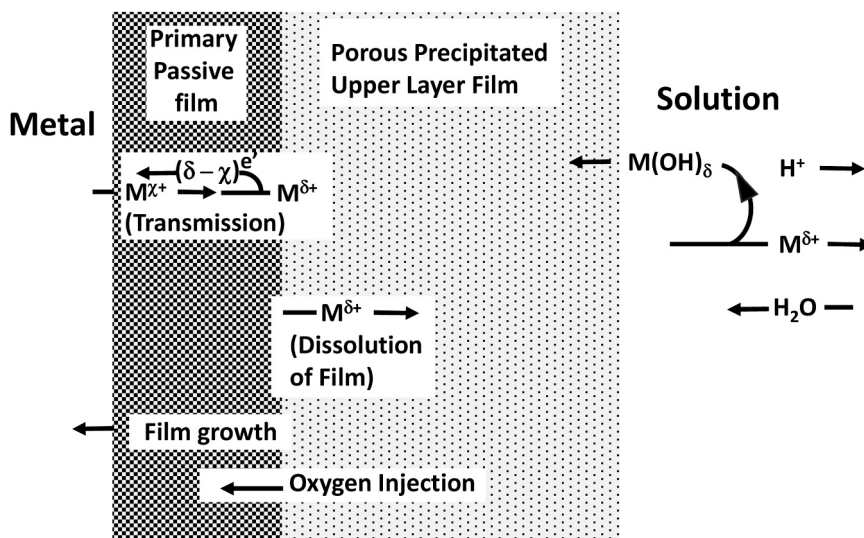


Fig. 8. Schematic of a point defective bi-layer displaying the formation of the barrier layer (primary passive layer) and the outer layer (porous, precipitated upper layer).

electrochemical interactions and, in some cases, potentially mitigating it by modifying the surface structure or creating protective biofilms.

One important characteristic of the PDM is that it yields many analytical relations available for evaluation against experimental data. To the authors' knowledge, the PDM has never been shown to be at odds with experiments when confluence exists between experiment and theory (*i.e.*, when the experiment performed on a system are consistent in detail with the basis of the model). For example, when evaluating the validity of the steady-state PDM, it is necessary to demonstrate that the experimental data are also in the steady state. This model has allowed the formulation of the criterion for the very existence of our reactive metals-based civilization by specifying the conditions that must be present for the existence of a meta-stable barrier layer on the surface.

The charge exchange across the passive layers of active-passive alloys has been extensively investigated over the past 40 years, cumulating with the development of the PDM [66]. The PDM is presented here because it is generally unfamiliar to the MIC community. It is

incorporated in the Mixed Potential Model (MPM) [67] to describe the partial anodic process of steel electro-dissolution associated with the partial cathodic process of the Hydrogen Electrode Reaction (HER) and/or the Oxygen Electrode Reaction (OER). The kinetics of the partial cathodic process are described by the Generalized Butler-Volmer equation (Eq. 10) [68]. The model is based on the bi-layer version of the PDM [66] shown in Fig. 9a. It takes into account the various ohmic drop contributions at the interfaces ( $\varphi_m - \varphi_{bl,1} + \varphi_{bl,1} - \varphi_{bl,2} + \varphi_{bl,2} - \varphi_{ol,1} + \varphi_{ol,1} - \varphi_{ol,2} + \varphi_{ol,2} - \varphi_R$ ) that decrease the value of the potential (V) applied to a metal immersed in a solution and measured vs a reference electrode (Eqs. 11 and 12):

$$V = \varphi_m - \varphi_R$$

$$= \varphi_m - \varphi_{bl,1} + \varphi_{bl,1} - \varphi_{bl,2} + \varphi_{bl,2} - \varphi_{ol,1} + \varphi_{ol,1} - \varphi_{ol,2} + \varphi_{ol,2} - \varphi_R \tag{11}$$

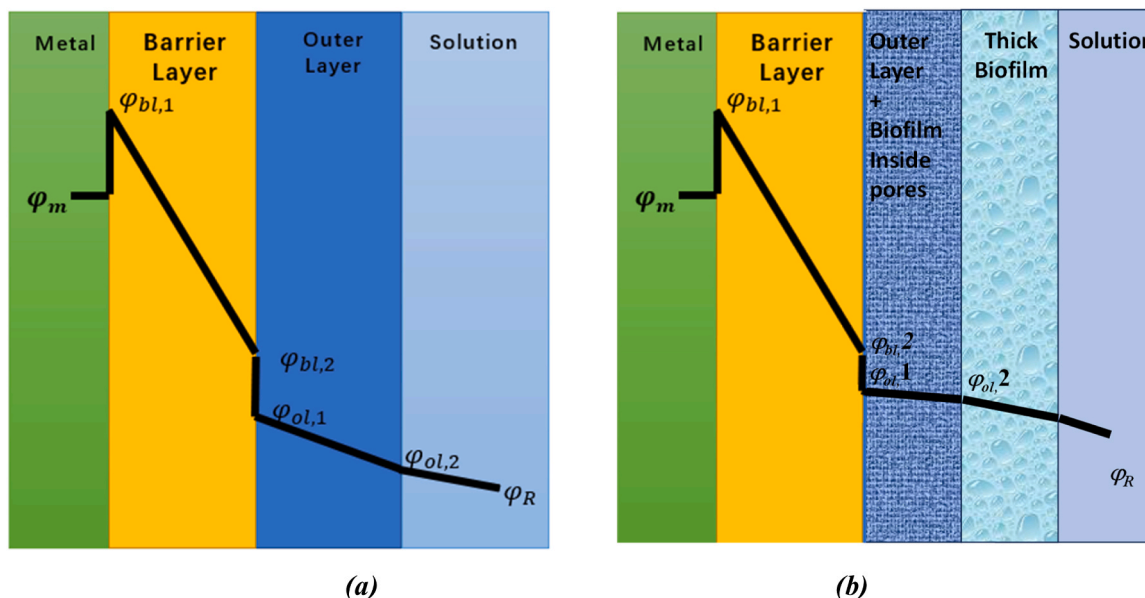


Fig. 9. Potential distribution across the barrier layer as envisioned by the PDM (a) in abiotic (a) and as it can be inferred for biotic conditions (b). Note that the electrostatic potentials at each interface are specified in the figure. The indicated potential drops are not to scale. (modified from ref. [65]).

$$V = \varphi_{bl}^m + \varepsilon_{bl}L_{bl} + \frac{\varphi_{bl}}{s} \pm \Delta\varphi_{ol} + \varphi_{Ref} \quad (12)$$

where  $\varphi_{bl}^m$  is the potential drop across the metal/barrier layer interface,  $\varepsilon_{bl}L_{bl}$  is the voltage drop across the barrier layer of thickness  $L_{bl}$ ;  $\frac{\varphi_{bl}}{s}$  is the voltage drop across the barrier layer/solution interface  $\varepsilon_{ol}L_{ol}$  across the barrier layer of thickness  $L_{ol}$ , and  $\varepsilon_{ol}$  are the corresponding quantities for the outer layer, ( $= \varphi_{bl,2} - \varphi_{ol,1}$ ), and  $\varphi_{Ref} = \varphi_{ol,2} - \varphi_R$  is a constant associated with the reference electrode. Now, from the PDM we may write Eq. 13:

$$\frac{\varphi_{bl}}{s} = \alpha V + \beta pH + \varphi_{bl}^0 \quad (13)$$

where  $\alpha$  is the polarizability of the bl/ol interface,  $\beta$  is the dependence of the potential drop across the bl/ol interface on pH, and  $\varphi_{bl}^0$  is a constant.

Combining Eqs. 12 and 13 yields the following expression:

$$\varphi_{bl}^m = (1 - \alpha)V - \varepsilon_{bl}L_{bl} - \beta pH - \frac{\varphi_{bl}^0}{s} - \Delta\varphi_{ol} - \Delta\varphi_{ref} \quad (14)$$

Eqs. 13 and 14 detail the potential drops at the barrier layer/solution and the metal/barrier layer interfaces, respectively. These potential drops drive the defect generation and annihilation reactions at the barrier layer interface. The schematic in Fig. 9b highlights that, in the case of biotic conditions, the potential drops of the outer layer from the barrier layer interface to the solution can be influenced by an active metabolism. To a first approximation, the biofilm could be included in the outer layer. This approximation is justified by noting that the biofilm and the outer layer interpenetrate and may be described as a single phase. The potential distribution profile can vary depending on the catalytic activity and conductivity of the biofilm.

The point defects of interest in the formation of the barrier layer are the cation vacancy ( $V_M^{\bullet}$ ) on the metal sublattice, the oxygen vacancy ( $V_O^{\bullet\bullet}$ ) on the oxygen sublattice, and the cation interstitial ( $M_i^{\bullet+}$ ) within the barrier layer. Other (non-point defect) species include the metal cation on metal sublattice ( $M_M$ ), the oxide ion on the oxygen sublattice ( $O_O$ ), the metal cation in the solution ( $M^{\delta+}$ ), the barrier layer oxide ( $MO_{\frac{\delta}{2}}$ ) and the components of the outer layer. These components vary with the system but are generally metal hydroxides, oxyhydroxides, oxides, and other precipitates like carbonates, sulfates, and sulfides, as well as microorganisms/biofilms. The potential distributions across the electrical double layer at the metal/solution interface, and across the barrier layer/solution interface are not shown. These distributions can be affected by biofilms in still unpredictable way.

The PDM concludes that the barrier layer grows into the metal, consistent with marker experiments [63–65,67], and that growth occurs through reactions describing the generation and annihilation of the point defects, as shown in Fig. 9. This model explains the formation of the point defective barrier layer on stainless steels, along with the formation of the outer layer. Both metal interstitials ( $M_i^{\bullet+}$ ) and the oxygen vacancy ( $V_O$ ) are electron donors, thus doping the barrier layer  $n$ -type. On the other hand, the cation vacancy ( $V_M^{\bullet}$ ) is an electron acceptor that dopes the  $p$ -type. Most studies show that the barrier layer on stainless steels is  $n$ -type in electron characteristics, demonstrating that the dominant point defects in the barrier layer are  $V_O$  and/or  $M_i^{\bullet+}$ , at least over the potential range of interest, depending upon the pH and  $V$ (vs. SHE). Some research indicates  $p$ -type behaviour at potentials outside of this range.

As shown in Fig. 9, seven fundamental point defect reactions are proposed to describe the growth and dissolution kinetics of the passive film. The rate constants for these reactions have been derived using the method of partial charges and are expressed in the form:

$$k_i = k_i^0 e^{a_i V} e^{b_i L_{ss}} e^{c_i pH} \quad (15)$$

where the coefficients are summarized in Table 1. The parameter  $k_i^0$  is the standard rate constant of the  $i_{th}$  reaction, and the expressions for  $k_i^0$  in terms of the base rate constant ( $k_i^{(0)}$ ) can be seen in [64].

At the steady-state, the rate of Reaction (3) equals the sum of the rates of Reaction (6) and Reaction (7), with allowances for differences in the stoichiometric coefficients for metals other than iron. These equalities lead directly to Eq. (2), predicting that the thickness of the barrier layer is a linear function of the applied voltage and the prevailing pH. On the other hand, from the equalities of the Rates of Reactions (3) and (6), we may write  $k_3 = k_6 C_O$  from which we can obtain the concentration of oxygen vacancies at the barrier layer/outer layer interface as:

$$C_O = \frac{k_3}{k_6} \quad (16)$$

Based on the PDM, the steady state barrier layer thickness ( $L_{ss}$ ) and the current density ( $j_{ss}$ ) can be expressed as Eq. (17) [64]:

$$L_{ss} = \left( \frac{1 - \alpha}{\varepsilon} \right) V + \left( \frac{c_7 - c_3}{b_3} \right) pH + \frac{1}{b_3} \ln \left[ \frac{k_7^0}{k_3^0} \left( \frac{C_H}{C_{H^+}^0} \right)^n \right] \quad (17)$$

and

$$j_{ss} = F \left[ \chi k_1 C_v^L + \chi k_2 + \chi k_3 + (\delta - \chi) k_4 + (\delta - \chi) k_5 C_i^0 + (\delta - \chi) k_7 \left( \frac{C_H}{C_{H^+}^0} \right)^n \right] \quad (18)$$

respectively, where  $C_v^L$  is the concentration of cation vacancies at the metal/barrier layer interface and  $C_i^0$  is the concentration of cation interstitials at the barrier layer/outer layer interface,  $C_H$  is the concentration of hydrogen ion at the barrier layer/outer layer interface and  $C_{H^+}^0$  is the standard concentration of hydrogen ion ( $1 \text{ mol L}^{-1}$ ),  $n$  is the kinetic order of the dissolution reaction of the barrier layer with respect to the hydrogen ion,  $\alpha$  is the polarizability of the barrier layer/outer layer interface,  $\varepsilon$  is the electric field strength within the barrier layer, and  $\delta$  and  $\chi$  are the oxidation state of cation in outer layer and barrier layer, respectively. Analytical analysis shows for Reactions (1) to (3) of Fig. 9 and that provided  $\chi = \delta$ , then  $a_i V + b_i L_{ss} = \text{constant}$ . Application of this condition results in an equation collapsing to Eq. 18. From this equation,

**Table 1**

Coefficients for the rate constants ( $k_i = k_i^0 e^{a_i V} e^{b_i L_{ss}} e^{c_i pH}$ ) of the reactions that generate and annihilate point defects at the metal/barrier layer interface and at the barrier layer/outer layer interface.

Reaction	$a_i$ ( $V^{-1}$ )	$b_i$ ( $cm^{-1}$ )	$i$	Units ( $k_i^0$ )
(1) $m + V_M^{\bullet} \xrightarrow{k_1} M_M + v_m + \chi e'$	$\alpha_1(1 - \alpha)\chi\gamma$	$-\alpha_1\chi K$	$-\alpha_1\beta\chi\gamma$	$cms^{-1}$
(2) $m \xrightarrow{k_2} M_i^{\bullet+} + v_m + \chi e'$	$\alpha_2(1 - \alpha)\chi\gamma$	$-\alpha_2\chi K$	$-\alpha_2\beta\chi\gamma$	$molcm^{-2} s^{-1}$
(3) $m \xrightarrow{k_3} M_M + \frac{\chi}{2} V_O^{\bullet\bullet} + \chi e'$	$\alpha_3(1 - \alpha)\chi\gamma$	$-\alpha_3\chi K$	$-\alpha_3\beta\chi\gamma$	$molcm^{-2} s^{-1}$
(4) $M_M \xrightarrow{k_4} M^{\delta+} + V_M^{\bullet} + (\delta - \chi)e'$	$\alpha_4\alpha\delta\gamma$		$\alpha_4\beta\delta\gamma$	$molcm^{-2} s^{-1}$
(5) $M_i^{\bullet+} \xrightarrow{k_5} M^{\delta+} + (\delta - \chi)e'$	$\alpha_5\alpha\delta\gamma$		$\alpha_5\beta\delta\gamma$	$cms^{-1}$
(6) $V_O^{\bullet\bullet} + H_2O \xrightarrow{k_6} O_O + 2H^+$	$2\alpha_6\alpha\gamma$		$2\alpha_6\beta\delta\gamma$	$cms^{-1}$
(7) $MO_{\frac{\delta}{2}} + \chi H^+ \xrightarrow{k_7} M^{\delta+} + \frac{\chi}{2} H_2O + (\delta - \chi)e'$	$\alpha_7\alpha(\delta - \chi)\gamma$		$\alpha_7(\delta - \chi)\beta\gamma$	$molcm^{-2} s^{-1}$

we conclude that the passive state is very tenuous and exists only when the rate of barrier layer formation exceeds the rate of dissolution at the interface with the outer layer. Violation of this condition leads to depassivation and often catastrophic corrosion. This underlines the crucial role of microorganisms that can inhabit the microporosities of the outer layer, directly interacting with the barrier layer.

2.2.2. Electron transfer across the passive layers

The electric charge transfer accompanying the reactions described by the PDM is analyzed in detail here.

For very thin barrier layers (< 3 nm thick), such as those on stainless steel, electron transfer across the barrier layer occurs via tunnelling (direct QMT) [69]. Since tunnelling is an isoenergetic process, an empty acceptor state in the quantized electronic energy levels of the cathodic reaction at the barrier layer/outer layer interface must be available at the same energy level as a donor state in the metal for the cathodic reaction to occur. For thicker barrier layers, electronic charge transfer is believed to occur via tunnelling between oxygen vacancies that act as quantized ('particle in a box') quantum wells. However, due to the strong electric field strength ( $\approx 3 \times 10^6$  V cm<sup>-1</sup>), it is doubtful that the required overlap between filled and empty states in neighbouring oxygen vacancies exists. It is envisioned that an electron will tunnel from a filled quantized state in the donor oxygen vacancy to an empty 'virtual' state in the acceptor oxygen vacancy, which is at much higher energy than the quantized states. The carrier in the virtual state loses energy through interaction with the oxide phonons, ultimately occupying a quantized state in the acceptor oxygen vacancy. This vacancy then acts as the donor state for the transfer of the carrier to another oxygen vacancy or 'virtual' acceptor state. The overall result being indirect QMT via the hopping of electronic charge carriers from oxygen vacancy to oxygen vacancy and the transfer of the carriers across the barrier layer from the metal to the cathodic reaction. The charge transfer rates due to direct and indirect QMT can vary over widely depending upon the thickness and height of the energy barrier.

The existence of free electrons (in the conduction band) and holes (in the valence band) generally requires an additional Randles circuit ( $R_{eh}/C_{eh}$ ) in the equivalent circuit summarized in Fig. 10 for their movement within the barrier layer. Note that the capacitance is included to account for reactance originating from the point defect reactions that are responsible for their generation and annihilation, as described by Bojinov [70–72] and later by Sharifi et al. [61]. In turn, and following this model, the impedance  $Z_e$  is calculated by using the Young relation, Eq. 19 [73]:

$$Z_e = \int_0^L \frac{dx}{\sigma_e(x) + j\omega\epsilon_0\epsilon} \tag{19}$$

where  $\sigma_e(x)$  is the electronic conductivity profile in the barrier layer,  $\omega$  is angular frequency,  $\epsilon$  is the dielectric constant of the film, and  $\epsilon_0$  is the dielectric permittivity of the vacuum and  $j$  the complex number ( $j^2 = -1$ ). The electronic conductivity of the barrier layer is proportional to the concentration of electronic charge carriers,  $C_T$ , i.e., Eq. 20:

$$C_T = \chi C_i + 2C_O + \chi C_V \tag{20}$$

The quantities  $C_i$ ,  $C_O$ , and  $C_V$  are the concentrations of metal interstitials, oxygen vacancies, and cation vacancies, respectively, within the barrier layer [74].

Thin films of the barrier layer can achieve the high capacitance performance of supercapacitors, ranging from 50 to 1100 F g<sup>-1</sup>, due to charge separation across a small distance in the electrical double layer created with the adjacent electrolyte. It's important to note that large number of pores within a high surface area of oxide layer contributes to enhanced capacitance properties. Inside the pores, indeed, energy storage involves rapid movement of the ions interacting with the oxide [74].

3. Electrochemical assessment of biofilms

Traditional EC techniques investigate the kinetics of anodic and cathodic processes on conductive surfaces at the macro-scale. These techniques involve applying an external input (current or potential) via a generator (galvanostat or potentiostat) and measuring the system's response. Continuous measurements of one or more electrochemical parameters, such as current density, potential differences, impedance, resistance, and capacitance, are conducted and subsequently analyzed. Advanced technologies can investigate conductive surfaces at a more microscopic scale than conventional methods, providing more detailed information on MIC mechanisms.

A notable example illustrating the need to move measurements to a microscopic scale is the work of Mollica et al. presented, for the first time, at Eurocorr 1996 [75]. They demonstrated that the potential ennoblement observed after a few days of immersion in natural seawater was correlated to the presence of active biofilm that covered only 2 % of the surface. Thus, it became evident that the global parameter (potential) was influenced by the local distribution of catalytic sites. Among the local techniques used for corrosion research, the Scanning Vibrating Electrode Technique (SVET), the Scanning Kelvin Probe (SKP), and

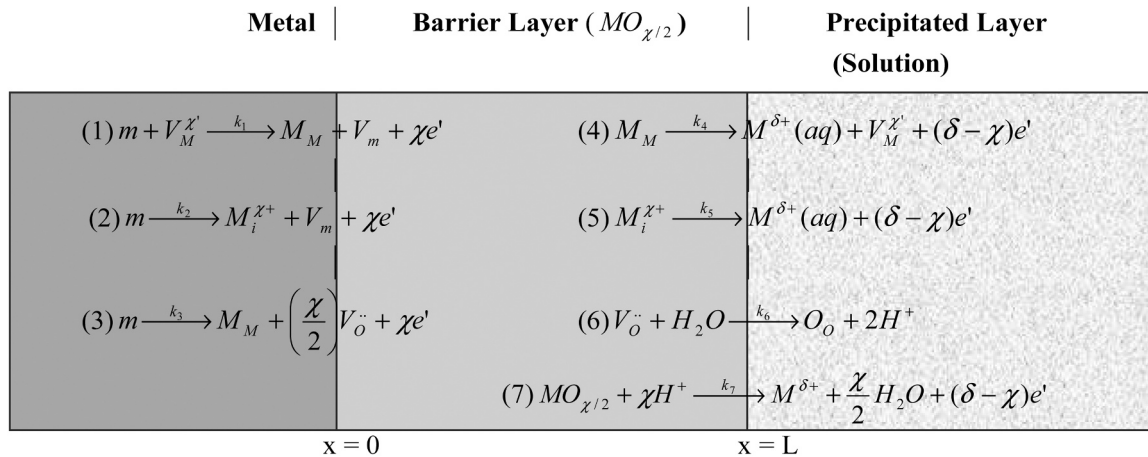


Fig. 10. Postulated defect generation and annihilation reactions at the metal/barrier layer and barrier layer/solution interfaces of the barrier oxide layer of a passive film on a metal.  $V_M^{\chi'}$  = cation vacancy,  $V_o^{\bullet}$  = oxygen (anion) vacancy,  $M_i^{\chi+}$  = cation interstitial,  $M^{\delta+}(aq)$  = cation in outer layer/solution interface,  $V_m$  = vacancy in the metal substrate,  $O_o$  = oxide ion in anion site on the oxygen sublattice,  $M_M$  = cation in cation site on the metal sublattice,  $MO_{\chi/2}$  = stoichiometric barrier layer oxide [65].

those that combine electrochemical microscopy with a system for scanning the metallic surface in two- or three dimensions. Scanning Electrochemical Microscopy (SECM) and localized electrochemical impedance spectroscopy (LEIS) are excellent examples of advanced techniques used to study corrosion at a microscopic scales.

### 3.1. Open circuit potential measurement

The Open Circuit Potential (OCP) is crucial for investigating corrosion processes, particularly MIC, as it avoids potentially destructive electric stimulations. Its value is determined by the dominant electrochemical processes generating charge exchanges at the interface metal-solution of the studied system. OCP is a mixed potential, measured by a high-impedance voltmeter as the voltage between the analyzed element and a stable reference electrode placed in the electrochemical system [31]. When corrosion is the dominant process driving current exchange, OCP also defines the corrosion potential ( $E_{\text{corr}}$ ) [76]. If the metal is non-corrodible, or a high overpotential impedes the corrosion process, OCP is dominated by the redox equilibria of elements dissolved at the metal-solution interface, under the biofilm. Therefore, several variables of the electrochemical system can affect OCP measurements. The magnitude and sign of OCP depend on the nature of the metal, the electrolytic medium (chemical composition, oxygen, pH), hydrodynamics and temperature [25]. It is also influenced by the microbial activity, which relies on the aerobic or anaerobic conditions of the media [77]. Positive or negative shifts may be observed and can be explained by interfacial changes [75,78,79]. The OCP ennoblement due to biofilm growth has been the main phenomenon observed for active-passive alloys when they are exposed to natural seawater [80–84]. If alloys suffer from pitting phenomena, the risk of pitting occurrence increases. A sudden negative shift in OCP after ennoblement indicates the initiation of accelerated corrosion attack due to bacteria. For stainless steels, OCP ennoblement has mainly been attributed to the catalysis of the oxygen reduction [23,24,83,85]. To explain the potential ennoblement due to biofilm activity, there must also be consideration of either enzyme involvement [86], the deposition of oxide layers such as manganese oxide [87], or the production of metabolic byproducts such as  $\text{H}_2\text{O}_2$  [88]. When the OCP is measured on uncolonized, totally inert electrode, such as platinum, it expresses the solution redox potential ( $E_{\text{redox}}$ ). Based on Nernst equation,  $E_{\text{redox}}$  can be used to characterize the aggressiveness of the solution. It usually indicates the aerobic conditions favourable for corrosion [1] or the aggressiveness of microbial metabolism occurring within the biofilm [1]. When the oxygen reduction (Eq. 21) is the main cathodic reaction [1], a Pt electrode can be used to estimate changes in the local oxygen concentration [76] based on the Nernst equation for this reaction (Eq. 22). The rates of oxidation and reduction at the platinum surface are assumed to be equal, and  $E_{\text{redox}}$  is a function of the oxygen concentration, temperature, and pH of the solution [25].



$$E = E^\circ + \frac{RT}{4F} \ln \frac{p_{\text{O}_2}}{a_{\text{OH}^-}^4} \quad (22)$$

where  $p_{\text{O}_2}$  is the partial oxygen pressure and  $a_{\text{OH}^-}$  the activity of  $\text{OH}^-$  species.

If the oxygen concentration increases or the pH decreases, the potential of Pt shifts in the positive direction. It must be emphasized that equilibrium conditions are required to achieve a stable  $E_{\text{redox}}$ , which is difficult to reach in biofilms with living systems. Living microorganisms dynamically consume and produce redox substances in response to external conditions and nutrient availability [25]. These phenomena are also responsible of the signal shift in online chlorine sensors based on redox potential, which are often used to monitor continuous low level chlorination treatments (less than  $1 \text{ mg L}^{-1}$  residual  $\text{Cl}_2$ ) in industrial waters for the biofouling control [89].

In corrosion monitoring, changes of  $E_{\text{corr}}$  and  $E_{\text{redox}}$  need to be associated with corrosion rate measurements. For instance, the single measurement of OCP, or its trend, can have contradictory interpretations for stainless steel. A low OCP can indicate a passive state in anaerobic condition and, conversely, severe localized corrosion in aerobic conditions. Therefore, OCP measurements should be used alongside other electrochemical techniques that provide an adequate reflection of the corrosion kinetics, to quantify and depict the corrosion process. Nevertheless, measuring  $E_{\text{redox}}$  together with  $E_{\text{corr}}$  and pH could be sufficient in some cases to assess whether the oxidizing conditions of the surrounding electrolyte medium can initiate MIC [76,90,91].

The non-destructive technique of Electrochemical Noise (EN) can also be mentioned, although its relevance has been limited over the past thirty years. This technique does not apply any electric stimulation to the sample under investigation, avoiding perturbations to operating systems [31]. In this approach, potential fluctuations are measured with a high-impedance voltmeter between two coupled nominally identical electrodes, and current fluctuations are measured through a zero-resistance ammeter (ZRA). The electrochemical noise resistance ( $R_n$ ), defined as the ratio of standard deviation of the measured potential and current noise, is inversely proportional to a uniform corrosion process [92], that can be correlated with a localization index for the localized corrosion [93]. The increase in current along with drop in potential has, in some cases related to localized corrosion due to the microbial activity [92–96]. In principle, it is suitable for studying MIC. However, analyzing the EN data can be challenging and requires advanced mathematical software to characterize the significance of the noise signal. Unstable electrical connections and variation in electrolyte composition during the measurement can also hinder achieving reliable results.

### 3.2. Local electrochemical scanning techniques

The OCP and EN parameters correspond to the global response of the entire test surface. To localise the anodic and cathodic zones present on the surface during corrosion, local electrochemical techniques have been developed [97,98]. These techniques allow a more in-depth understanding of the phenomena of localised corrosion, where the reactive surface is small compared to the non-active areas. Advanced software now enables a more sophisticated statistical analysis of the large electrochemically data sets. However, interpreting responses from these new tools can again be challenging if numerous perturbations and physical entities produce similar responses to MIC from an inhomogeneous macroscopic area of the sample. Modern software enables more advanced statistical analysis of the large of data sets produced through electrochemical processes.

#### 3.2.1. Scanning vibrating electrode technique

The scanning vibrating electrode technique (SVET) is a non-destructive method that provides a sensitive means of locating anodic and cathodic zones using a vibrating microelectrode. The technique does not alter the corrosion process or change the local environment of the sites and electrochemical counterparts. Variations in current densities on a microscopic scale on a corrosive metal are obtained by measuring the potential gradients developed in the solution due to ionic flows [99–105]. During SVET measurement, the Pt microprobe vibrates at a frequency of 80 Hz an amplitude of around  $30 \mu\text{m}$ , perpendicularly to the surface being scanned. The difference in potentials of the probe tip at the vibrating peak and valley,  $\Delta E$ , is transformed into a current using Ohm's law. The potential is directly related to the electrochemical activity of the monitored material in the test environment. Scanning the surface produces a map showing the spatial distribution of anodic and cathodic sites, allowing the study of oxidation–reduction reactions in the micro-range. Moreover, the vibration above the surface creates an alternating potential signal, which is then filtered to increase the signal to noise ratio. This allows the monitoring of very small current

variations over a metal surface even at OCP. This non-destructive technique can locate any surface heterogeneities like inclusions, observe the initiation and the growth of pits and cracks in real time under straining conditions, and observe galvanic coupling and catalytic reaction. In MIC studies, SVET can provide qualitative and quantitative data about biofilms and their components [76,106–108]. The example given in Fig. 11 illustrates how SVET can be used to investigate oxygen reduction catalysis due to the presence of enzyme in an aerobic medium. Hemin, a heme protoporphyrin, was chosen to represent the catalytic centre of the enzymes involved in oxygen reduction. Hemin, dissolved in DMSO, was deposited on stainless steel by adsorption, creating a simple configuration that mimicked the presence of enzymes. The areas where hemin was deposited exhibited a cathodic current (blue colour), indicating a catalytic effect, while the adjacent areas without hemin displayed a pronounced anodic behaviour (red colour). SVET thus enabled the identification of active catalytic centres and the evaluation of the enzyme contribution to the formation of galvanic cells, which can lead to localised corrosion [107].

Thus, SVET can be regarded as a useful tool for studying the interaction between biological media and metallic surfaces, offering a new approach for visualizing and understanding MIC. SVET can also be corroborated with optical microscopy to show the variation in surface morphology. For example, SVET combined with optical microscopy was used to investigate the MIC mechanism of 304 L stainless steel in treated urban wastewater [108]. Initially (1 h), a random distribution of cathodic and anodic low currents was detected, and few white spots, assigned to the pioneering attachment of microbes, were observed using optical microscopy (Fig. 12). As bacterial colonization progressed and a mixed biofilm formed, the potential distribution on the electrode surface lost its uniformity, and relatively large cathodic zones (blue colour) were observed [108]. The results confirmed that the electrode surface became heterogeneous when porous corrosion products combined with biofilm formed on the stainless steel surface.

### 3.2.2. Scanning Kelvin probe

The Scanning Kelvin Probe (SKP) is a local technique capable of measuring the contact potential difference between a working electrode and a vibrating reference electrode using a Kelvin probe. It provides high-resolution maps for the distribution of possible galvanic elements [109]. The main disadvantage of SKP and its combined techniques is that they cannot be employed in aqueous solutions, making online measurement of MIC impossible with this approach [110]. However, the measured potential ( $E_{kp}$ ) is linearly related to the corrosion potential of the metal, as  $E_{corr} = a + bE_{kp}$ .

The SKP technique is applicable for characterizing passive film developed on passive-active metals such as either stainless steel or titanium [111]. When the  $E_{kp}$  of the whole surface is uniform and positive,

it indicates stable passive behaviour and the absence of localized corrosion. It should be mentioned that  $E_{kp}$  is not the Volta potential distribution, but rather the difference between a specific probe tip and particular material surface [109]. Often, a two-dimensional map of Volta surface potential distribution is collected by SKP to reveal the metallic interface resistance to external change.

SKP technique has been also used in MIC studies, where the potential distribution has been reported to indicate the formation of biofilm and corrosion products. In this context, fluctuation of  $\Delta E_{kp}$  can determine the presence of localized corrosion on metal surfaces. An example is shown in Fig. 13, where the  $E_{kp}$  distribution on the surface of a X80 pipeline steel is plotted for different exposure times in the sterile artificial Beijing soil, with or without the presence of a nitrate reducing bacterium, *B. cereus* [110]. After one day,  $E_{kp}$  exhibited an almost a uniform distribution with small potential differences, indicating that the sample was covered by a uniform corrosion layer (Fig. 13a). However, in the presence of *B. cereus*,  $E_{kp}$  shifted in a positive direction, and surface potential distribution of X80 steel became scattered. This suggests an enhancement in the formation of biofilm and corrosion products, resulting the surface being divided into two distinct cathode and anode areas. This process became more noticeable with time. After 18 days of immersion, the potential fluctuation became disordered due to the deformation and biofilm detachment [110]. Additionally, the  $\Delta E_{kp}$  for the inoculated medium was much higher (about three times) than  $\Delta E_{kp}$  in sterile medium, indicating the surface potential heterogeneity and severe pitting [112].

SKP can be combined with other microscopy techniques, such as AFM, to visualize both topography and Volta potential variations on local surface areas [111]. SKPFM has also become a powerful method for determining local potential differences in many alloy systems, especially aluminum and magnesium alloys. This technique achieves a lateral resolution of less than 1  $\mu\text{m}$ , allowing precise measurement of surface potential and to study the corrosion mechanisms on and around intermetallic precipitates [113]. In SKPFM, the signal is expected to strongly depend on the tip-sample distance, as the contribution of the cantilever becomes increasingly significant when the distance between sample and tip is increased. In addition, the measured potential differences on a sample usually do not represent the real potential differences between the tip and sample because it is difficult to prevent the cantilever contribution [109]. SKPFM is highly promising for studies into the heterogeneous electrochemistry at the biofilm/ metal interface due to its high resolution and non-destructive nature [111].

To date, SKPFM is seldom used in MIC investigations to its necessity of only being able to scan initial microbe attachment and thin biofilm layers. Since the heterogeneity and structure of biofilm cannot be controlled, these techniques should be combined with numerical simulations to obtain reliable results [114]. An example of SKPFM

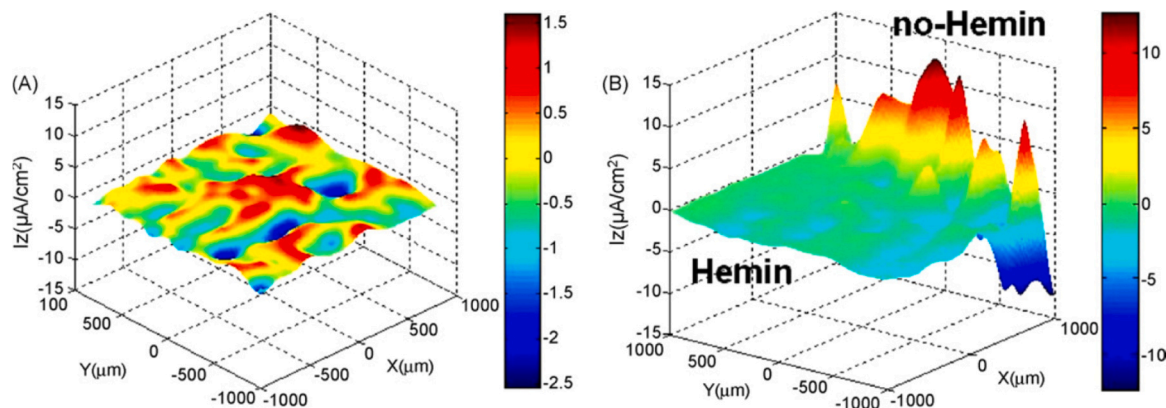
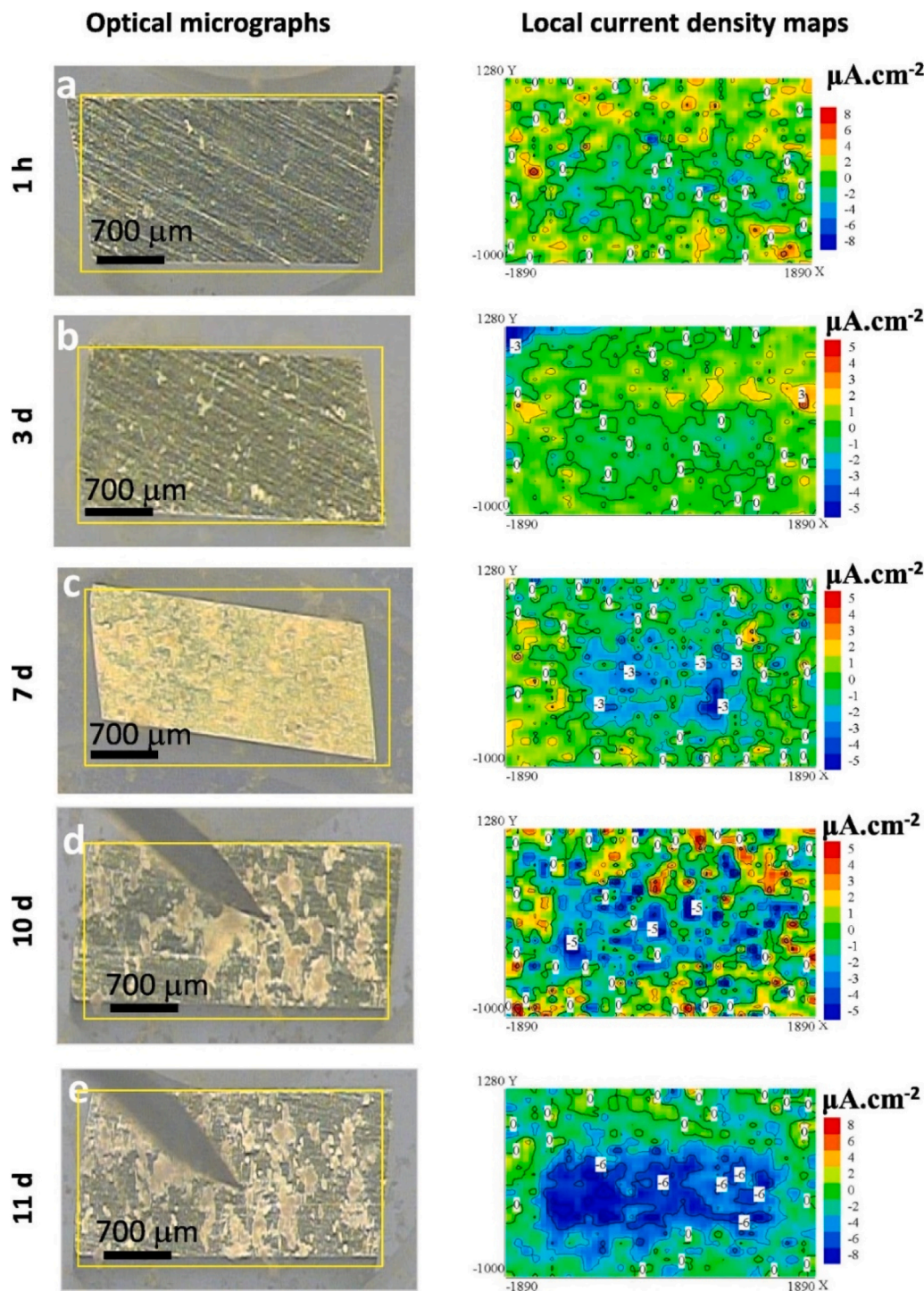


Fig. 11. Local current map (3D) obtained by SVET in 0.001 M NaCl at open circuit potential on stainless steel: (A) control without hemin; (B) interface hemin/no hemin (from ref. [107]).



**Fig. 12.** Optical micrographs and SVET current density maps of 304 L SS immersed in treated urban wastewater for: (a) 1 h, (b) 3 days, (c) 7 days, (d) 10 days and (e) 11 days (from ref. [108]).

application in MIC is the study of the effect of SRB on stress corrosion of 2205 duplex stainless steel (2205 DSS) [114]. In this work, 2205 DSS samples were immersed in a bacterial solution for different exposure times. The samples were then removed from solutions, and the biofilms were fixed using glutaraldehyde before being observed using SKPFM. The results showed a sharp increase of SRB cells and biofilms on the surface over time, along with a significant difference in Volta surface potential between the austenite and ferrite phase before incubation, indicating the presence of galvanic current. However, when the biofilm covered the surface, the differences became smaller. In addition, the

austenite phase under the biofilm became more positive, creating a micro-galvanic corrosion area between high-stress and low-stress regions. Indeed, SRB preferentially grew on the austenite phase, causing sulfidation and chromium depletion of the passive films [114].

Finally, it should be noted that SKP, as a dynamic scanning probe technique is combined with SECM as a static scanning probe technique for multifunctional measurements. Several studies [115,116] describe the application of SKP-SECM to study corrosion mechanisms by measuring the contact potential difference under various conditions without requiring a sample change or working electrode replacement,



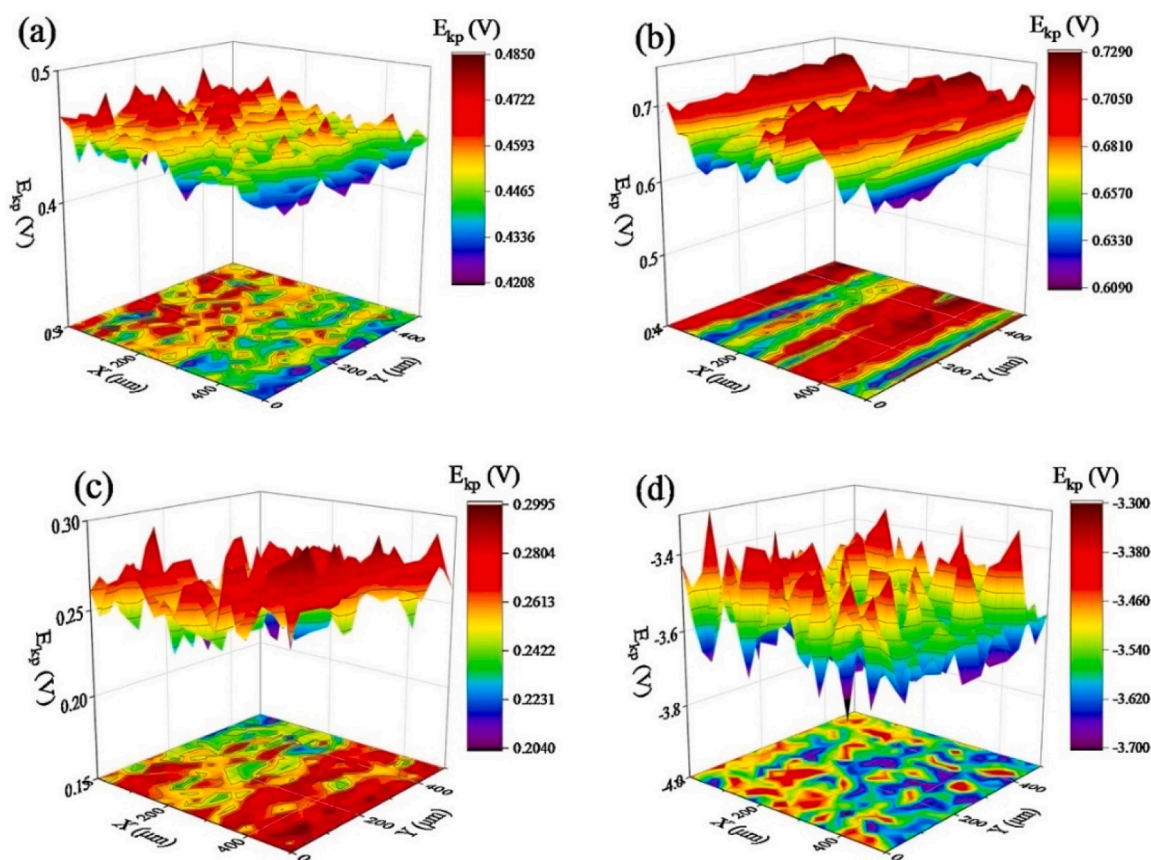


Fig. 13. SKP distribution of potential on X80 pipeline steel in artificial Beijing soil with (a-c) and without *B. cereus* (d) at 30 °C for different times: (a) 1 day; (b) 6 days; (c) 18 days; (d) 18 days (from ref. [110]).

due to the non-destructive nature of this technique [117]. However, there are no reports on the application of this technique in MIC, possibly due to its limitations. One requirement for the SKP-SECM approach is a fast measurement speed to visualize rapid events such as pitting initiation. The maximum scan speed can be adjusted to be up to several tenths of  $\text{mm s}^{-1}$  [118]. In addition, despite the reliability of SECM to obtaining spatially resolved *in situ* electrochemical information, SKP is not valid for assessing potential corrosion behaviour [118].

#### 4. Direct Current (DC) stimulation

While non-destructive techniques like OCP have limitations, DC current techniques described in this section provide valuable insights into MIC development. However, they can be highly destructive and require careful application to avoid interference with microbial activities. These methods, combined with biofilm monitoring, are primarily used to understanding and mitigate MIC in industrial environments.

Non-destructive techniques are useful for observing MIC phenomena. Monitoring the OCP or mapping surfaces at local scale are valuable tools for evaluating the impact of microorganisms and biofilms on the corrosion behaviour of metal. Nonetheless, in microbial systems, especially SRBs, which contain numerous chemicals, OCP trends are often misleading and not reflect the true corrosion tendency. Therefore, they are completely unusable in supporting weight loss data trends. This is not surprising, since OCP provides no corrosion kinetics insight. Consideration must also be given to the fact that an oxidation reaction on a working electrode can exhibit a rather negative OCP, while its related corrosion kinetics may be negligible, while a different reaction with a less negative OCP is kinetically favoured. Furthermore, when the working electrode is covered with a biofilm, the biofilm can donate electrons harvested from organic carbon oxidation to the working

electrode, as in microbial fuel cells (MFCs). Therefore, OCP may become the output of an MFC process rather than a reflection of the sole working electrode's susceptibility to oxidation. Recently, MFC output variations due to corrosion phenomena were investigated in lab experimentations, such as [119], providing indirect insights on the progression of corrosion phenomena. Previously, the catalytic effect of biofilm in oxidizing organics was also detected using other electrochemical techniques, such as the Zero Resistance Ammetry, which was proposed by Little and Lee [120] for MIC studies. This biocatalytic effect prevents this technique from establishing a direct correlation between the measured current and the corrosion rate.

In contrast, numerous MIC studies have shown that active scans utilizing external and controlled current signals are reliable when properly performed in support of weight loss data trends, which reflect the much mass of the working electrode in favour of the biofilm. Nevertheless, it should be noted that  $j_{\text{corr}}$  (corrosion current density) from polarization performed at the end of MIC incubation cannot accurately reflect weight loss because the latter is cumulative and depends on a corrosion rate that can vary significantly during the test period. It is generally acknowledged that electric stimulation by direct current, using stationary (chronoamperometry) or transitory (potentiodynamic) EC techniques, can provide insights into the impact of microorganisms/biofilm on the corrosion behaviour and the mechanisms of metallic interfaces. This will be critically discussed in the following sections.

##### 4.1. Chronoamperometry

Chronoamperometry (CA) is an electrochemical technique that involves imposing a constant potential (anodic or cathodic) and measuring the variation of current as a function of time [121]. It is an effective

method for obtaining data about the long-term steady-state reaction rate. This approach can be used for electrodeposition, evaluating the formation and repair of passive film on metal surfaces [122]. In MIC studies, both the kinetics and mechanisms of electron transfer can be investigated using this technique. One example involves marine biofilms, which catalyses the oxygen reduction on stainless steel [23,24,75, 82]. When polarized at a fixed cathodic potential in natural seawater (around  $-0.2$  V vs. SCE in this case), the electrodes exhibit the current-time response shown in Fig. 14. Initially, when the electrodes were first immersed, the current is low (less than  $1 \text{ mA m}^{-2}$ ). After a period of a few days, depending on the water temperature and the season, the current was seen to increase rapidly as microbial colonisation proceeds, via microbiological attachment and growth processes. Once the biofilm is formed, the current reaches a plateau, with an intensity can be more than 100 times greater when compared to electrodes without a biofilm [221].

#### 4.2. Biofilm monitoring probes

After biofilm ennoblement was first reported for non-corrodible alloys, light polarized electrochemical probes were developed to monitor in the early stages of biofilm growth in real time and online, in various environments (water and soil) [123–125]. The BIOX probe [123] is one of the first types of these electrochemical probes. It detects and measures biofilm growth on an inert cathode (either stainless steel or titanium) that is slightly polarized by coupling with a sacrificial zinc anode through an electric resistance (Fig. 15 insert). The current response of the probe (measured as a resistance voltage) is due to cathode ennoblement, as the zinc corrodes, behaving like an almost unpolarizable electrode. It should be stressed that the presence of oxidants in the aqueous medium, due to biocide treatments such as chlorination, also increases the potential of the cathode electrode. However, the signal increase due to chemical dosage is immediate, whereas for biofilm growth it is slow (see Fig. 15). By analyzing the electrochemical signal trends, it becomes feasible to optimize biocide treatments. Several biofilm electrochemical probes, *i.e.*, BiGeorge [126], ALVIM [127], and others integrated with LPR are available on the market [128]. These industrial devices exemplify how electrochemistry aids operators in monitoring and mitigating microbial corrosion risks across a number of industrial sectors [124,125,129]. Another notable example is the direct electron transfer (DET) between sulfate-reducing bacteria (SRB) and carbon steel in anaerobic conditions [130]. When polarized at  $-0.740$  V vs. SCE, a cathodic current was reported exclusively in the presence of an SRB medium during biofilm formation. This DET explains the observed ennoblement of the corrosion potential.

Moreover, the role of bacterial enzymes can be highlighted using the CA technique. For instance, hydrogenase from *Clostridium acetobutylicum* has been reported to accelerate the corrosion process on mild steel [131]. CA performed at a cathodic potential demonstrated that

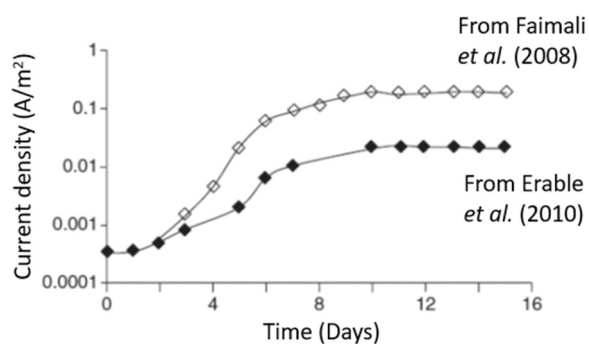


Fig. 14. Cathodic current collected on stainless steel electrode polarized at  $-0.2$  V vs Ag/AgCl in seawater in the CNR/IAS (ex ISMAR) marine station at Genova harbour (from ref.[221]).

hydrogenase catalyses the electrochemical reduction of protons or water into hydrogen gas (HER) through direct electron transfer (Fig. 16a), indicating its involvement in the OCP ennoblement (Fig. 16b).

Finally, it should be mentioned that CA is widely used in bio-electrochemical systems, such as microbial fuel cells and bio-electrosynthesis cells, to highlight and enhance electron transfer phenomena between conductive (non-corrodible) materials and electroactive microbial species [132–138]. Fig. 17 illustrates the behaviour of a stainless steel electrode when anodically polarized in a deaerated medium containing bacterium *Geobacter sulfurreducens*. Three distinct phases are observed: 1) a latency period with low currents, 2) current increase due to the growth of the electroactive biofilm that catalyses the oxidation of acetate, and 3) a current decrease due to acetate (soluble substrate) consumption. When the test medium was refreshed, the current increased again. Similarly, when the electrode was cleaned (biofilm removed), the current dropped significantly, and it took a few days to observe the microbial catalysis phenomenon again. The maximum current density depends on the applied potential, microbial activity, and the ability of the substrate to be oxidized or reduced.

It is also worth noting that several microbial species can exchange electrons with a solid substrate in both anodic and cathodic directions, depending on the electrode potential and the composition of the test medium in which they develop [132,133,139]. An example is shown in Fig. 18, where *Shewanella loihica* PV-4 [139] demonstrates its ability to catalyze the lactate oxidation on carbon cloth electrode at  $0.000$  V vs. Ag/AgCl (outward Bielectrochemical Stimulation) and the reduction of nitrate at  $-0.500$  V vs. Ag/AgCl. This phenomenon of extracellular electron transfer (EET) is also relevant in biocorrosion studies, where environmental and surface conditions change over time.

#### 4.3. Linear polarization resistance

Linear polarisation resistance (LPR) is a well-established potential sweep technique operating within a narrow potential range around  $E_{\text{corr}}$ , typically  $\pm 20$  mV. It is used for continual monitoring of the instantaneous corrosion rate of a metal or alloy exposed to a corrosive environment ( $j_{\text{corr}}$ ). Based on the Stern and Geary theory [140], the relationship between  $E$  and  $j_{\text{corr}}$  is generally linear (Eq. 23) around  $E_{\text{corr}}$ , where anodic and cathodic reactions are both reversible, close to their equilibrium.

$$R_p = \frac{B}{j_{\text{corr}}} \quad (23)$$

The evaluation of  $j_{\text{corr}}$  from  $R_p$  (Eq. 24) requires prior data of the anodic and cathodic Tafel slopes ( $b_a$  and  $b_c$ ) [141], which are determined using polarization curves conducted far from  $E_{\text{corr}}$ , and utilised in Eq. 25.

$$j_{\text{corr}} = \frac{B}{R_p} \quad (24)$$

$$B = \frac{b_a b_c}{2.303(b_a + b_c)} \quad (25)$$

Eq. 24 estimates the linear polarization resistance  $R_p$  evaluated by Stern and Geary from Ohm's law. The method is validated for cases of uniform corrosion and at low pH, which are not common conditions. Furthermore, it should be noted that in presence of a coating, mass transport limitation, or kinetic with different steps, the currents do not follow Tafel kinetics making it impossible to determine a value of  $j_{\text{corr}}$ . In such cases, other theoretical relations between  $j_{\text{corr}}$  and  $R_p$  must be used to address scenarios where anodic and cathodic kinetics are not charge transfer controlled [142]. Consequently, it is not prudent to use fixed values of  $b_a$  and  $b_c$  to calculate the MIC corrosion rate since these values can vary significantly within the same microbial culture at different incubation times, as well as different MIC systems. These varying  $b_a$  and  $b_c$  values have been reported in Tafel parameter tables in numerous MIC

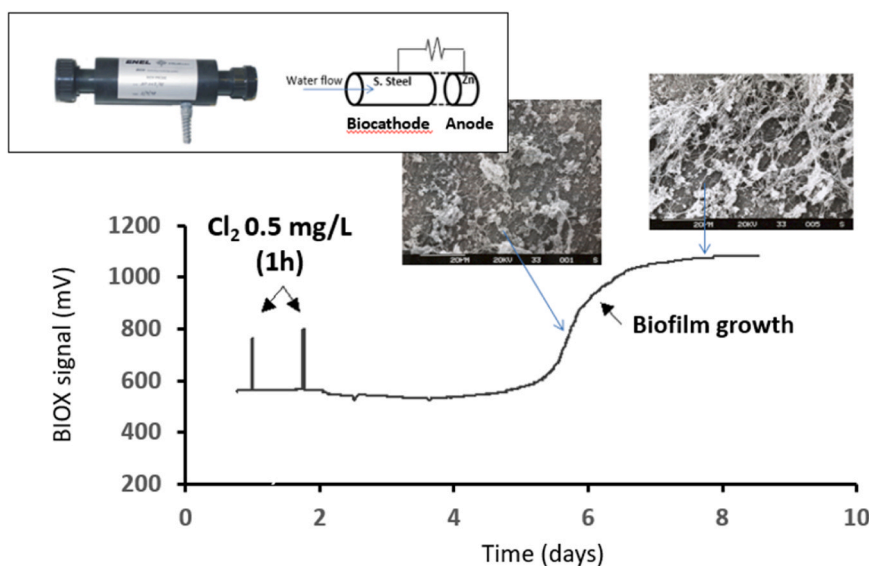


Fig. 15. The typical signal trend of a BIOX probe inserted in a marine cooling circuit. SEM micrographs show the biofilm development at different signal levels (blue rows). Image of a BIOX probe and schematic of the electrochemical cell is also reported (from ref. [144]).

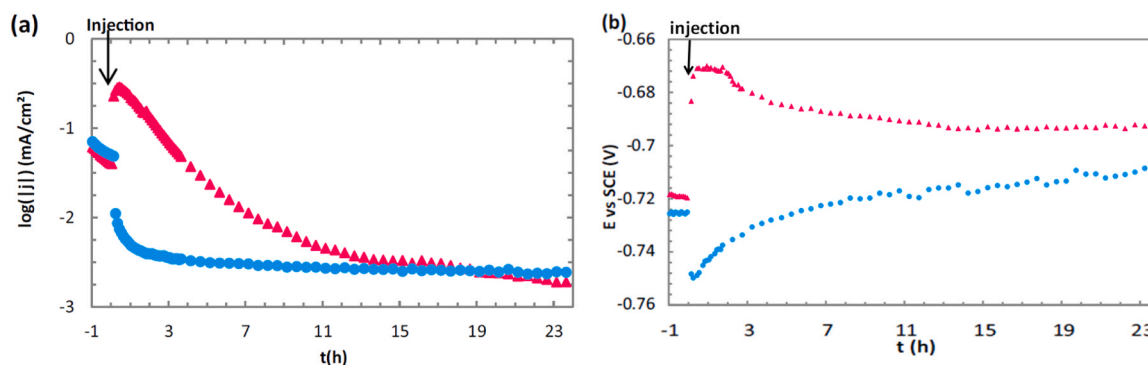


Fig. 16. Cathodic polarisation plotted at  $-100\text{ mV}$  vs OCP (a), and OCP versus time for S235JR mild steel electrodes in  $0.1\text{ M}$  Tris-HCl pH7 medium inside a dialysis bag (b). Injection at  $t = 0$  + of  $75\text{ }\mu\text{L}$  hydrogenase solution (pink triangles) and  $75\text{ }\mu\text{L}$  Control solution (blue circles). Modified from ref. [131].

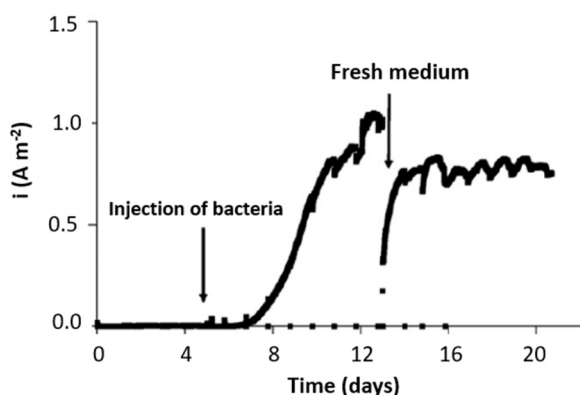


Fig. 17. Time evolution of the current density obtained on stainless steel polarized at  $+0.2\text{ V}$  vs Ag/AgCl in a deaerated growth medium with  $10\text{ mM}$  acetate. The inoculation of bacteria (*Geobacter sulfurreducens*) and the replacement of the medium are indicated by the arrows (from ref. [132]).

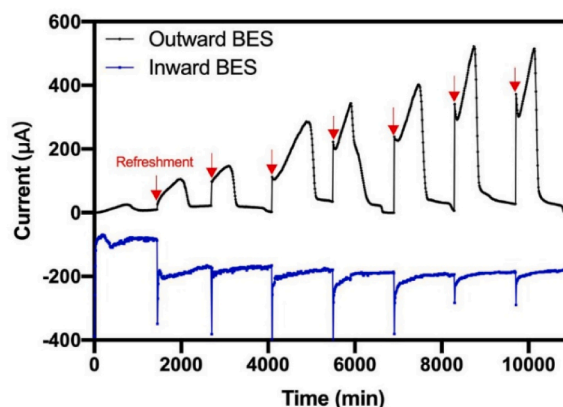


Fig. 18. Current evolution for bidirectional EET performance of *S. loihica* PV-4 on carbon cloth electrode. Applied potential is  $0\text{ V}$  vs Ag/AgCl in outward BES and  $-0.5\text{ V}$  vs Ag/AgCl in inward BES (fro ref. [139]).

publications, for instance in [143]. Fig. 19 shows that despite fluctuations in  $R_p$  data, they correctly reflect the weight loss trend for treatments using different biocide dosages, with and without biocide enhancement [143]. Consequently,  $R_p$  data have been proven valuable

when used qualitatively to support weight loss data trends, while also providing additional transient corrosion rate information that cumulative weight loss data do not offer. Moreover, despite the simplicity of this technique, significant calculation errors can occur in cases of the low

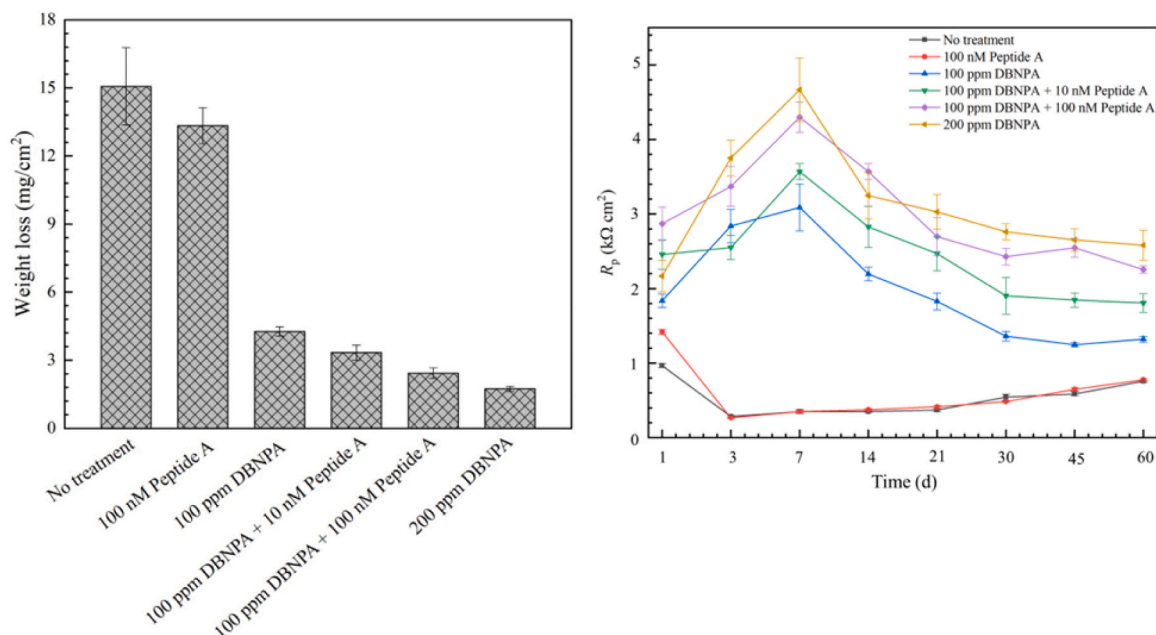


Fig. 19.  $R_p$  responses supporting weight loss trend in assessing enhanced biocide treatment of carbon steel MIC by an oilfield biofilm consortium (Modified from ref. [143]).

electrolyte conductivity or localized corrosion. Since the sum of  $R_p$  and the solution resistance ( $R_s$ ) between electrodes is measured, relevant noise can be introduced in the measurement when the electrolyte conductivity is lower than about  $0.5 \text{ mS cm}^{-1}$ , depending on the probe geometry [144]. Low conductivities can be found in oligotrophic freshwaters, tap waters, boiler waters, and similar environments. For highly conductive waters, the geometry of the monitored samples and their surface finish can play a crucial role in MIC monitoring, as biofilm growth is strongly influenced by hydrodynamics and surface roughness. In case of crevices, secondary electrochemical reactions which are controlled by diffusion of reaction species and passivation, are not accounted for [145]. Conversely, Gonzalez *et al.* [146] have stated that when the corrosion systems are under mass transfer control, even a small potential perturbation as low as 10 mV can cause changes in the measurement. In this case, LPR cannot provide adequate information, particularly regarding the initiation and growth of passivation or passivation breakdown [145]. For high capacitance systems, such as carbon steel in anaerobic environment, LPR tends to overestimate the corrosion rate [76]. This high capacitance is often associated with corrosion product deposits.

For active-passive metal alloys, since MIC is frequently accompanied with pitting and localized corrosion, the LPR technique cannot, in principle, provide accurate information about the actual weight loss. Nevertheless, LPR is widely used to monitor corrosion rate in field and industrial applications, where corrosion phenomena are usually localized and occur in near neutral pH environments. Indeed, commercial corrosionimeters are usually based on a variation of the LPR technique. They scan the potential in the range of the  $E_{ocp} \pm 5\text{--}10 \text{ mV}$ , close to the open circuit potential of the corrosion process. Operating in a non-destructive manner, the measurement provides an almost immediate response (in a few seconds), allowing for frequent repeat measurements over time. By monitoring the trend of collected data, it enables real-time extraction of information linked to the overall corrosion process and the effectiveness of anticorrosive treatments/mitigation strategies.

The practical application of LPR to monitor microbial corrosion of copper alloys in industrial environments, such as marine cooling circuits, has demonstrated the usefulness of this technique for localized corrosion as well [144]. Empirically estimated values of  $B$  (Tafel factor, see Eq. 25) for copper alloys usually falls within the range of 10 and

20 mV, with  $j_{corr}$  usually validated by gravimetric assessment [124,147]. Fig. 20 provides an example of integrated corrosion monitoring of 70/30 cupronickel samples, biofilm growth using a BIOX probe, and other parameters such as temperature and turbidity [147]. The corrosion trends, estimated in  $\mu\text{m y}^{-1}$  by LPR measurements and corroborated by BIOX signal, highlight how corrosion increases, especially in case of new (unpassivated) sample of the copper alloy, when the antifouling treatment (chlorination) is interrupted in a cooling circuit supplied with sediment-rich seawater (as highlighted by the increase in turbidity signal).

For MIC studies accessing the Tafel slopes is not feasible, LPR can be used to track the corrosion rate evolution via  $1/R_p$  without estimating  $j_{corr}$  during the immersion test. This approach can also determine the role of microbial activity (i.e., biofilm and enzymes) in corrosion performance. Fig. 21 illustrates how LPR is performed and how it can help assess the influence of hydrogenase in the corrosion of mild steel [131]. In this case, it is clearly shown that hydrogenase increased the corrosion rate and induced grain boundary degradation, which was not observed in the control medium.

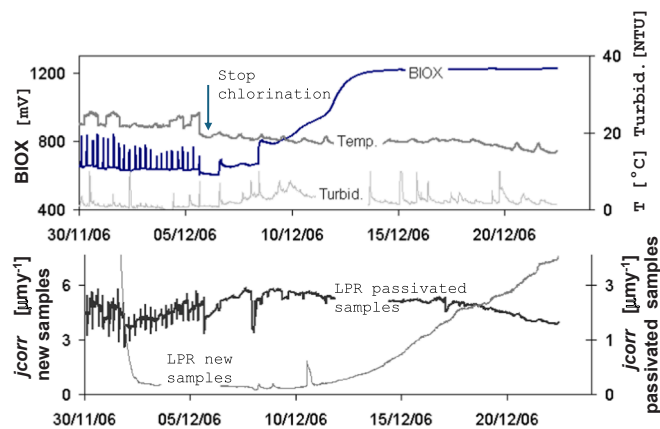
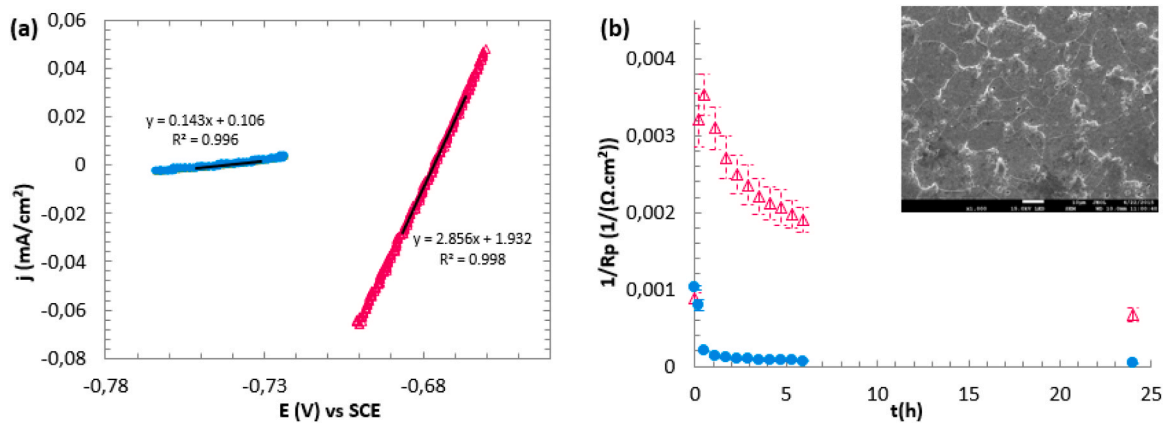


Fig. 20. Integrated monitoring of corrosion of CuNi 70/30 samples by LPR, biofilm (BIOX probe), temperature and turbidity (due to mud incoming) in a seawater cooling circuit of a power plant (from ref. [147]).



**Fig. 21.** Determination and evolution in time of the inverse of polarization resistance ( $1/R_p$ ) for S235JR mild steel electrodes in 0.1 M Tris-HCl pH7 medium inside a dialysis bag. Injection at  $t = 0$  + of solution with or without hydrogenase. (a) Examples of polarization curves to determine  $1/R_p$  (slope of the curve), obtained after 10 minutes of immersion with 75  $\mu\text{L}$  hydrogenase solution (pink curve) and with 75  $\mu\text{L}$  control solution (blue curve). (b)  $1/R_p$  versus time for experiments performed with 75  $\mu\text{L}$  hydrogenase solution (pink point) and with 75  $\mu\text{L}$  control solution (blue points). SEM images of the S235JR mild steel electrode surface after 24 hours of immersion with hydrogenase (modified from ref. [131]).

#### 4.4. Potentiodynamic polarization technique

The potentiodynamic polarization (PDP) technique is more intrusive than the LPR technique. It scans a wide range of potentials, typically  $\pm 0.5$  to  $\pm 1.0$  V vs. OCP, to extrapolate Tafel curves, the pitting potential  $E_{\text{pit}}$ , and the protection potential  $E_{\text{prot}}$ . The analysis is generally performed by considering the reactions at the steady state, can be approximated using a low potential scan rate. For corrosion tests, this means a scan rate of less than  $5 \text{ mV s}^{-1}$ , and usually  $1.666 \text{ mV s}^{-1}$  (equivalent to  $100 \text{ mV min}^{-1}$ ).

Polarization curves provide an overview of the reaction kinetics for a given corrosion system, including charge-transfer or mass-transfer controlled reactions, passivity, transpassivity, and localized corrosion phenomena [76]. Tafel curves offer mechanistic insights into the rates of anodic and cathodic reactions, which can behave differently, especially during when active-passive transition, thereby determining the limiting step of the corrosion reaction. Under these conditions, passivation properties can be evaluated based on the critical potential  $E_{\text{crit}}$ , critical ( $j_{\text{crit}}$ ), and passive ( $j_{\text{pass}}$ ) current densities for passivation. The PDP technique is widely used to study dynamic changes of anodic and cathodic processes caused by microorganisms or a biofilm [1,148]. However, high-field polarization can alter the electrochemical conditions at the metal-solution interfaces, affecting bacteria attachment and biofilm formation. Therefore, anodic and cathodic polarization should be performed separately, starting from the corrosion potential. Despite this, MIC researchers often use a continuous scan towards electropositive potentials on a single electrode instead of using two replicate electrodes to obtain separate cathodic and anodic curves. Indeed, an electropositive potential scan (Fig. 22 yellow curve A5) can result a lower  $j_{\text{corr}}$  (often 50 % or more), along with significant compression of the cathodic curve (in voltage range) and elongation of the anodic curve when compared to the half-scan curves obtained separately (Fig. 22 black curve standard WEs) [149]. This is because when a living biofilm is suddenly exposed to the lowest voltage (e.g., an overpotential of  $-200 \text{ mV}$ ), the biofilm has no time to adapt to the external DC voltage, unlike the case when the scan pattern starts at OCP (no external voltage). Moreover, when the dual-half scan scheme is adopted to scan a single electrode with a cathodic scan from OCP to  $-200 \text{ mV}$  overpotential and then an anodic scan from OCP to  $+200 \text{ mV}$  overpotential, the  $j_{\text{corr}}$  deviation is greatly reduced, resulting in more symmetric anodic and cathodic curves (Fig. 22 curves A1 and A2). Furthermore, with the mild dual-half scan scheme, the same electrode covered with a biofilm can often be repeatedly scanned without severe deterioration (Fig. 22 curves A3 and A4) [149].

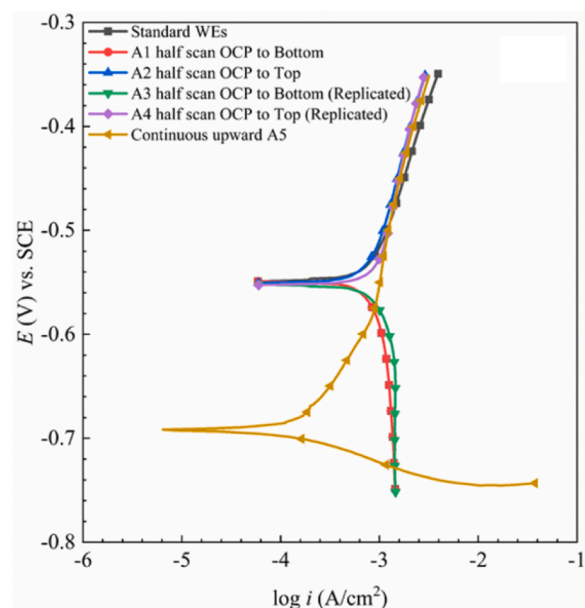


**Fig. 22.** Potentiodynamic polarization curves for C1018 carbon steel MIC by *Desulfovibrio ferrophilus* biofilm using continuous upward scan scheme (from  $-200 \text{ mV}$  vs. OCP to  $+200 \text{ mV}$  vs. OCP) and dual-half scan scheme with each half scan starting from OCP (from ref. [149]).

Regarding pitting corrosion performance,  $E_{\text{pit}}$  (pitting potential or breakdown potential,  $E_b$ ) can be determined when the anodic curve shows a sharp increase, even in the presence of bacteria.  $E_{\text{pit}}$  provides data on the tendency for pitting but not the pit propagation rate [76]. Therefore, it is useful to assess the repassivation curve by reversing the polarisation, allowing the current density to decrease to the passive current density at the repassivation potential ( $E_r$ ). Consequently, the  $E_r$  and the area under the repassivation curve give the extent of pit propagation. For example, it was reported that the *Geobacter species* influence the pitting behaviour of 304 L stainless steel differently depending on the test medium in which the biofilms develop (Fig. 22). In acetate-lacking media, pitting occurred with and without bacteria within the same potential range of, but the presence of bacteria markedly increased the pit size [150]. In fumarate-lacking conditions (Fig. 22b), the biofilm exhibited a protective effect by shifting the  $E_{\text{pit}}$  to

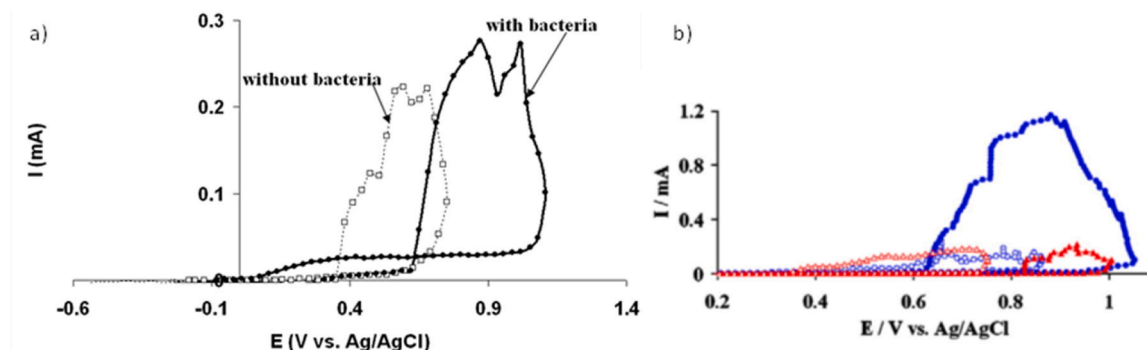


Fig. 23. Influence of medium composition on pitting curves ( $0.5 \text{ mV s}^{-1}$ ) in presence of *Geobacter sulfurreducens* for 304 L stainless steel electrode a) medium containing 5 mM acetate (e- donor) and 25 mM fumarate (e- acceptor) (from ref. [148]) and b) after 20 days immersion in a medium containing 10 mM acetate and (○ blue) 25 mM fumarate or (Δ red) 0 mM fumarate. Closed and open symbols represent, respectively the presence of 5 % v/v *G. sulfurreducens* and the absence of bacteria (from ref. [151]).

more positive potentials and improved the repassivation conditions [151]. However, disadvantages of this technique can be highlighted as follows:

1. Large polarizations alter the electrochemical conditions, which can be deleterious to the biofilm microorganisms, especially when a large potentials (high-field) are used or a continuous electropositive scan is used [25,149].
2. This technique alone cannot provide information about the local contribution of biofilm to corrosion.
3. The choice of potential scan rate is crucial in MIC studies to minimize effects on biofilm structure and characteristics. Faster scan rates have less the impact on microbial activities.
4. Slow potential sweep rates can affect localized conditions at the metal-solution interface [87].

A fast potential scan usually leads to the formation of an electric double layer of charge at the metal-solution interface. This non-faradaic charging current constitutes a significant source of error in estimating the faradaic current density, which influences the equilibria of the redox reactions occurring at the metal surface [145].

#### 4.4.1. Cyclic voltammetry

Cyclic voltammetry (CV) is a potentiodynamic technique to study the reversible, irreversible or quasi-irreversible behaviour of redox couples at metal-solution interface. It involves applying a rapid triangular potential scan to the working electrode, in a cyclic manner, inducing the oxidation of electroactive redox species followed by their reduction (or vice-versa). Single redox species generate peaks in the  $E-I$  curve both in the anodic and cathodic regions when the induced redox process is reversible. For irreversible processes peaks appear only in one region (Fig. 24). In CVs, the scan rate ( $\nu \text{ mV s}^{-1}$ ) is the most important parameter, as it affects the intensity and the shape of the redox peaks. Lower scan rates result in lower peak heights, while higher scan rates produce sharper redox peaks. For bioelectrochemistry systems and consequently MIC studies, CV is useful for highlighting the electroactivity of a biofilm that forms on an electrode [24,152–154]. Some examples are shown in Fig. 25 with an anodic biofilm (a) formed from garden compost, that oxidizes acetate [155]. In this case, the shape of the anodic curve is a wave with a  $j_{\text{max}}$  that indicates a limiting phenomenon, which can be attributed to the diffusion of substrates and/or metabolites, the electron transfer rate and the microbial kinetics. These curves can be fitted with the Nernst-Michaelis expression, see Eq. 7.

Fig. 25b shows the CVs obtained with a cathode biofilm of *Algoriphagus yeomjeoni*, a species isolated from a marine biofilm that catalyses oxygen reduction [221]. It is interesting to note the shift of the cathodic curve, corresponding to the reduction of oxygen, towards

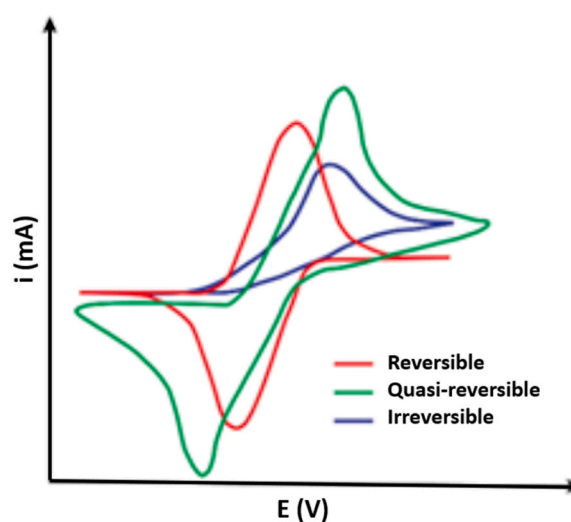
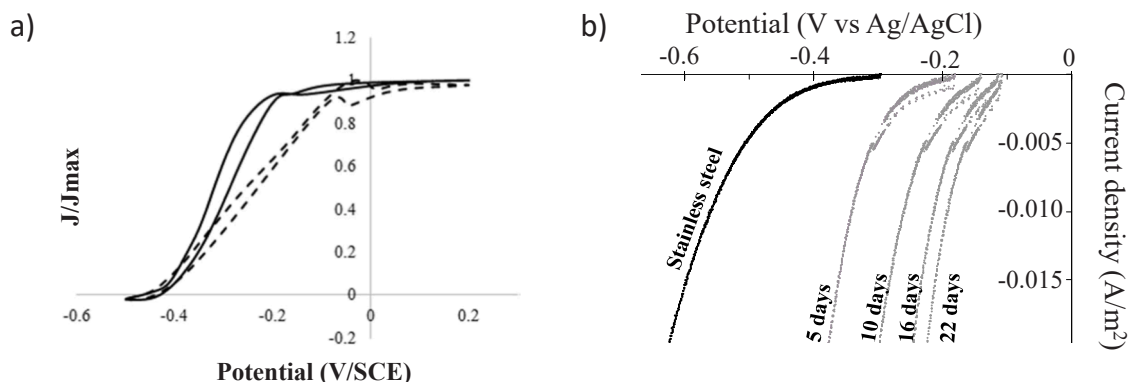


Fig. 24. Schematic CV curves for reversible, quasi-reversible and irreversible redox process.

electropositive potentials, indicating the reduction catalysis by the biofilm. CV is extensively used to identify the redox activity at the biofilm/metal interface and to study the EET pathways of electroactive bacteria and to calculate the standard EET rate constant and diffusion coefficients [154,156–162]. For example, numerous bacteria isolated from electro-active marine biofilms have shown high efficiencies in oxygen reduction catalysis through CVs performed on inert glassy carbon (Fig. 26). This activity was attributed not only to direct electron transfer between adhered cells and electrode but also to redox compounds present in test medium [154]. Fig. 27 provides another example where CVs, obtained with a pencil graphite electrode covered by a cultivated SRB biofilm (*Desulfovibrio singaporensis*) showed a reversible peak due to the presence of redox mediator and the contribution of the electroactive biofilm, as well as c-type cytochrome activity [158]. The redox peak currents were enhanced by between 1.5 and 2.5 times with riboflavin and cytochrome c, respectively, confirming the positive connection of the attached biofilm with soluble riboflavin and cytochrome c in EET.

The CV technique can effectively highlight the catalytic effects of enzymes and other molecules. Fig. 28 shows the irreversible wave of oxygen reduction catalysed by (a) laccase and (b) Hemin, an iron protoporphyrin.

However a possible disadvantage of CV, is that the faradaic current can be masked by a high resistive and/or capacitive behaviour of the electrode surface [163] as illustrated in Fig. 29. Although the different



**Fig. 25.** CV curves ( $1 \text{ mV}\cdot\text{s}^{-1}$ ) for a) microbial anodes, formed after 10 days' polarization at  $0.2 \text{ V/SCE}$  in garden compost leachate, E-I curves drawn in a synthetic medium with  $20 \text{ mM}$  acetate,  $9\text{-cm}^2$  (continuous line) and  $50\text{-cm}^2$  (dotted line) anodes made of flat carbon cloth [160] and b) microbial stainless steel cathodes, formed after different times of polarization at  $-0.2 \text{ V}$  vs  $\text{Ag/AgCl}$  in seawater inoculated with *Algoriphagus yeomjeoni*, an electroactive species extracted from marine biofilm.(modified from ref. [221]).

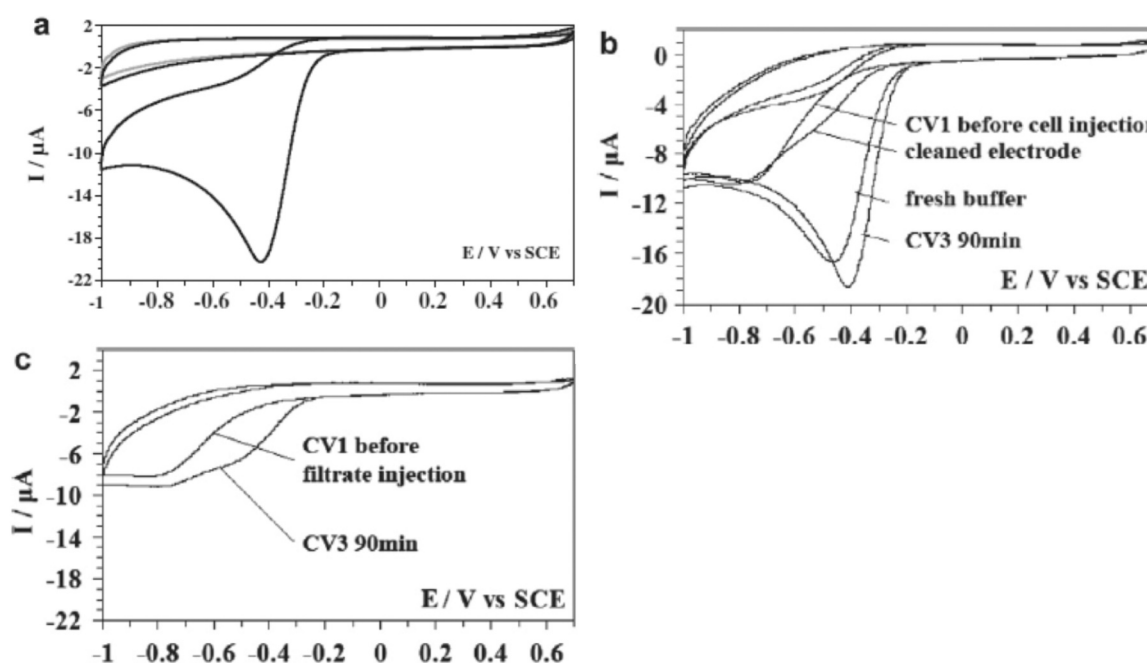


**Fig. 26.** Roles of dissolved oxygen, adhered bacteria and released compounds (GC electrode and cell suspension of *Roseobacter* sp.). (a) CV1 and CV3 were recorded in deoxygenated solution and CV4 after 10 minutes of air bubbling (*Roseobacter* sp. R-26140). (b) CV1 and CV3 were recorded following the standard procedure, then the cell suspension (*Roseobacter* sp. R-28704) was replaced by fresh buffer that did not contain cells and, finally, the electrode was cleaned. (c) CV1 and CV3 (standard procedure) obtained with the filtrate of bacterial cell suspension (*Roseobacter* sp. R26140). Modified from ref. [154].

surface treatments (Acid – A, Electrochemical E, or the both A+E) of the graphite electrodes enabled the generation of microbial bioanodes delivering significantly higher current densities than the untreated control electrode (table in Fig. 29) after microbial colonization in domestic wastewater (end of the 25-day of experiment), the CV graph of the electrode A+E is very different from the others. In fact, for the A, E and control electrodes, the CV graphs displayed a shape characteristic of bioanodes oxidizing organic matter with, however, a higher capacitive current for the electrode E ( $C = 248 \text{ mF}$ ). In contrast, the A+E electrode presented a steady state current equal to that of the A one and yet the CV graphs showed a strongly capacitive ( $C = 627 \text{ mF}$ ) and resistive (inclination of the I/V curve) behavior that masked the oxidation phenomenon. Furthermore, while CV is mainly used to analyze solutions, it often struggles to clearly observe detect reactions in weakly concentrated electroactive species in solution. Applying CV to solid samples, such as the biofilm/metal interface, necessitates more advanced strategies, as

the technique measures impedance of the entire electrochemical cell.

## 5. Alternating Current (AC) stimulation

Methods based on the perturbation of an electrochemical system in equilibrium or steady state, through the application of a sinusoidal input (AC voltage or AC current) over a wide range of frequencies, and the monitoring of the resulting sinusoidal response (current or voltage, respectively), are powerful tools for investigating the electrical properties of interfaces, passive layers of corrosion products, and insulating coatings. These methods also provide detailed mechanistic insights into microbial corrosion and the role of biofilms in corrosion processes. However, their successful application requires advanced analytical techniques (now included in specific software) and a thorough understanding of the electrical aspects of corrosion phenomena.

Unlike DC methods, where current flows only in one direction, in AC methods current periodically reverses direction and changes its

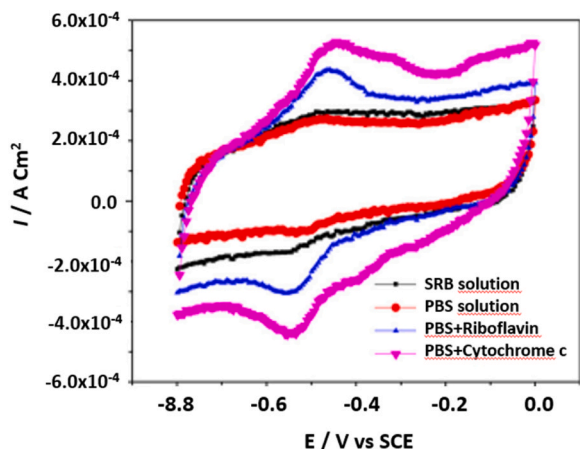


Fig. 27. CV curves for the pencil graphite electrode covered by a cultivated SRB biofilm in a 10 % carbon source medium for 15 days in different solutions: SRB solution (culture medium with planktonic cells), PBS medium (fresh abiotic medium) and PBS medium with addition of riboflavin or cytochrome c (from ref. [158]).

magnitude continuously with time. Similar to DC, AC stimulation can be a non-destructive technique or can influence the measured phenomenon, depending on the current intensity. The frequency of the

stimulation can also strongly impact the process under investigation.

### 5.1. Electrochemical Impedance Spectroscopy

Electrochemical impedance spectroscopy (EIS) is an effective non-destructive method for mechanistic studies of various corrosion phenomena, not limited to MIC. In this method, the working electrode at the corrosion potential is generally stimulated by a small amplitude sinusoidal voltage at variable frequencies. The response of the working electrode to this perturbation, in terms of: current, signal amplitude, and phase, is recorded [1]. By dividing the imposed voltage by the induced current, the impedance of the system at all excited frequencies. The applied voltage perturbation covers a wide frequency range, from millihertz (mHz) to megahertz (MHz), allowing the characterization of all the phenomena occurring at the solid/solution interface [164]. Each elementary phenomenon can be observed and characterized at a specific frequency range that corresponds to its own time constant (the relaxation time to return to steady state). Rapid electrochemical phenomena (such as charge transfer) are revealed at high frequencies, whereas slow phenomena, such as diffusion (mass-transfer) or adsorption are observed at low frequencies. Experimentally, at high frequencies, only the ohmic component due to the solution resistance is measured. When the measured  $|Z|$  increases inversely with frequency (on a log scale), it demonstrates the characteristics of a pure capacitance. Thus, EIS enables the distinction between different phenomena that are stimulated at

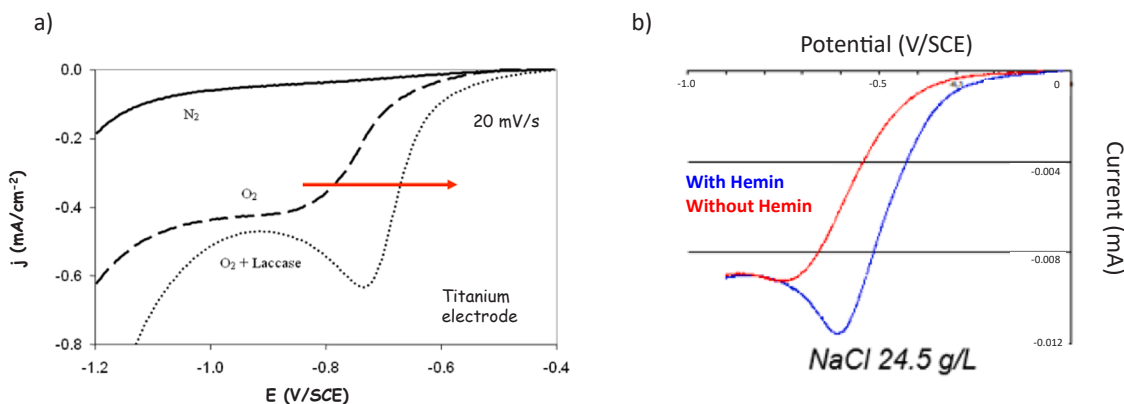


Fig. 28. Catalysis of oxygen reduction by a) laccase from *Trametes versicolor* on a titanium electrode in 0.1 M citrate-phosphate solution at pH 3.0, deaerated or oxygen saturated at atmospheric pressure with and without Laccase confined near the electrodes and b) the iron protoporphyrin Hemin, adsorbed on a stainless steel electrode in NaCl solution. Modified from ref. [107].

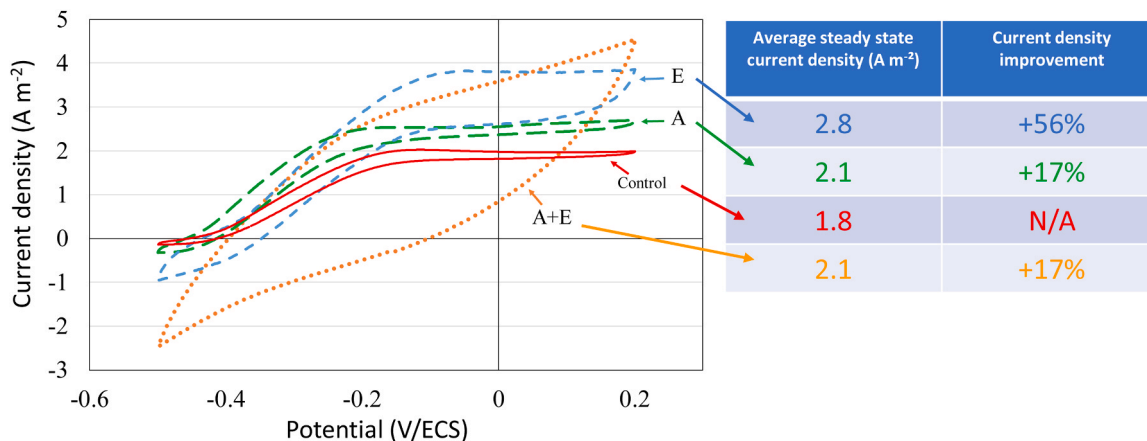


Fig. 29. CV performed in domestic wastewater on treated graphite surfaces (A+E, A, E) and non-treated commercial graphite surface (Control) after microbial colonization (end of the 25-day experiment). The correspondent steady state current densities (at 25-days) are given in the table as well as the improvement over the Control. Scan rate: 1 mV s<sup>-1</sup>. A: acid, E: electrochemical. Modified from ref. [163].



different frequencies. EIS can be performed as a high-resolution technique to achieve kinetic parameters, determine reaction mechanisms, and measure electrolyte and electrode conductivities, as well as the influence of a biofilm on the metallic surface. EIS can thus be used to characterize non-conducting or semi-conducting passive layers, coating on the surface [45,165–170]. For example, Fedrizzi *et al.* reported that high-frequency peaks were associated with coating performance, whereas the other peaks were related to activation of electrochemical processes [45].

EIS data can be interpreted using various plots such as Nyquist, Bode-modulus, Bode-phase, and Cole-Cole plots. The Bode plots display information on impedance, frequency, and phase angle [87]. For instance, the Bode-phase plot can provide insights into pitting corrosion when combined with optical microscopy. It has been observed that when the phase angle reaches a minimum at the lowest frequencies, pitting can be initiated, and the growth of active pits increases the capacitance [171, 172]. It must be noted that the breakdown of the passive layer, accompanied by pitting corrosion process, is critical to detect by EIS since their initiation and development are unstable processes. In such cases, EIS provides only qualitative, not quantitative, results. The

interpretation of the EIS data is not straightforward and requires understanding of the physical meaning of the electric components to model an effective equivalent circuit of the corrosion process, including microbial interactions for MIC. To address this, an integrated approach combining experimental observation, model development, and error analysis has been proposed by Orazem and Tribollet [173]. Moreover, dedicated software packages are also available to mathematically generate equivalent electrical circuits from the raw EIS data. These packages use a structural identification approach that involves the generalized deconvolution of the impedance data without requiring priori chosen assumptions. For example, Differential Impedance Analysis (DIA) is a technique that applies a structural identification approach to time constants [174]. It ensures both structural and parametric identification based on a single experimental data. The method applies a local operating model (LOM) for the parametric analysis by scanning along the analytical coordinate frequency. The LOM describes a simple first-order inertial system extended with an additive term. A deterministic approach is used by extending of the initial set of data ( $Z_{\text{real}}$  and  $Z_{\text{imag}}$  components of the impedance and frequency  $\omega$ ) with two additional terms – the derivatives of  $Z_{\text{real}}$  and  $Z_{\text{imag}}$  with respect to the

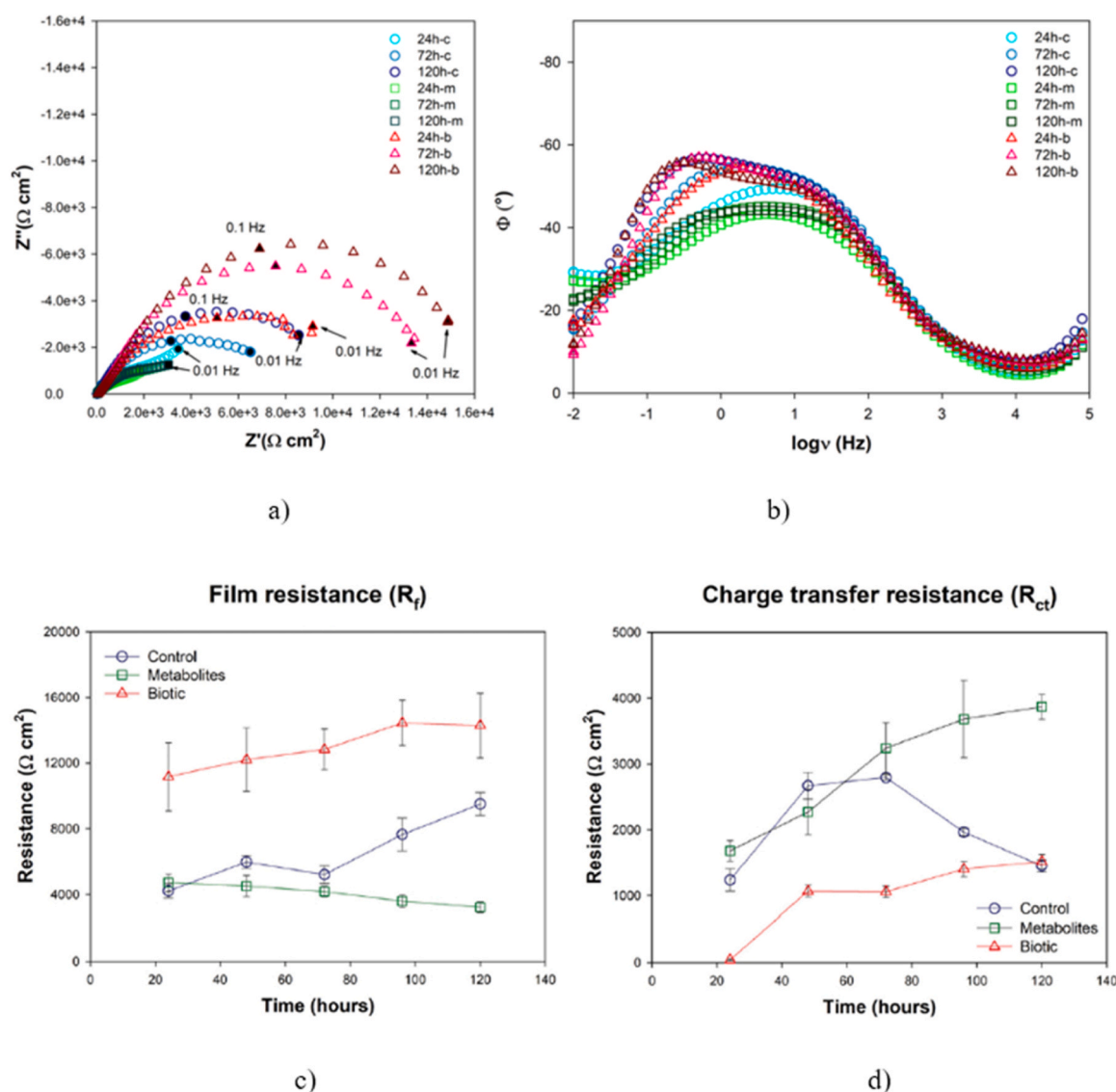


Fig. 30. Nyquist (a) and Bode (b) plots of an aluminum bronze showing the most significant EIS spectra achieved during exposition in a control solution of 0.1 M of NaCl solution (Circles); filtered biotic solution with metabolites (squares) and biotic solution containing *Pseudomonas fluorescens* bacteria (triangles) at different exposition time; c) Trends of calculated film resistance  $R_f$  and d) trends of Charge transfer resistance  $R_{ct}$  (from ref. [30]).

frequency. The number of plateaus found in the frequency range where the LOM corresponds to the object's behaviour, is the number of time constants. The temporal analysis can qualitatively estimate frequency distribution, indicated by deviations from the plateau-behaviour. However, for precise quantitative analysis, *i.e.*, for structural and parametric identification, another algorithm called Secondary DIA [175], and complex non-linear regression least squares fitting procedure [176] must be performed based on the results obtained by DIA. Despite the complexity of this method, it was successfully applied recently in MIC studies of copper alloys, supported by microscopy observations, Raman data, and other electrochemical techniques [21], [220]. EIS techniques also allowed us to demonstrate how the aerobic metabolism of *Pseudomonas fluorescens* promotes the formation of a stable and highly resistive oxide film, which inhibits the corrosion of Aluminum bronze. Although this bacterium initially produced an electroactive mediator (pyocyanin) that increases charge transfer, corrosion was ultimately inhibited. This is due to the enhanced metal dissolution being followed by the re-precipitation of metal ions in a more stable (higher capacitive and resistive) passive layer compared to the sterile and metabolite control tests ([30], Fig. 30).

Wharton et al. [177,178] report a study monitoring aerobic marine biofilms on electrode surfaces, and the influence of nitric oxide attachment control as an innovative method for detecting and monitoring marine bacterial biofilms using EIS. The study effectively demonstrates the use of microelectrodes to monitor the condition film, biofilm formation and the impact of nitric oxide on biofilm dispersal (Fig. 31). A key aspect of this investigation is its novel application of EIS for real-time biofilm monitoring, which is crucial for understanding biofilm dynamics and developing mitigation strategies, which incorporated confocal microscopy to validate the electrochemical data. However, the study has limitations. The experimental setup, although detailed, may not fully replicate the complex conditions of natural marine environments, potentially limiting the applicability of the findings. Additionally, a more thorough discussion on the long-term stability and reproducibility of the sensor system under varying environmental conditions would have been useful. While the innovative use of microelectrodes offers high sensitivity and specificity, the potential scalability issues could limit practical applications. Overall, the study provided insights into biofilm detection and control, although further studies are needed to address its limitations and improve its practical applications.

It is worth noting that equivalent circuit models often cannot accurately represent the corrosion process due to its complexity. Multiple interfaces involving partial coverages, mixtures of corrosion products, elements with different geometries, and porosity can co-exist on the

surface [78,173]. Additionally, biofilms are also dynamic entities that cause short-term fluctuations in the electrochemistry at the metal/film interface, making localized corrosion under the biofilm difficult to detect. The period of these fluctuations is shorter than the time for gathering EIS data through a full frequency sweep, meaning that not all frequencies of the applied signal respond to the same electrochemical conditions [25]. Nevertheless, many EIS reports monitoring bacterial cell attachment [78,179] and biofilm formation [87,171,180,181], bacterial electroactivity and conductivity of biofilm, often misinterpret the equivalent circuits, and incorrectly attribute the double layer response of corrosion products to the biofilm.

When analyzing EIS data linked to MIC or biofilm studies, it is important to remember that the biofilm is mostly composed of water [38] and is a good electrolyte. Therefore, it cannot exhibit a capacitive behaviour itself, although it can influence the charge transfer in several ways. For the study of MIC mechanisms, low frequency data are of greater interest. In conclusion, the EIS technique can be a useful for studying biofilm and its effects on corrosion if the experimental data are well analysed. EIS is non-destructive to the biofilm, and electrochemical conditions on electrodes change very little after the EIS measurements [1]. Several studies have demonstrated that the small signals required for EIS do not adversely affect the numbers, viability, and activity of microorganisms within a biofilm [76,78,181]. Conversely, cell populations can be significantly reduced on the polarized surface when subject to either PP or CV [182].

Although the EIS cannot directly determine the corrosion current density and biofilm thickness, it can estimate the passive layer thickness under the biofilm. The high-frequency impedance range (40 MHz down to 100 Hz) corresponds apparently to a pure capacitive behaviour [183]. At infinite frequency, all resistances are negligible compared to the impedance corresponding to the capacitance [184]. Therefore, extrapolating of the complex-capacitance diagram can reliably determine the thickness of the capacitive layer [184]. The complex capacitance ( $C$ ) is calculated using the impedance data corrected for the electrolyte resistance ( $R_e$ ) (Eq. 26).

$$C(\omega) = \frac{1}{j\omega(Z(\omega) - R_e)} \quad (26)$$

The physical meaning of this capacitance is linked with the dielectric properties of the electrochemical interface. Using the known dielectric constant of oxides, the capacitance estimated in the high-frequency domain using Eq. 27 allows the calculation of the oxide layer thickness  $\delta$  as described in Eq. 28 (used for plate capacitors):

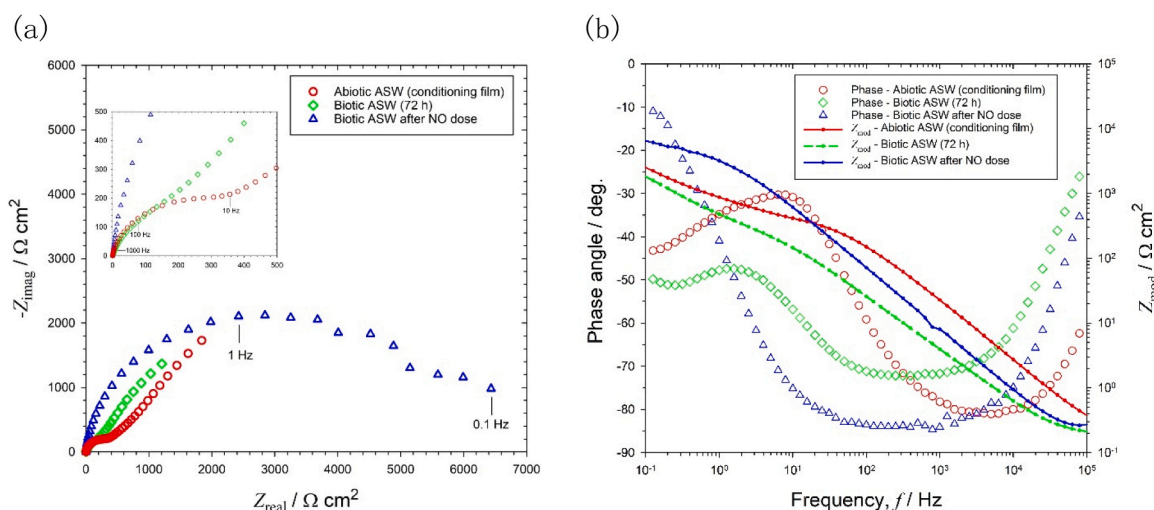


Fig. 31. EIS for abiotic and abiotic artificial seawater before and after nitric oxide dosing: (a) Nyquist ( $-Z_{imag}$  vs.  $Z_{real}$ ) and (b) Bode phase (deg. vs.  $f$ ) and Bode modulus ( $Z_{mod}$  vs.  $f$ ). From ref. [177,178].

$$C_{\text{ox}} = \frac{\epsilon \epsilon_0}{\delta} \quad (27)$$

Where  $\epsilon_0$  is the permittivity of vacuum ( $\epsilon_0 = 8.85 \times 10^{-14} \text{ Fcm}^{-1}$ ) and  $\epsilon$  is the dielectric constant for metal oxide. In practice, the high-frequency capacitance is determined at frequencies above 25 kHz [185].

### 5.1.1. Mott-Schottky plots to study passive films

Mott-Schottky (M-S) is another method that can be used to understand how the biofilm affects passive layers of metallic surfaces from EIS data. M-S plots show changes of capacitance at an electrochemical interface under voltage fluctuations and are typically used to determine the semiconductor property of passive films. The Mott-Schottky analysis expressions are as follows (see Eqs. 28–29):

$$\frac{1}{C_{\text{SC}}^2} = \frac{2}{\epsilon \epsilon_0 e N_{\text{D}}} \left( E - E_{\text{FB}} - \frac{k_{\text{B}} T}{q} \right) \text{ for } n\text{-type semiconductor} \quad (28)$$

$$\frac{1}{C_{\text{SC}}^2} = \frac{2}{\epsilon \epsilon_0 e N_{\text{A}}} \left( E - E_{\text{FB}} - \frac{k_{\text{B}} T}{q} \right) \text{ for } p\text{-type semiconductor} \quad (29)$$

Where  $e$  is the electron charge,  $N_{\text{D}}$  and  $N_{\text{A}}$  are the donor and acceptor densities ( $\text{cm}^{-3}$ ),  $\epsilon$  is the dielectric constant of the passive film ( $\epsilon = 12$  for iron/steel substrates),  $\epsilon_0$  is the vacuum permittivity  $k_{\text{B}}$  is the Boltzmann constant ( $1.38 \times 10^{-23} \text{ J K}^{-1}$ ),  $T$  is the absolute temperature and  $E_{\text{FB}}$  is the flat band potential. The interfacial capacitance,  $C$  is also explained in Eq. 30:

$$C = \frac{1}{\omega Z_{\text{imag}}} \quad (30)$$

where  $Z_{\text{imag}}$  is the imaginary component of the impedance and  $\omega = 2\pi f$  is the angular frequency [186]. In corrosion science, this technique is often employed when the double layer capacitance is negligible. Under these conditions, the measured capacitance ( $C$ ) is equivalent to the space charge capacitance ( $C_{\text{SC}}$ ). Consequently, a plot of  $1/C_{\text{SC}}^2$  versus  $E_{\text{FB}}$  is generated. In these plots, positive slopes indicate the presence of  $n$ -type semiconductor behaviour at all formation potentials. From the linear portion of the slopes, the donor density can be estimated. This method calculates the dopant density near the alloy/passive film interface, where the concentrations of oxygen vacancies and metal interstitials are expected to be the highest [186]. Thus, understanding the nature of the passive film is crucial for comprehending the corrosion properties of engineering metals and alloys [187]. For instance, M-S analysis is performed to investigate how the electronic properties of the passive film change with an increase in solution temperature.

An important consideration in the M-S analysis is the influence of frequency on the measured capacitance. To determine the optimized frequency, capacitance should be measured across a range of frequencies. The highest frequency at which the capacitance does not significantly decrease should be selected as a reference frequency for M-S analysis [188]. It is important to note that M-S analysis is not suitable for analyzing biofilms, as they do not have a capacitive character, a fact sometimes overlooked in some publications. However, M-S analysis can be used to study the impact of biofilms on the characteristics of the passive layers beneath them [189–192]. For instance, a study presented M-S plots for the passive films on 304 SS after 14 days of exposure to both sterile and inoculated media. In both conditions, two linear regions were observed. This confirmed that the biofilm did not change the semiconductor properties of the passive film. However, the increase in donor density ( $N_{\text{D}}$ ) and acceptor density ( $N_{\text{A}}$ ) indicated enhanced electron transfer within the passive film, accelerating its dissolution [192]. Notably, the increase of these parameters also suggests that the passive film became more defective. Thus, it is expected that the biofilm compromise the barrier function of the passive film, increasing the likelihood of pitting corrosion [192]. Fig. 32 shows an example of M-S plots with two distinct regions of semi-conductivity for stainless steel

under various test conditions. The positive slopes, found at potentials more positive than about  $-0.5 \text{ V vs. SCE}$  correspond to  $n$ -type behaviour. Conversely, the negative slopes, observed at potentials more negative than around  $-0.7 \text{ V vs. SCE}$  denote  $p$ -type behaviour. Additionally, there is a flat band potential ( $E_{\text{FB}}$ ) region between  $-0.504 \text{ V}$  and  $-0.686 \text{ V vs. SCE}$ , which represents the transition between  $p$ -type and  $n$ -type conductivity. Both  $N_{\text{D}}$  and  $N_{\text{A}}$  calculated from the linear portions of the slopes were of the order of  $10^{21}$  and progressively decreased with the development of biofilm and reduction of the light levels [189]. Alternatively, another study shows that M-S analysis can elucidate why a *G. sulfurreducens* biofilm on 254SMO stainless steel exhibited higher cathodic current densities compared to biofilms on 316 L stainless steel. It was found that at the cathodic potential used for biofilm formation (below the  $E_{\text{FB}}$ ), 316 L displayed slight  $p$ -type behaviour, whereas 254SMO did not show any semi-conductive behaviour. The  $p$ -type behaviour in 316 L indicates a lack of available electrons near the surface, which is detrimental for the cathodic process. In contrast, the absence of this  $p$ -type behaviour in 254SMO explains the superior electrochemical performance of biocathodes formed on it [193].

### 5.1.2. Dynamic electrochemical impedance spectroscopy

Another potentially relevant technique for studying the dynamic effects induced by a biofilm on protective oxides and anticorrosive coatings is Dynamic Electrochemical Impedance Spectroscopy (DEIS). DEIS is powerful for investigating mechanisms in surface electrochemical reactions by applying an AC signal while sweeping the potential [194]. This novel approach provides impedance data from non-stationary systems [194]. DEIS can be distinguished from conventional EIS through the use of advanced software, ensuring precise measurements in critical applications [195]. The technique achieves a frequency limitation as low as  $0.1 \text{ Hz}$ , validated through the Kramers-Kronig transform and consistency tests [196]. The mechanisms of electrochemical systems can be analysed qualitatively and quantitatively, enabling time-resolved studies of various physicochemical processes across different time scales. Different acquisition strategies and correction algorithms facilitate high-precision dynamic impedance spectra and cyclic voltammetry measurements, addressing the challenge of high-frequency artefacts caused by non-ideal instrument behaviour, which can lead to incorrect interpretations down to  $0.1 \text{ Hz}$ . By leveraging advanced computing to reduce computation time, DEIS can effectively study corrosion, inhibitors, pitting, organic coating damage, cavitation and battery discharge processes [196]. This makes DEIS a

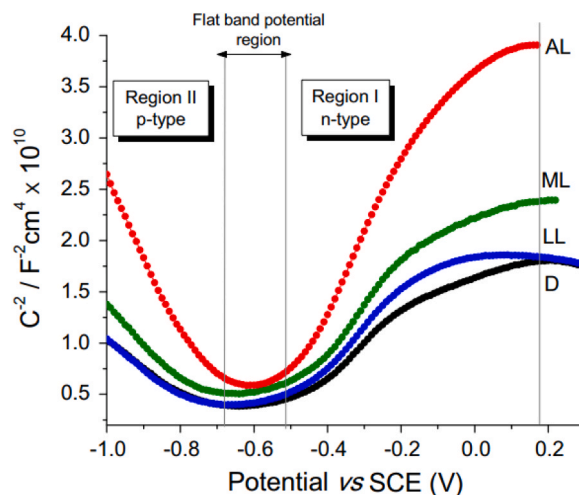


Fig. 32. M-S plots obtained for biofilm formed on stainless steel surfaces immersed in coastal seawater for 37 d at different test conditions of ambient light (AL), moderate light (ML), low light (LL), and full darkness (D). From ref. [189].

powerful tool for advancing the understanding and monitoring of complex electrochemical phenomena. Although it has not yet been applied to MIC scenarios, DEIS is valuable for analysing non-stationary systems. It allows for time-resolved studies of various electrochemical processes, including those occurring in biofilms, to examine the dynamic effects induced by biofilms on protective oxides and anticorrosive coatings. Therefore, it shows promise for studying microbial corrosion in real time for laboratory experiments.

### 5.1.3. Electrochemical frequency modulation

Electrochemical frequency modulation (EFM) is a modern, non-destructive technique that applies a dual frequency potential perturbation to measure the current density response at sums, differences, and multiples of the input frequencies [145]. Simpler and faster than EIS, EFM provides data about corrosion parameters, such as corrosion rate and polarization resistance of metals and alloys undergoing electrochemical corrosion, without requiring prior knowledge of the Tafel slopes. It validates the accuracy of results obtained using causality factors (CF-2 and CF-3) [197]. The EFM approach can also interpret the corrosion mechanism as either activation, diffusion, or passivation-controlled phenomena based on the potential-current relationship involved in the corrosion process [145]. Consequently, EFM is suggested as a good alternative to the conventional electrochemical techniques.

Bosch and co-workers [198] modified the Stern-Geary equation and derived mathematical expressions for the theoretical calculation of corrosion current density, Tafel slopes (constants) and causality factors CF-2 and CF-3 from the current peaks at harmonic and intermodulation frequencies. (see Eqs. 31–34):

$$j_{\text{corr}} = \frac{i_{\omega_1, \omega_2}^2}{\sqrt{8 i_{\omega_1, \omega_2} i_{2\omega_2 \pm \omega_1} - 3i_{\omega_2 \pm \omega_1}^2}} \quad (31)$$

$$\beta_a = \frac{b_a}{\ln 10} = \frac{i_{\omega_1, \omega_2} \Delta E}{\omega_2 \pm \omega_1 \sqrt{8i_{\omega_1, \omega_2} i_{\omega_2 \pm \omega_1} - 3i_{\omega_2 \pm \omega_1}^2}} \quad (32)$$

$$\beta_c = \frac{b_c}{\ln 10} = \frac{i_{\omega_1, \omega_2} \Delta E}{-\omega_2 \pm \omega_1 \sqrt{8i_{\omega_1, \omega_2} i_{\omega_2 \pm \omega_1} - 3i_{\omega_2 \pm \omega_1}^2}} \quad (33)$$

$$\text{CF} - 2 = \frac{i_{\omega_2 \pm \omega_1}}{i_{2\omega_1}} \text{ and } \text{CF} - 3 = \frac{i_{2\omega_2 \pm \omega_1}}{i_{3\omega_1}} \quad (34)$$

where  $\omega_1$  and  $\omega_2$  are the (angular) perturbation frequencies in  $\text{rad s}^{-1}$  (and  $\omega = 2\pi f$ , with the frequency  $f$  in Hertz), and  $\Delta E$  is the perturbation potential.

Compared to conventional techniques such as LPR and PP, EFM offers several advantages. Firstly, it is less susceptible to errors caused by the bulk medium in which the metal corrosion is analyzed, such as the solution resistance and the double layer charging during potential perturbation. Secondly, the causality factors help detect the initiation of phenomena like active-passive transition and localized pitting and crevice corrosion. EFM provides accurate values of Tafel constant and corrosion current density, even when the metal is under passivated condition, pitting or diffusion control [145]. The experimental values of CF-2 and CF-3 obtained during an EFM measurement are usually compared with theoretically established values. If the theoretical and experimental values are close, it means the EFM experiments are verifiable. It is important to use low frequencies in EFM experiments to avoid the influence of the capacitive behaviour of the electrochemical double layer.

The  $R_p$  derived from EFM can be comparable to  $R_p$  obtained from EIS and polarization techniques, but only when the metal corrosion is charge-transfer controlled. In the case of diffusion controlled and passivation, these parameters are not comparable and  $R_p$  derived from EFM is generally more reliable [145]. Despite reliability of EFM

compared to conventional electrochemical methods, there are only a few reports on the application of EFM in MIC investigations [197,199]. In one study [200], iron corrosion in a culture media inoculated with *Desulfovibrio sp. strain HS3* was investigated using EFM. A significant deviation between the corrosion rates measured by EFM and LPR was observed after five days of incubation, attributed to the onset of severe localized corrosion of the iron surface by the bacteria communities. In addition, localized colonization distorted the active surface area measured by both EFM and LPR, leading to an underestimation of the corrosion rate by LPR and an overestimation by EFM, compared with average from long term incubation studies. The overestimation by EFM was attributed to a shift in the impedance of the corrosion system towards lower frequencies, causing the EFM input frequencies to fall into the capacitive region [200]. However, EFM was able to detect significant changes in its causality factors CF-2 and CF-3 [145], indicating when the MIC transitions from uniform to localized behaviour and when corrosion rate monitoring breaks down. This capability of EFM could be a distinct advantage over other electrochemical methods for MIC monitoring [200].

### 5.2. Localized Electrochemical Impedance Spectroscopy

The localized application of EIS (LEIS) was firstly introduced by Isaacs in 1992 [201]. In LEIS, the applied voltage is similar to the conventional EIS typically involving sinusoidal amplitudes of 10 mV and a DC potential scan rate of  $1 \text{ mV s}^{-1}$ . However, LEIS measures the local potential difference using a moveable probe that scans the sample surface. The potential difference between micro-probes is then used to accurately calculate the local current on the sample. This technique involves a two-step process and can be customised as needed [202]. Initially, the probe is polarized at a fixed frequency and moved over the sample to identify the area of interest, for instance defects and discontinuities in the passive film with low impedance. Subsequently, a systematic variable perturbation is applied above the area of interest, potentially using the second probe. In this configuration, complete impedance spectra over some frequencies can be acquired [203]. Three-dimensional graphs of the explored area, usually coloured as a function of capacitance, are then produced. An example of such data processing is shown in Fig. 33a [223].

The spatial resolution of this technique is governed by several parameters, including size and distances between microelectrodes, as well as the distance between the probe and substrate. To obtain reliable data, it is crucial to consider the dependency of potential differences on the distance of microelectrodes. In addition, the measured potential will be smaller if the probe is positioned farther from the substrate during interface mapping [202].

By equipping dynamic LEIS with two digital-analogue cards for measurement of current and voltage signals, EIS spectra can be determined over narrow time periods. This makes the method suitable for investigating pitting corrosion, as the breakdown of passive layers is usually accompanied by this corrosion type. A recent review on LEIS [202] highlighted that the shape of the curves and the low frequency limit of the impedance diagrams were correlated with the potential at the bottom of the pit formed on stainless steel (see Fig. 33b [202]).

Hence, another feature of LEIS is its ability to measure the impedance during the propagation of a pit. However, this technique can be limited at low frequency ranges, where capacitive and inductive elements in the measurement setup and the electrochemical cell itself can introduce artifacts, resulting in negative polarization resistances. To overcome this limitation, the conventional EIS and LEIS are usually conducted to simplify interpretation of the LEIS data [202].

## 6. Advanced localized electrochemical techniques

*Localized Electrochemical Impedance Spectroscopy (LEIS) and Scanning Electrochemical Microscopy (SECM) are advanced techniques for studying*

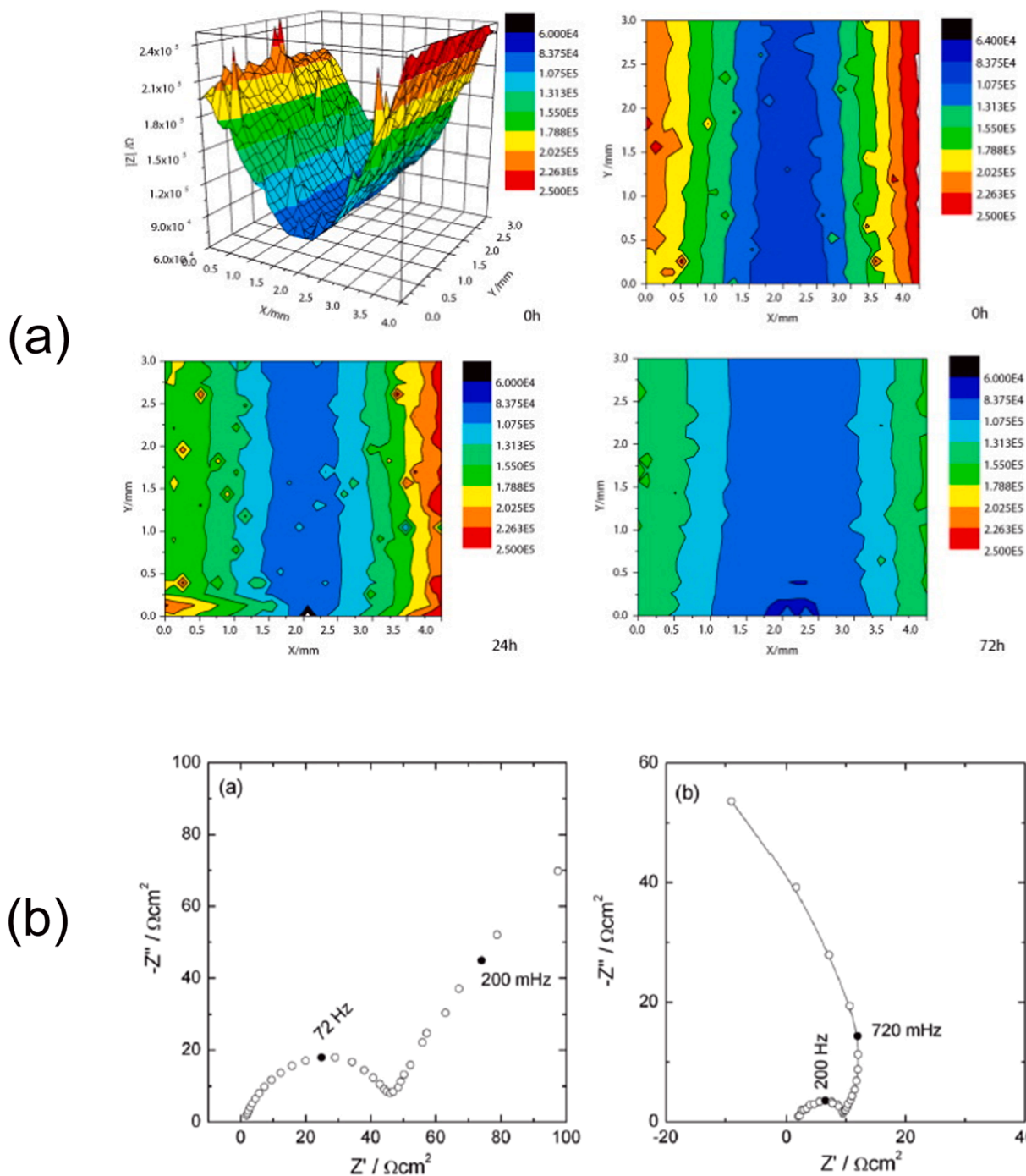


**Fig. 33.** Example of LEIS profiles and their projections in time (a): aluminum alloys under salt spray test from ref. [223]; (b): LEIS diagrams obtained above a propagating pit on 316L steel in different media, from ref. [202]

*MIC. LEIS maps corrosion sites by measuring local impedance, making it ideal for detecting pitting corrosion, although it has limitations at low frequencies. SECM uses a microelectrode to scan surfaces and monitor localized corrosion, biofilm activity, and redox reactions, providing detailed insights into biofilm-electrode interactions. Both techniques offer high spatial resolution but face challenges such as slow scanning speeds and sensitivity to environmental conditions. Combining SECM with Atomic Force Microscopy (AFM) enhances both topographical and electrochemical analysis, offering a more comprehensive understanding of the corrosion/MIC processes.*

### 6.1. Scanning ElectroChemical Microscopy

Scanning ElectroChemical Microscopy (SECM) is highly effective technique for studying of a wide range of electrochemical processes, including biological processes, surface reactivity, local corrosion, and charge transfer mechanisms. The setup of SECM involves an ultra-microelectrode (UME) probe that scans the working electrode surface, while a two-channel potentiostat monitors the potentials of both the UME probe and the working electrode. The working electrode, where electrochemical processes occur, perturbs the electrochemical response of the UME probe. This perturbation provides information about the nature and properties of the working electrode [204]. The distance

between the UME and the electrode surface is controlled by a three-dimensional positioning stepper motor and a piezoelectric motor for precise adjustments. Results from SECM are presented by three-dimensional graphs showing current versus distance. While the current of the working electrode does not depend on the UME tip-to-electrode distance, the response of the UME probe highly dependent on this distance. This is one of the most relevant factors that can limit this technique.

Furthermore, the tip is often very fragile at dimensions of just a few hundreds of nanometres and is fabricated of glass; therefore probe/substrate crashes are a regular occurrence in SECM analysis [205]. To allow the piezo to respond to height variations, it is necessary to slowly scan small areas. Consequently, the time frame for SECM is relatively long, with an area of just a few square millimetres taking over 10 h to fully scan. This extended scanning time can lead to issues such as substrate fouling and aging, solvent evaporation, and irreversible chemical reaction in the solution [205]. Therefore, SECM is ideal for small surface areas on the microscale. Despite its limitation, SECM has become valuable in corrosion science due to its ability to probe surface reactivity of wetted materials at microscopic scales. SECM can be used to study the MIC in real-time, detecting chemical reactions occurring at the interface between two regions (such as metal/air or metal/electrolyte interfaces) in a corrosion process, providing insights into the pathways and speed of such reactions with spatial resolution. In addition, SECM can probe the diffusion layer of specific chemicals on the working electrode surface and convert chemical signals into visual electrical signals [206].

The application of SECM for MIC studies offers two significant advantages: (1) it provides detailed data on localized corrosion, and (2) it delivers insights into absorbed electroactive species (oxidation or reduction enzymes) on the electrode. Thus, the technique has a bright future to study MIC and EET-MIC mechanisms in particular [207,208].

An MIC application example is illustrated in the Fig. 34 [206]. This work utilised SECM to study the influence of catalase on the MIC of 304 stainless steel in presence of *archaeon N. tibetense*. A platinum UME was utilized as the SECM probe, with the distance between the probe tip and

the sample surface maintained at a micron scale. The current drop on the UME revealed pit on anodic regions of the stainless steel surface (Fig. 34a). These pits appear only in inoculated media, and their occurrence is intensified by the addition of catalase (Fig. 34c). Conversely, SECM images under sterile conditions showed no changes or current fluctuations (Fig. 34b).

In other studies, SECM has been widely used to investigate the formation and conductivity of biofilms of various bacteria, including *Escherichia coli* [209], *Staphylococcus aureus* [210], *Salmonella typhimurium* [211], *Rhodobacter sphaeroides* [212] and *Paracoccus denitrificans* [213]. In these cases, the early detection of biofilm formation is crucial, especially when microorganisms are present at relatively low densities on metal surfaces. Under these conditions, the concentration of signal molecules is low and can be easily disturbed by the background signals from metal substrates and electrolytes [214], making detection challenging. However, SECM uniquely enables the quantitative monitoring the redox-active molecules in biofilms [204]. SECM is also used to monitor the distribution and activity of enzymes immobilized on flat surfaces, enhancing the sensitivity of this technique, through the use alternating current mode (AC-SECM) [97].

Zhang *et al.* [215] investigated the EET mechanisms using SECM to examine the formation process of *Shewanella* biofilm on an electrode. As the bioelectrogenic process progressed, the SECM tip moved vertically to trigger positive feedback, while the feedback current decreased at each vertical point. This current change was influenced by two factors: the increased electrochemical activity, which raised the current, and the shielding effect of the insulating biofilm, which lowered it. These findings demonstrated that SECM characterization can accurately reflect the biofilm thickness and conductive properties. Given the complexity of the biofilm and MIC reactions on metal surfaces, as well as the influence of metabolites, chemical signal molecules and electron shuttles on surface, modern techniques such as SECM are essential for detecting local electrochemical variations near the biofilm. This helps establish relationships between chemical species and the electrochemical corrosion process at metal surfaces. When a potential is applied at the SECM tip,

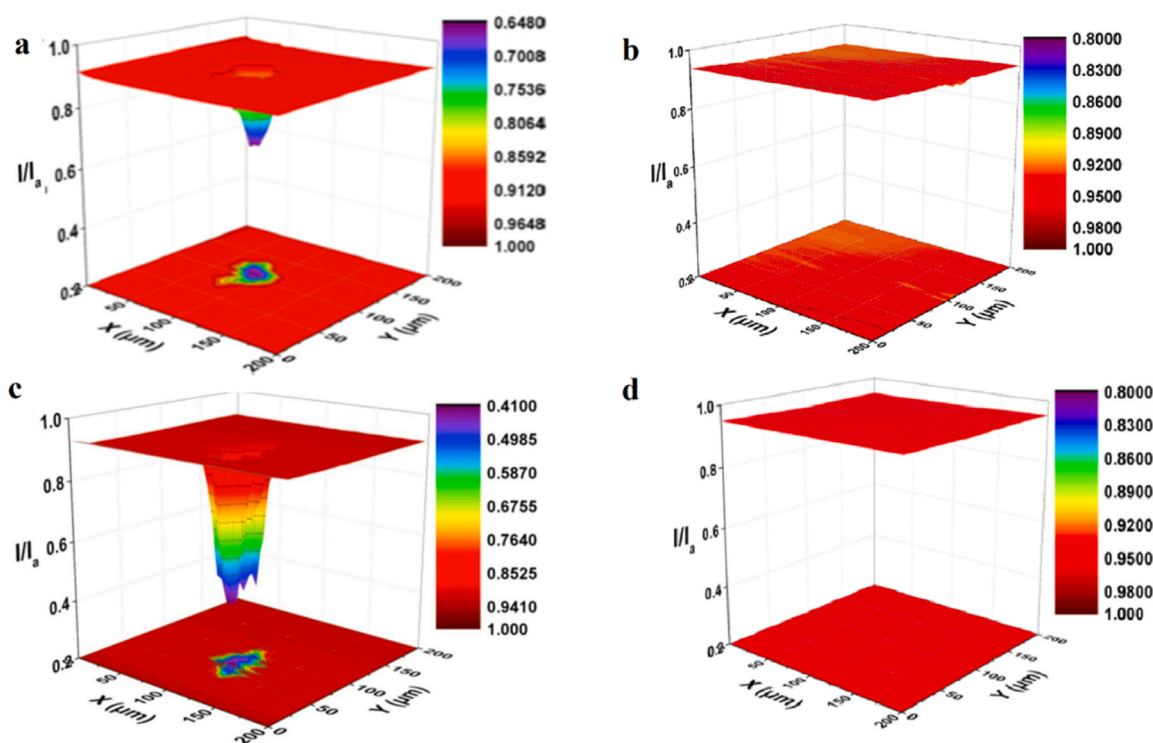


Fig. 34. SECM image of the stainless-steel samples in the inoculated culture media (a without catalase, c with 0.3 mg/mL catalase) and sterile medium (b with 0.15 mg/mL catalase, d with 0.3 mg/mL catalase) on the 7th day (from ref. [206]).

the oxidation or reduction of specific chemical species in the culture media or the biofilm can be observed. The resulting current map can provide insights into the interactions within the biofilm [208].

Li *et al.* [190] applied this technique to investigate the local concentration of riboflavin as a redox-active mediator and to monitor its interactions with a stainless steel surface during the EET-MIC process. Through starvation tests, one of common method to investigate the mechanism of EET, Huang *et al.* [216] also applied SECM to reveal the acceleration of MIC for 304 stainless steel in the presence of *Pseudomonas aeruginosa* and absence of an electron acceptor. Through starvation tests, a common method to investigate the EET mechanism, it was attributed to the bio-reduction of the passive film in micro-local regions. Multi-mode SECM was used to probe the environmental changes around the biofilm ( $\sim 30 \mu\text{m}$ ) caused by respiratory metabolism, including  $\text{Fe}^{2+}$ ,  $\text{O}_2$  and pyocyanin.

Aside from various enzymes, certain metabolic products and pH variations near or within the extracellular polymeric substances (EPS)

can become focal points in SECM-based MIC research [214]. The main limitation lies in the uncontrollable environmental conditions that hinder tracking variations in biological and electrochemical processes, as samples are typically immersed in nutrient-rich culture media for extended periods. Another major limitation is the relatively low temporal resolution, since the *in situ* detection of MIC is a time-dependent process. Improving the high-speed SECM mode [214] presents a real challenge to overcome these limitations. In addition to AC-SECM mode, which is particularly well-suited bacterial behaviour and biofilm activity in biological systems, there are several other operating modes. These include Generation and Collection Mode, Redox Competition Mode, and Potentiometric Mode, which utilize an ion selective electrode.

The SECM approach can be successfully combined with atomic force microscopy (AFM-SECM) to probe the local electrochemical responses in liquid while studying the native topography of biological components [217]. For instance, the AFM-SECM has been used to simultaneously investigate pit nucleation electrochemically and topographical imaging

**Table 2**  
Methods without externally applied electrical stimulation.

Acronym: name	Method	Strengths	Limitation	Notes
OCP: Open Circuit Potential	Measure of the voltage vs. a reference electrode.	Non-destructive. Simple to apply in both laboratory and field.	Does not measure the corrosion rate. A stable (reference) electrode is necessary. Different phenomena (oxygen conc., pitting, sulphides, etc.) can lead to similar variations.	For passivable alloys, anaerobic conditions induce a negative shift, while the cathodic effect of a biofilm induces a positive shift.
EN: Electrochemical Noise	Measure of the stochastic fluctuations of the current and potential between two nominally identical sample surfaces, typically in the range of mV or $\mu\text{A}$ .	Non-destructive and allows for the evaluation between uniform and localized corrosion.	Requires complex mathematical approaches to characterize the significance of the signal. The noise induced by the setup can be of the same order or higher than the measured parameter.	The increase in current, along with drop in potential can be associated with localized microbial activity.
SVET: Scanning Vibrating Electrode Technique	Measure of the local ionic current in an electrolyte near the surface of a sample using a vibrating microelectrode. This technique maps the spatial distribution of anodic and cathodic sites.	Non-destructive and capable of mapping corrosion activity and surface morphology in real-time. It allows the identification of the active catalytic centers, such as enzymes, within the biofilm.	For laboratory studies only. The conductivity of the solution must be low, and it can change if ions are released by the mapped surface. The microelectrode can displace and disrupt the biofilm, if it is too thick.	Provides qualitative and quantitative data about biofilms and their component distribution. It can also be corroborated with optical microscopy.
SKP: Scanning Kelvin Probe	Measures the contact potential difference between a sample and a vibrating reference electrode using a Kelvin probe.	Non-destructive Provides high-resolution maps for the possible galvanic element distribution of possible galvanic elements.	It cannot be employed immersed in aqueous solutions, and online measurement of MIC is not possible. For laboratory studies only.	The SKP technique can be combined with AFM (SKPFM) to visualize both topography and Volta surface potentials on small surface area.

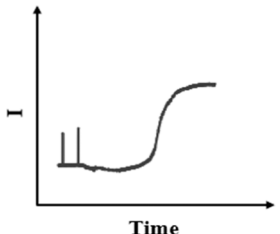
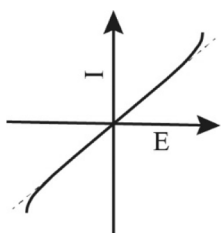
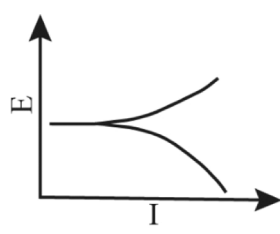
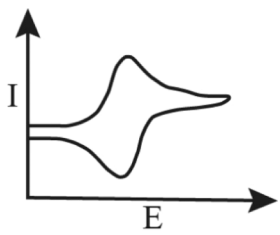
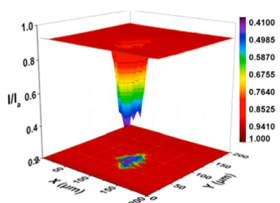
of pit formation on aluminum alloy AA1050 [218]. This method provides pit distributions and detailed information about localized corrosion and intermetallic particles, offering real-time data with high spatial resolution (in the micron or submicron range).

## 7. Conclusive remarks

This review critically examined both conventional and advanced EC techniques used in-field and laboratory corrosion studies within the context of MIC investigations, as summarized in Tables 2 – 4. While EC

techniques generally do not specifically target MIC, they can monitor specific MIC conditions and corrosion rates. However, no single technique can fully address all aspects of the complex MIC process. The diverse chemical and physical characteristics, along with the thermodynamics of corrosion layers and their surface distribution, influence metal corrosion behaviour and the impact of microorganisms. These microorganisms form heterogeneous biofilms that interface with and adapt to varying environmental conditions at the metal-solution boundary. Consequently, environmental changes due to corrosion can affect the microbial communities within biofilms. Although the

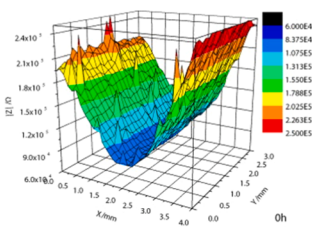
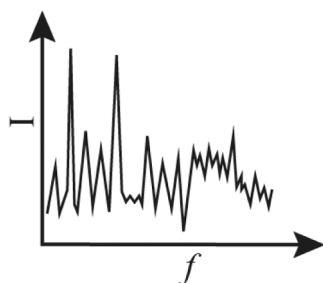
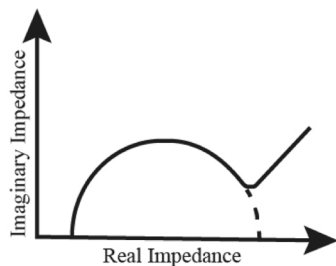
**Table 3**  
Direct Current (low/high perturbation) Methods.

Acronym: name	Method	Strengths	Limitation	Notes	
CA: Chrono Amperometry	Imposes a fixed potential and measures the current response with time.	It investigates electron transfer kinetics and allows online and long-time monitoring of the steady-state.	Does not measure the corrosion rate. The conditions do not correspond to the pure spontaneous process.	Industrial biofilm monitoring probes are based on this technique. They measure biofilm growth on a specific material (stainless steel or titanium) that can be different than on other materials.	
	LPR: Linear Polarization Resistance	Perform a potential sweep within a narrow range of a few millivolts around the corrosion potential.	It is non-destructive and allows the estimation of instantaneous corrosion rates both in the field and in laboratory. The theory was validated for cases of uniform corrosion, confirmed in laboratory settings at neutral pH and in field conditions.	Issues in correlate $R_p$ with corrosion current: suitable coefficients from weight losses or Tafel plots are mandatory.	Commercial corrosion meters for field and industry are most often based on the LPR technique, despite its limitations.
	PDP: Potentiodynamic Polarization	Scan of a wide range of potential ( $\pm 0.5$ to $\pm 1$ V vs OCP) at scan rates of $< 5 \text{ mV s}^{-1}$ (typically, $1.666 \text{ mV s}^{-1}$ ).	Provides an overview of corrosion reactions, charge transfer, diffusion-controlled reactions, passivity, transpassivity, and localized corrosion.	The anodic sweep is invasive, particularly deleterious to microorganisms within the biofilm. It is unusable if system is under diffusion control.	The impact on microbial activities decrease as the scan rate increases.
	CV: Cyclic Voltammetry	A rapid triangular potential scan cyclically applied to the working electrode, at a fast scan rate (i.e., $10 - 50 \text{ mV s}^{-1}$ ).	The highest scan rate emphasizes sharp redox peaks, such as the ones resulting to enzymatic activity, making it useful for highlighting biofilm electroactivity.	Faradaic current can be masked by high resistive and/or capacitive characteristics of the surface. Weakly concentrated electroactive species in solution may not be detected.	It examines the reversible, irreversible or quasi-irreversible behaviour of redox couples at the metal-solution interface.
	SECM: Scanning Electro Chemical Microscopy	The surface of the working electrode is scanned in three-dimensional manner using a polarized microprobe.	It is ideal for studying the surface at the level of individual microbes and the activity of redox enzymes. It can focus at nanometric scale (the most sensitive).	Measurement can take over 10 h to fully scan, leading substrate fouling and aging, solvent evaporation, and irreversible chemical reactions in solution.	SECM can be combined with the atomic force microscopy (AFM-SECM) to study in a liquid phase the topography of biological components.
					



**Table 4**  
Sinusoidal Stimulation (Low Perturbation) Methods.

Acronym: name	Method	Strengths	Limitations	Notes
EIS: Electrochemical Impedance Spectroscopy	The steady-state is disturbed by a low-amplitude sinusoidal voltage (10 mV) at variable frequencies ranging from 0.01 Hz – 10 <sup>5</sup> Hz.	Allows the characterization of the electric phenomena (capacitance, resistance, inductance) occurring at the solid/solution interface, both in the laboratory and in the field.	To analyze the data, specialized software and a physical model are essential. MIC can deviate from a steady-state condition during the measurement. The low frequency response is the most relevant for MIC.	While EIS cannot directly determine the corrosion current density and biofilm thickness, it is capable of estimating the thickness of the passive oxide layer thickness beneath the biofilm.
EFM: Electrochemical Frequency Modulation	A dual frequency potential perturbation is applied, and the current density response is traced. The generated spectrum of multiples harmonics, is analyzed.	Simpler and faster than EIS, it can provide data on corrosion rate and polarization resistance, activation, diffusion, or passivation-controlled phenomena.	The $R_p$ derived EFM can be comparable with the $R_p$ derived from EIS and polarization techniques, only when the corrosion of metal is subject to an activation-controlled process.	This method is well-suited for MIC because it is less prone to the errors caused by solution resistance and the double layer charging during potential perturbation.
LEIS: Localized Electrochemical Impedance Spectroscopy	A sinusoidal amplitude as for traditional EIS. However, a local potential difference is measured at a moveable microelectrode that explore the sample surface.	Insights into local resistive, capacitive, or diffusional properties of the surface. It is a two-step method that can be suitably personalized.	As for other EIS techniques, can be limited at low frequency ranges, where capacitive and inductive artifacts can cause a polarization resistance with negative values. Resolution depends on the size of the probe and its distance from the surface.	The output is a complex impedance 3D plots (Nyquist, Bode) or spatial maps of capacitance (presented in different colors). Suitable for complex electrochemical studies.



evolution of chemical and microbial components over time effectively assessed, the overall process remains largely unpredictable, making it challenging to accurately replicate biofilm development and MIC at the laboratory scale. Ultimately, it is crucial to emphasize that combining electrochemical techniques with complementary methods -such as microscopy and advanced molecular analyses, including next-generation sequencing of specific genes - forms a powerful multi-evidence approach. This integrative strategy can provide unparalleled insights into the roles of biofilms, specific microbial groups, enzymes, and individual cells, offering a deeper understanding of the complex systems across the taxonomic kingdoms of microorganisms involved in MIC.

Despite present limitations, EC techniques offer innovative methods for studying microbial corrosion across various scales. New online probes can assist plant operators in preventing corrosion by optimizing biocide treatments. Additionally, the ability to visualize and electrochemically characterize surface regions as small as 1  $\mu\text{m}$  enables more precise analysis of MIC-induced localized degradation under controlled laboratory conditions. In conclusion, advanced EC techniques, combined with microelectrodes and microscopy, now enable more effective exploration of MIC phenomena at the microscale. These methods can evaluate the effects of individual microorganisms rather than merely integrating the impact of complex biofilms. Additionally, advanced statistical methods can efficiently process the large volumes of data produced by these techniques, promising a deeper understanding of the interactions between bacteria and metallic surfaces, as well as the associated redox reactions, in both spatial and temporal contexts.

#### CRediT authorship contribution statement

**Regine Basseguy:** Writing – review & editing. **Digby Macdonald:** Writing – review & editing. **Tingyue Gu:** Writing – review & editing. **Dawei Zhang:** Writing – review & editing. **Pierangela Cristiani:** Writing – review & editing, Conceptualization. **Masoumeh Moradi:** Writing – review & editing, Data curation, Conceptualization. **Dake Xu:** Writing – review & editing, Supervision. **Julian A. Wharton:** Writing – review & editing.

#### Declaration of Competing Interest

The authors declare that they have no known competing financial interests or personal relationships that could have appeared to influence the work reported in this paper.

#### Acknowledgement

Authors thanks the COST Action European MIC Network—New paths for science, sustainability and standards (Euro-MIC) [CA20130] for supporting this work. RSE contribution to this work has been financed by the Research Fund for the Italian Electrical System under the Three-Year Research Plan 2025-2027 (MASE, Decree n.388 of November 6<sup>th</sup>, 2024), in compliance with the Decree of April 12<sup>th</sup>, 2024.

## Data Availability

No data was used for the research described in the article.

## References

- [1] J.W. Costerton, G.G. Geesey, T.I. Ladd, C. Nickel, M. Dasgupta, T.I. Marrie, Bacterial biofilms in nature and disease, *Annu. Rev. Microbiol.* 41 (1987) 435–464, <https://doi.org/10.1146/annurev.mi.41.100187.002251>.
- [2] H.A. Videla, L.K. Herrera, Microbiologically influenced corrosion: looking to the future, *Int. Microbiol.* 8 (3) (2005) 169–180. PMID: 16200495.
- [3] W.P. Iversen, Corrosion of iron and formation of iron phosphide by desulfovibrio desulfuricans, *Nature* 217 (5135) (1968) 1265–1267, <https://doi.org/10.1038/2171265a0>.
- [4] I. Beech, J. Sunner, Biocorrosion: towards understanding interactions between biofilms and metals, *Curr. Opin. Biotechnol.* 15 (3) (2004) 181–186, <https://doi.org/10.1016/j.copbio.2004.05.001>.
- [5] D.C. White, P.D. Nichols, A.T. Mikell, B.D. Kerger, J.M. Henson, G.G. Geesey, C. K. Clarke, Role of aerobic bacteria and their extracellular polymers in the facilitation of corrosion: use of Fourier transforming infrared spectroscopy and 'signature' phospholipid fatty acid analysis, in: S.C. Dexter (Ed.), *Biologically induced corrosion*, NACE, Houston, TX, (1986), pp. 233–243.
- [6] S.P. Kotu, A. Jayaraman, Emerging molecular techniques for studying microbial community composition and function in microbiologically influenced corrosion, *Int. Biodeter. Biodegr.* 144 (2019), <https://doi.org/10.1016/j.ibiod.2019.104722>.
- [7] D.H. Leary, L.J. Hamdan, W.J. Hervey, N. Lebedev, Z. Wang, J.R. Deschamps, A.W. Kusterbeck, G.J. Vora, Integrated metagenomic and metaproteomic analyses of marine biofilm communities (in eng), *Biofouling* 30 (10) (2014) 1211–1223, <https://doi.org/10.1080/08927014.2014.977267>.
- [8] S.M. Poulsen U.S. Thomsen Th Lundgaard, "Use of Advanced Molecular Microbiology Methods to Manage Microbial Corrosion Issues in Topside Facilities 2016 Abu Dhabi, UAE." <https://doi.org/10.2118/183526-MS>.
- [9] J.M. Suflita, A.L. Oldham, B.M. Perez-Ibarra, K. Duncan, Molecular tools to track bacteria responsible for fuel deterioration and microbiologically influenced corrosion, *Biofouling* 28 (9) (2012) 1003–1010, <https://doi.org/10.1080/08927014.2012.723695>.
- [10] S.J. Salgar-Chaparro, Complementary DNA/RNA-Based Profiling: Characterization of Corrosive Microbial Communities and Their Functional Profiles in an Oil Production Facility, *Front. Microbiol.* 10 (2019) 2587, <https://doi.org/10.3389/fmicb.2019.02587>.
- [11] S.C. Whitby, T.L. Skovhus, *Applied Microbiology and Molecular Biology in Oil Field Systems*, Conference Proceedings, Springer Publisher, 2011, <https://doi.org/10.1007/978-90-481-9252-6>.
- [12] J.L. Wood, S.A. Wade, High taxonomic diversity in ship bilges presents challenges for monitoring microbial corrosion and opportunity to utilize community functional profiling, *Appl. Environ. Microbiol.* 87 (18) (2021) e00890–21, <https://doi.org/10.1128/AEM.00890-21>.
- [13] B.J. Little, D.J. Blackwood, J. Hinks, F.M. Lauro, E. Marsili, A. Okamoto, S. A. Rice, S.A. Wade, H.-C. Flemming, Microbially influenced corrosion—Any progress? *Corros. Sci.* 170 (2020) <https://doi.org/10.1016/j.corsci.2020.108641>.
- [14] J.P.G. Stott, "What progress in the understanding of microbially induced corrosion has been made in the last 25 years? A personal viewpoint, *Corros. Sci.* 35 (1) (1993) 667–673, [https://doi.org/10.1016/0010-938X\(93\)90202-R](https://doi.org/10.1016/0010-938X(93)90202-R).
- [15] F. Mansfeld, B.J. Little, A technical review of electrochemical techniques applied to microbiologically influenced corrosion, *Corros. Sci.* 32 (3) (1991) 247–272, [https://doi.org/10.1016/0010-938X\(91\)90072-W](https://doi.org/10.1016/0010-938X(91)90072-W).
- [16] D.A. Jones B. Pitonzo P. Castro P.S. Amy Electrochemical characteristics of MIC, Conference Paper osti 509472. <https://www.osti.gov/biblio/509472>.
- [17] R. Jia, T. Unsal, D. Xu, Y. Leckbach, T. Gu, Microbiologically influenced corrosion and current mitigation strategies: a state of the art review, *Int. Biodeterior. Biodegrad.* 137 (2019) 42–58, <https://doi.org/10.1016/j.ibiod.2018.11.007>.
- [18] M. Saleem Khan, Z. Li, K. Yang, D. Xu, C. Yang, D. Liu, Y. Leckbach, E. Zhou, P. Kalnaowakulet, et al., Microbiologically influenced corrosion of titanium caused by aerobic marine bacterium *Pseudomonas aeruginosa*, *J. Mater. Sci. Technol.* 35 (1) (2019) 216–222, <https://doi.org/10.1016/j.jmst.2018.08.001>.
- [19] S. Yu, Y. Lou, D. Zhang, E. Zhou, Z. Li, C. Du, H. Qian, D. Xu, T. Gu, Microbiologically influenced corrosion of 304 stainless steel by nitrate reducing *Bacillus cereus* in simulated Beijing soil solution, *Bioelectrochemistry* 133 (2020) 107477, <https://doi.org/10.1016/j.bioelechem.2020.107477>.
- [20] E. Zhou, F. Li, D. Zhang, D. Xu, Z. Li, R. Jia, Y. Jin, H. Song, H. Li, Q. Wang, J. Wang, X. Li, T. Gu, A.M. Homborg, J.M.C. Mol, J.A. Smith, F. Wang, D. R. Lovley, Direct microbial electron uptake as a mechanism for stainless steel corrosion in aerobic environments, *Water Res* 219 (2022) 118553, <https://doi.org/10.1016/j.watres.2022.118553>.
- [21] G. Ghiara, R. Spotorno, S. Delsante, G. Tassistro, P. Piccardo, P. Cristiani, "Dezincification inhibition of a food processing brass OT60 in presence of *Pseudomonas fluorescens*, *Corros. Sci.* 157 (2019) 370–381, <https://doi.org/10.1016/j.corsci.2019.06.003>.
- [22] W. Dou, W. Cai, D. Wang, R. Jia, S. Chen, T. Gu, Electrochemical investigation of increased carbon steel corrosion via extracellular electron transfer by a sulfate reducing bacterium under carbon source starvation, *Corros. Sci.* 150 (2019) 258–267, <https://doi.org/10.1016/j.corsci.2019.02.005>.
- [23] A. Bergel, D. Féron, A. Mollica, "Catalysis of oxygen reduction in PEM fuel cell by seawater biofilm, *Electrochem. Commun.* 7 (9) (2005) 900–904, <https://doi.org/10.1016/j.elecom.2005.06.006>.
- [24] M. Mehana, R. Basseguy, M.L. Delia, B. Erable, A. Bergel, Effect of *Geobacter sulfurreducens* on the microbial corrosion of mild steel, ferritic and austenitic stainless steels, *Corros. Sci.* 51 (11) (2009) 2596–2604, <https://doi.org/10.1016/j.corsci.2009.06.041>.
- [25] S.C. Dexter, D.J. Duquette, O.W. Siebert, H.A. Videla, Use and limitations of electrochemical techniques for investigating microbiological corrosion, *Corrosion* 47 (4) (1991) 308–318, <https://doi.org/10.5006/1.3585258>.
- [26] M. Stipančević, O. Rosas, R. Basseguy, F. Turcu, Electrochemical and fractographic analysis of microbiologically assisted stress corrosion cracking of carbon steel, *Corros. Sci.* 80 (2014) 60–70, <https://doi.org/10.1016/j.corsci.2013.11.009>.
- [27] H. Venzlaff, J. Srinivasan, K.J.J. Mayrhofer, A.W. Hassel, F. Widdel, M. Stratmann, Accelerated cathodic reaction in microbial corrosion of iron due to direct electron uptake by sulfate-reducing bacteria, *Corros. Sci.* 66 (2013) 88–96, <https://doi.org/10.1016/j.corsci.2012.09.006>.
- [28] M. Moradi, Z. Sun, Z. Song, H. Hu, "Effect of proteases secreted from a marine isolated bacterium *Bacillus vietnamensis* on the corrosion behaviour of different alloys, *Bioelectrochemistry* 126 (Apr 2019) 64–71, <https://doi.org/10.1016/j.bioelechem.2018.08.003>.
- [29] M. Moradi, Z. Song, L. Yang, J. Jiang, J. He, Effect of marine *Pseudoalteromonas* sp. on the microstructure and corrosion behaviour of 2205 duplex stainless steel, *Corros. Sci.* 84 (2014) 103–112, <https://doi.org/10.1016/j.corsci.2014.03.018>.
- [30] G. Ghiara, R. Spotorno, S. Delsante, F. Formicola, A. Franzetti, P. Cristiani, Opposite corrosion behaviour of aluminum bronze induced by *Pseudomonas fluorescens* and its metabolites, *Corros. Sci.* 208 (2022) 110656, <https://doi.org/10.1016/j.corsci.2022.110656>.
- [31] F. Mansfeld, "The use of electrochemical techniques for the investigation and monitoring of microbiologically influenced corrosion and its inhibition – a review, *Mater. Corros.* 54 (7) (2003) 489–502, <https://doi.org/10.1002/maco.200390111>.
- [32] I. Beech, J.A. Sunner, Microbe–Surface interactions in biofouling and biocorrosion processes, *Int. Microbiol.* 8 (2005) 157–168. PMID: 16200494.
- [33] D.J. Beale, A.V. Karpe, S. Jadhav, T.H. Muster, E.A. Palombo, "Omics-based approaches and their use in the assessment of microbial-influenced corrosion of metals 34 (1–2) (2016) 1–15, <https://doi.org/10.1515/correv-2015-0046>.
- [34] D.J. Beale, A.V. Karpe, W. Ahmed, Beyond Metallomics: A Review of Multi-Omics-Based Approaches, in: D. Beale, K. Kouremenos, E. Palombo (Eds.), *Microbial Metallomics*, Springer, Cham., 2016, [https://doi.org/10.1007/978-3-319-46326-1\\_10](https://doi.org/10.1007/978-3-319-46326-1_10).
- [35] Y. Jin, T. Ueki, D. Zhang, Y. Fan, D. Xu, F. Wang, D.R. Lovley, "Accelerated microbial corrosion by magnetite and electrically conductive pili through direct fo-to-microbe electron transfer, *Angew. Chem. Int. Ed.* 62 (18) (2023) 2023, <https://doi.org/10.1002/anie.202309005>.
- [36] H.Q. Tianyu Cui, Weiwei Chang, Huaibei Zheng, Dawei Guo, Chi Tat Kwok, Lap Mou Tam, Dawei Zhang, "Towards understanding *Shewanella algae*-induced degradation of passive film of stainless steel based on electrochemical, XPS and multi-mode AFM analyses, *Corros. Sci.* 218 (2023) 111174, <https://doi.org/10.1016/j.corsci.2023.111174>.
- [37] Y. Gao, M. Zhang, Y. Fan, Z. Li, P. Cristiani, X. Cheng, D. Xu, F. Wang, and T. Gu, "Marine *Vibrio* spp. protect carbon steel against corrosion through secreting extracellular polymeric substances, *npj Mater. Degrad.* 6 (1) (2022), <https://doi.org/10.1038/s41529-021-00212-2>.
- [38] W.G. Characklis, Attached microbial growths—II. Frictional resistance due to microbial slimes, *Water Research* 7 (9) (1973) 1249–1258, [https://doi.org/10.1016/0043-1354\(73\)90002-X](https://doi.org/10.1016/0043-1354(73)90002-X).
- [39] P.L. Bishop, T. Yu, "A microelectrode study of redox potential change in biofilms, *Water Sci. Technol.* 39 (7) (1999) 179–185, [https://doi.org/10.1016/S0273-1223\(99\)00166-3](https://doi.org/10.1016/S0273-1223(99)00166-3).
- [40] E. Guerrini, M. Grattieri, S.P. Trasatti, M. Bestetti, P. Cristiani, "Performance explorations of single chamber microbial fuel cells by using various microelectrodes applied to biocathodes, *Int. J. Hydrog. Energy* 39 (36) (2014) 21837–21846, <https://doi.org/10.1016/j.ijhydene.2014.06.132>.
- [41] X. Bai, G.W. Luther, "Application of EIS with Au–Hg microelectrode in determining electron transfer mechanisms, *Electrochim. Acta* 51 (8–9) (2006) 1524–1533, <https://doi.org/10.1016/j.electacta.2005.02.139>.
- [42] W. Chang, Z. Li, A. Mol, D. Zhang, "Application and prospect of localized electrochemical techniques for microbiologically influenced corrosion, *Corros. Sci.* 236 (2024) 112246, <https://doi.org/10.1016/j.corsci.2024.112246>.
- [43] D. Blackwood, "An electrochemist perspective of microbiologically influenced corrosion, *Mater. Degrad.* 1 (1) (2018) 59–76, <https://doi.org/10.3390/cmd1010005>.
- [44] A. Kumar, L. Huan-Hsuan Hsu, P. Kavanagh, F. Barrière, P.N.L. Lens, L. Lapinonniere, V. Lienhard, J. H. Schröder, U. Jiang, X. Leech, D. "The ins and outs of microorganism–electrode electron transfer reactions, *Nat. Rev. Chem.* 1 (2017), <https://doi.org/10.1038/s41570-017-0024>.
- [45] P.L. Bonora, F. Deflorian, L. Fedrizzi, "Electrochemical impedance spectroscopy as a tool for investigating underpaint corrosion, *Electrochim. Acta* 41 (7) (1996) 1073–1082, [https://doi.org/10.1016/0013-4686\(95\)00440-8](https://doi.org/10.1016/0013-4686(95)00440-8).
- [46] M. Selvakumar, Bhat, LiClO4 doped cellulose acetate as biodegradable polymer electrolyte for supercapacitors, *J. Appl. Polym. Sci.* 110 (2008) 594–602, <https://doi.org/10.1002/app.28671>.
- [47] J.A. Dean, "Lange's handbook of chemistry," 1992. McGraw Hill, Inc.

- [48] N.S. Malvankar, K.P. Nevin, A.E. Franks, M.T. Tuominen, D.R. Lovley, "Electrical conductivity in a mixed-species biofilm, *Appl. Environ. Microbiol.* 78 (2012) 5967–5971, <https://doi.org/10.1128/AEM.01803-12>.
- [49] Z.M. Summers, "Direct exchange of electrons within aggregates of an evolved syntrophic coculture of anaerobic bacteria, *Science* 330 (2010) 1413–1415.
- [50] S. Malvankar, Z.M. Summers, L. Giloteaux, A.E. Rotaru, C. Rotaru, D.R. Lovley, "Potential for direct interspecies electron transfer in methanogenic wastewater digester aggregates, *mBio* 2 (2011), <https://doi.org/10.1128/mbio.00159-11>.
- [51] G.G.M. Moradi, R. Spotorno, D. Xu, P. Cristiani, "Understanding biofilm impact on electrochemical impedance spectroscopy analyses in microbial corrosion and microbial corrosion inhibition phenomena, *Electrochim. Acta* 426 (2022), <https://doi.org/10.1016/j.electacta.2022.140803>.
- [52] N.S. Malvankar, Microbial nanowires: a new paradigm for biological electron transfer and bioelectronics, *ChemSusChem* 5 (2012) 1039–1046, <https://doi.org/10.1002/cssc.201100733>.
- [53] M. Cordes, "Electron transfer in peptides and proteins, *Chem. Soc. Rev.* 38 (2009) 892–901, <https://doi.org/10.1039/b805743p>.
- [54] A. Marcus, Electron transfers in chemistry and biology, *Biochim. Biophys. Acta* 811 (1985) 265–322, [https://doi.org/10.1016/0304-4173\(85\)90014-X](https://doi.org/10.1016/0304-4173(85)90014-X).
- [55] B. Gray, Electron tunneling through proteins, *Q. Rev. Biophys.* 36 (2003) 341, <https://doi.org/10.1017/s0033583503003913>.
- [56] C. Moser, S.E. Chobot, P.L. Dutton, "Electron tunneling chains of mitochondria, *Biochim. Biophys. Acta* 1757 (2006) 1096, <https://doi.org/10.1016/j.bbabi.2006.04.015>.
- [57] H.R. Williamson, V.L. Davidson, "Mechanisms for control of biological electron transfer reactions, *Bioorg. Chem.* 57 (2014) 213–221, <https://doi.org/10.1016/j.bioorg.2014.06.006>.
- [58] H.A. Kumar, P. Kavanagh, F. Barrière, P.N.L. Lens, L. Lapinonniere, V.J. H. Lienhard, U. Schröder, X. Jiang, D. Leech, "The ins and outs of microorganism–electrode electron transfer reactions, *Nat. Rev. Chem.* 1 (2017) 0024, <https://doi.org/10.1038/s41570-017-0024>.
- [59] R.P. Buck, Electron hopping in one dimension: Mixed conductormembranes, *J. Phys. Chem.* 92 (1988) 4196–4200, <https://doi.org/10.1021/j100325a040>.
- [60] C.I. Torres, H.S. Lee, P. Parameswaran, R. Krajmalnik-Brown, B.E. Rittmann, "A kinetic perspective on extracellular electron transfer by anode-respiring bacteria, *FEMS Microbiol. Rev.* 34 (1) (2010) 3–17, <https://doi.org/10.1111/j.1574-6976.2009.00191.x>.
- [61] T.S. Sharifi-Asl, Z. Lu, G.R. Engelhardt, B. Kursten, D.D. Macdonald, Modeling of the electrochemical impedance spectroscopic behavior of passive iron using a genetic algorithm approach, *Electrochim. Acta* 102 (2013) 161–171.
- [62] J. Bao, D. Macdonald, the tunneling current, Oxidation of hydrogen on oxidized platinum at elevated temperatures, part, *J. Electroanal. Chem.* 600 (2007) 205–216, <https://doi.org/10.1016/j.jelechem.2006.07.024>.
- [63] D. Macdonald, "On the existence of our metals-based civilization: i. phase-space analysis, *J. Electrochem. Soc.* 153 (7) (2006) B213, <https://doi.org/10.1149/1.2195877>.
- [64] D.D. Macdonald, "Passivity—the key to our metals-based civilization, *Pure Appl. Chem.* 71 (6) (1999) 951–978, <https://doi.org/10.1351/pac199971060951>.
- [65] D. Macdonald, "The point defect model for the passive state, *J. Electrochem. Soc.* 139 (12) (1992) 3434, <https://doi.org/10.1149/1.2069096>.
- [66] D. Macdonald, G. Englehardt, "The point defect model for bi-layer passive films, *ECS Trans.* 28 (24) (2010) 123, <https://doi.org/10.1149/1.3496427>.
- [67] D. Macdonald, "The history of the Point Defect Model for the passive state: a brief review of film growth aspects, *Electrochim. Acta* 56 (4) (2011) 1761–1772, <https://doi.org/10.1016/j.electacta.2010.11.005>.
- [68] D. Macdonald, "Viability of hydrogen water chemistry for protecting in-vessel components of boiling water reactors, *Corrosion* 48 (03) (1992).
- [69] A.P. Lu, B. Kursten, D. Macdonald, "The irreversibility of the passive state of carbon steel in the alkaline concrete pore solution under simulated anoxic conditions, *J. Electrochem. Soc.* 162 (2015) C572–C581.
- [70] M. Bojinov, T. Laitinen, K. Makela, T. Saario, G. Sundholm, "Coupling between ionic defect structure and electronic conduction in passive films on iron, chromium and iron–chromium alloys, *Electrochim. Acta* 45 (2000) 2029.
- [71] M. Bojinov, P. Kinnunen, T. Laitinen, K. Makela, T. Saario, G. Sundholm, "Electrochemical study of the passive behaviour of Ni–Cr alloys in a borate solution – a mixed-conduction model approach, *J. Electroanal. Chem.* 504 (2001) 29.
- [72] M. Bojinov, K. Makela, T. Saario, G. Sundholm, "Conduction mechanism of the passive film on iron based on contact electric impedance and resistance measurements, *J. Electrochem. Soc.* 148 (2001) B243, <https://doi.org/10.1149/1.1371976>.
- [73] T. Fromhold, "Diffusion currents in large electric fields for discrete lattices, *J. Appl. Phys.* 38 (1967) 1546.
- [74] C.D. Lokhande, D.P. Dubal, O.-S. Joo, "Metal oxide thin film based supercapacitors, *Curr. Appl. Phys.* 11 (3) (2011) 255–270, <https://doi.org/10.1016/j.cap.2010.12.001>.
- [75] A. Mollica, E. Traverso, D. Thierry, "On oxygen reduction depolarisation induced by biofilm growth on stainless steel in sea water, *Eur. Fed. Corros. Ser., Inst. Mater.* (22) (1997) 51–63.
- [76] B.J. Little, P.A. Wagner, Application of Electrochemical Techniques to the Study of Microbiologically Influenced Corrosion, in: J.O.M. Bockris, B.E. Conway, R. E. White (Eds.), in *Modern Aspects of Electrochemistry*, Boston, MA: Springer, US, 2002, pp. 205–246.
- [77] B.J. Little, J.S. Lee, R.I. Ray, "The influence of marine biofilms on corrosion: a concise review, *Electrochim. Acta* 54 (1) (2008) 2–7, <https://doi.org/10.1016/j.electacta.2008.02.071>.
- [78] D.E. Nivens, R.J. Palmer Jr., D.C. White, "Continuous nondestructive monitoring of microbial biofilms: a review of analytical techniques," *J. Ind. Microbiol.* 15 (4) (1995) 263–276, <https://doi.org/10.1007/BF01569979>.
- [79] M. Urquidí-Macdonald, D.D. Macdonald, "Modeling mechanisms in biocorrosion, *Underst. Biocorrosion* (2014) 243–277.
- [80] S.T.Y. Ishihara, S. Motoda, Y. Suzuki, "Effect of environmental factors on ennobled electrode potential attained in natural sea water for stainless steels, *Corros. Eng.* 44 (6) (1995) 355–363.
- [81] M. Eashwar, S. Maruthamuthu, "Ennoblement of stainless alloys by marine biofilm: an alternative mechanism, *NACE Int.* (1993) 3708–3716.
- [82] A. Mollica, "Biofilm and corrosion on active-passive alloys in seawater, *Int. Biodeterior. Biodegrad.* 29 (3) (1992) 213–229, [https://doi.org/10.1016/0964-8305\(92\)90045-P](https://doi.org/10.1016/0964-8305(92)90045-P).
- [83] V. Scotto, R.D. Cintio, G. Marcenaro, "The influence of marine aerobic microbial film on stainless steel corrosion behaviour, *Corros. Sci.* 25 (3) (1985) 185–194, [https://doi.org/10.1016/0010-938X\(85\)90094-0](https://doi.org/10.1016/0010-938X(85)90094-0).
- [84] H.J. Zhang, S.C. Dexter, "Effect of biofilms on crevice corrosion of stainless steels in coastal seawater, *Corrosion* 51 (1) (1995) 56–66, <https://doi.org/10.5006/1.3293578>.
- [85] V. Scotto, M.E. Lai, "The ennoblement of stainless steels in seawater: a likely explanation coming from the field, *Corros. Sci.* 40 (6) (1998) 1007–1018, [https://doi.org/10.1016/S0010-938X\(98\)00038-9](https://doi.org/10.1016/S0010-938X(98)00038-9).
- [86] J. Landoulsi, K.E. Kirat, C. Richard, D. Feron, S.J.E.S. Pulvin, technology, *Enzym. Approach Microb. -Influ. Corros.: a Rev. Based Stainl. Steels Nat. Waters* 42 (7) (2008) 223–2242.
- [87] L. Trif, A. Shaban, J.J.C.R. Telegdi, Electrochemical and surface analytical techniques applied to microbiologically influenced corrosion investigation 36 (4) (2018) 349–363, <https://doi.org/10.1515/correv-2017-0032>.
- [88] M. Gulppi, L. MuNzon, N. Vejar, J.M. Blamery, E. Gonzales, M. Azocar, M. Sancy, P. Molina, J.H. Zagal, M.Paez, "Electrochemical dynamic sensing of hydrogen peroxide in the presence of microorganisms, *Electrochim. Acta* 305 (2019) 416–422, <https://doi.org/10.1016/j.electacta.2019.03.076>.
- [89] P. Cristiani, in: S. W. J. Chan, S. Wong Eds (Eds.), Electrochemical technologies for antifouling treatments of cooling circuits," in *Biofouling Types, Impact and Anti-Fouling*, Nova Science Pub Inc, ISBN-13: 978-1608765010, 2010, pp. 175–198.
- [90] P. Linhardt, Corrosion of metals in natural waters influenced by manganese oxidizing microorganisms, *Biodegradation* 8 (1997) 201–210 doi:10.1023/A:1008294003160.
- [91] D.A. Jones, P.S. Amy, A Thermodynamic Interpretation of Microbiologically Influenced Corrosion, *CORROSION* 58 (8) (2002) 638–645, <https://doi.org/10.5006/1.3287692>.
- [92] C. Chandrasatheesh, J. Jayapriya, R.P. George, U. Kamachi Mudali, Detection and analysis of microbiologically influenced corrosion of 316 L stainless steel with electrochemical noise technique, *Engineering Failure Analysis* 42 (2014) 133–142, <https://doi.org/10.1016/j.engfailanal.2014.04.002>. ISSN 1350-6307.
- [93] A. Padilla-Viveros, E. Garcia-Ochoa, D. Alazard, Comparative electrochemical noise study of the corrosion process of carbon steel by the sulfate-reducing bacterium *Desulfovibrio alaskensis* under nutritionally rich and oligotrophic culture conditions, *Electrochim. Acta* 51 (18) (2006) 3841–3847, <https://doi.org/10.1016/j.electacta.2005.11.001>.
- [94] M.J. Hernández Gayosso, G. Zavala Olivares, N. Ruiz Ordaz, C. Juárez Ramirez, R. García Esquivel, A. Padilla Viveros, Microbial consortium influence upon steel corrosion rate, using polarisation resistance and electrochemical noise techniques, *Electrochim. Acta* 49 (25) (2004) 4295–4301, <https://doi.org/10.1016/j.electacta.2004.03.038>.
- [95] A.M. Homborg, C.F. Leon Morales, T. Tinga, J.H.W. de Wit, J.M.C. Mol, "Detection of microbiologically influenced corrosion by electrochemical noise transients, *Electrochim. Acta* 136 (2014) 223–232, <https://doi.org/10.1016/j.electacta.2014.05.102>.
- [96] M. Stipanicev, F. Turcu, L. Esnault, O. Rosas, R. Basseguy, M. Sztyler, I.B. Beech, "Corrosion of carbon steel by bacteria from North Sea offshore seawater injection systems: laboratory investigation, *Bioelectrochemistry* 97 (Jun 2014) 76–88, <https://doi.org/10.1016/j.bioelechem.2013.09.006>.
- [97] W. Nogala, M. Burchardt, M. Opallo, J. Rogalski, G. Wittstock, "Scanning electrochemical microscopy study of laccase within a sol-gel processed silicate film, *Bioelectrochemistry* 72 (2) (Apr 2008) 174–182, <https://doi.org/10.1016/j.bioelechem.2008.01.010>.
- [98] V.M.R. Oltra, R. Akid, P. Marcus, Local probe techniques for corrosion research, Editors: R Oltra, V Maurice, R Akid, P. Marcus, EFC 'Green. Book 45 (2007). ISBN: 9781845692360.
- [99] D. Fix, E.V. Skorb, D.G. Shchukin, H. Möhwal, "Quantitative analysis of scanning electric current density and pH-value observations in corrosion studies, *Meas. Sci. Technol.* 22 (7) (2011), <https://doi.org/10.1088/0957-0233/22/7/075704>.
- [100] M.J. Franklin, D.C. White, H.S. Isaacs, "Pitting corrosion by bacteria on carbon steel, determined by the scanning vibrating electrode technique, *Corros. Sci.* 32 (9) (1991) 945–952, [https://doi.org/10.1016/0010-938X\(91\)90014-G](https://doi.org/10.1016/0010-938X(91)90014-G).
- [101] H. Krawiec, V. Vignal, R. Oltra, "Use of the electrochemical microcell technique and the SVET for monitoring pitting corrosion at MnS inclusions, *Electrochem. Commun.* 6 (7) (2004) 655–660, <https://doi.org/10.1016/j.elecom.2004.05.001>.
- [102] M. Refass, R. Sabot, M. Jeannin, C. Berziou, P. Refait, "Effects of phosphate species on localised corrosion of steel in NaHCO<sub>3</sub>+NaCl electrolytes, *Electrochim. Acta* 54 (18) (2009) 4389–4396, <https://doi.org/10.1016/j.electacta.2009.03.014>.
- [103] R. Souto, J. Izquierdo, J.J. Santana, S. González, "Scanning microelectrochemical techniques: a highly sensitive route to evaluate degradation reactions and

- protection methods with chemical selectivity", *Eur. J. Sci. Theol.* 9 (04/01 2013) 71–89.
- [104] H. Uchida, M. Yamashita, S. Inoue, K.J.M.S. Koterazawa, In-situ observations of crack nucleation and growth during stress corrosion by scanning vibrating electrode technique, *Materials Science and Engineering: A*, Volumes 319–321 (2001) 496–500, [https://doi.org/10.1016/S0921-5093\(01\)01011-5](https://doi.org/10.1016/S0921-5093(01)01011-5).
- [105] B. Vuillemin, X. Philippe, R. Oltra, V. Vignal, L. Coudreuse, L.C. Dufour, and E. Finot, "SVET, AFM and AES study of pitting corrosion initiated on MnS inclusions by microinjection", *Corros. Sci.* 45 (2003) 1143–1159, [https://doi.org/10.1016/S0010-938X\(02\)00222-6](https://doi.org/10.1016/S0010-938X(02)00222-6).
- [106] Z. Guo, T. Liu, Y.F. Cheng, N. Guo, Y. Yin, "Adhesion of *Bacillus subtilis* and *Pseudoalteromonas lipolytica* to steel in a seawater environment and their effects on corrosion, *Colloids Surf. B Biointerfaces* 157 (Sep 1 2017) 157–165, <https://doi.org/10.1016/j.colsurfb.2017.05.045>.
- [107] H. Iken, L. Etcheverry, A. Bergel, R. Basseguy, Local analysis of oxygen reduction catalysis by scanning vibrating electrode technique: A new approach to the study of biocorrosion, *Electrochim. Acta* 54 (1) (2008) 60–65, <https://doi.org/10.1016/j.electacta.2008.02.120>.
- [108] I. Ziadi, M.M. Alves, M. Taryba, L. El-Bassi, H. Hassairi, L. Bousselmi, M. F. Montemor, H. Akrouf, Microbiologically influenced corrosion mechanism of 304L stainless steel in treated urban wastewater and protective effect of silane-TiO<sub>2</sub> coating, *Bioelectrochemistry* 132 (2020) 107413, <https://doi.org/10.1016/j.bioelechem.2019.107413>.
- [109] M. Rohwerder, F. Turcu, "High-resolution Kelvin probe microscopy in corrosion science: scanning Kelvin probe force microscopy (SKPFM) versus classical scanning Kelvin probe (SKP)", *Electrochim. Acta* 53 (2) (2007) 290–299, <https://doi.org/10.1016/j.electacta.2007.03.016>.
- [110] B. Liu, M. Sun, F. Lu, C. Du, X. Li, "Study of biofilm-influenced corrosion on X80 pipeline steel by a nitrate-reducing bacterium, *Bacillus cereus*, in artificial Beijing soil, *Colloids Surf. B Biointerfaces* 197 (Jan 2021) 111356, <https://doi.org/10.1016/j.colsurfb.2020.111356>.
- [111] C. Örnek, C. Leygraf, J. Pan, "Passive film characterisation of duplex stainless steel using scanning Kelvin probe force microscopy in combination with electrochemical measurements, *npj Mater. Degrad.* 3 (1) (2019), <https://doi.org/10.1038/s41529-019-0071-8>.
- [112] B. Liu, Z. Li, X. Yang, C. Du, X. Li, "Microbiologically influenced corrosion of X80 pipeline steel by nitrate reducing bacteria in artificial Beijing soil, *Bioelectrochemistry* 135 (Oct 2020) 107551, <https://doi.org/10.1016/j.bioelechem.2020.107551>.
- [113] W. Wang, X. Zhang, J. Wang, "Heterogeneous electrochemical characteristics of biofilm/metal interface and local electrochemical techniques used for this purpose, *Mater. Corros.* 60 (12) (2009) 957–962, <https://doi.org/10.1002/maco.200905227>.
- [114] A. Davoodi, J. Pan, C. Leygraf, S. Norgren, "Integrated AFM and SECM for in situ studies of localized corrosion of Al alloys, *Electrochim. Acta* 52 (27) (2007) 7697–7705, <https://doi.org/10.1016/j.electacta.2006.12.073>.
- [115] A. Maljusch, C. Senöz, M. Rohwerder, W. Schuhmann, "Combined high resolution Scanning Kelvin probe—scanning electrochemical microscopy investigations for the visualization of local corrosion processes, *Electrochim. Acta* 82 (2012) 339–348, <https://doi.org/10.1016/j.electacta.2012.05.134>.
- [116] C. Senöz, A. Maljusch, M. Rohwerder, W. Schuhmann, "SECM and SKPFM Studies of the local corrosion mechanism of Al alloys - a pathway to an integrated SKP-SECM system, *Electroanalysis* 24 (2) (2012) 239–245, <https://doi.org/10.1002/elan.201100609>.
- [117] A. Maljusch, B. Schönberger, A. Lindner, M. Stratmann, M. Rohwerder, W. Schuhmann, "Integrated scanning Kelvin probe-scanning electrochemical microscope system: development and first applications," (in eng), *Anal. Chem.* 83 (15) (Aug 1 2011) 6114–6120, <https://doi.org/10.1021/ac200953b>.
- [118] A. Nazarov, N. Le Bozec, D. Thierry, "Scanning Kelvin Probe assessment of steel corrosion protection by marine paints containing Zn-rich primer, *Prog. Org. Coat.* 125 (2018) 61–72, <https://doi.org/10.1016/j.porgcoat.2018.08.024>.
- [119] L. Iannucci, P. Cristiani, R. Ferrero, E. Angelini, S. Grassini, "A novel approach for microbial corrosion assessment," *IEEE Transactions on Instrumentation and Measurement*, vol. 68, no. 5, IEEE1570417904, pp. 1424–1431, doi: <https://doi.org/10.1109/TIM.2019.2905734>.
- [120] J. L. B. Little, Jason Lee "Microbiologically Influenced Corrosion " in *International Materials Reviews*, 2009 DOI: 10.1002/0471238961.micrlitt.a01.
- [121] F. Allen-J. Bard, L.R. Faulkner, *ELECTROCHEMICAL METHODS Fundamentals and Applications* (2000), John Wiley & Sons, 978-0-471-04372-0.
- [122] J.L. Trompette, L. Massot, "Chronoamperometric study of the passive behaviour of tantalum in hostile media during water addition, *Corros. Sci.* 57 (2012) 174–181, <https://doi.org/10.1016/j.corsci.2011.12.020>.
- [123] A. Mollica, P. Cristiani, On-line biofilm monitoring by electrochemical probe BIOX, *IWA J. Water Technol.* 47 (5) (2003) 45–49, <https://doi.org/10.2166/wst.2003.0277>.
- [124] P. Cristiani, G. Perboni, Corrosion monitoring in microbial environments, Editor (s): Lietai Yang, In Woodhead Publishing Series in: Metals and Surface Engineering, Techniques for Corrosion Monitoring, Second Edition, Woodhead Publishing, ISBN 9780081030035, 2021, pp. 335–377. <https://doi.org/10.1016/B978-0-08-103003-5.00015-1>.
- [125] P. Cristiani, A. Franzetti, G. Bestetti, "Monitoring of electro-active biofilm in soil, *Electrochim. Acta* 54 (1) (2008) 41–46, <https://doi.org/10.1016/j.electacta.2008.01.107>.
- [126] G. Licina, G. Nekoksa, and R. Howard, "An Electrochemical Method for On-Line Monitoring of Biofilm Activity in Cooling Water Using the BioGEORGE™ Probe." *Microbiologically Influenced Corrosion Testing*. Ed. Kearns, J., & Little, B. 100 Barr Harbor Drive, PO Box C700, West Conshohocken, PA 19428-2959: ASTM International, 1994.
- [127] G. Pavanello, A. Mollica, M. Faimali, "Wrapped by bacteria: biofilm detection and removal in paper mills", *Journal of science & technology for forest products and processes (Online)* 6 (4), pp. 6–12. WOS:000422806400002.
- [128] P. Cristiani, "Risk assessment of biocorrosion in condensers, pipework and other cooling system components", in *Understanding Biocorrosion: Fundamentals and Applications*, Ed. T. Liengen, R. Basseguy, D. Feron, I. Beech, V. Birrien, EFC book n. 66, 2014, 357–384, DOI:10.1533/9781782421252.3.357.
- [129] P. Cristiani, G. Perboni, Antifouling strategies and corrosion control in cooling circuits, *Bioelectrochem.* 97 (2014) 120–126, <https://doi.org/10.1016/j.bioelechem.2014.01.002>.
- [130] L. Yu, J. Duan, X. Du, Y. Huang, B. Hou, "Accelerated anaerobic corrosion of electroactive sulfate-reducing bacteria by electrochemical impedance spectroscopy and chronoamperometry, *Electrochem. Commun.* 26 (2013) 101–104, <https://doi.org/10.1016/j.elecom.2012.10.022>.
- [131] I. Rouvre, R. Basseguy, "Exacerbation of the mild steel corrosion process by direct electron transfer between [Fe-Fe]-hydrogenase and material surface, *Corros. Sci.* 111 (2016) 199–211, <https://doi.org/10.1016/j.corsci.2016.05.005>.
- [132] C. Dumas, R. Basseguy, A. Bergel, Electrochemical activity of *Geobacter sulfurreducens* biofilms on stainless steel anodes, *Electrochimica Acta* 53 (2008) 5235–5241, <https://doi.org/10.1016/j.electacta.2008.02.056>.
- [133] C. Dumas, A. Mollica, D. Féron, R. Basséguy, L. Etcheverry, A. Bergel, "Marine microbial fuel cell: Use of stainless steel electrodes as anode and cathode materials, *Electrochim. Acta* 53 (2) (2007) 468–473, <https://doi.org/10.1016/j.electacta.2007.06.069>.
- [134] A.A. Karbelkar, A.R. Rowe, M.Y. El-Naggar, "An electrochemical investigation of interfacial electron uptake by the sulfur oxidizing bacterium *Thiohalobacterium electrotropha* EIOx9, *Electrochim. Acta* 324 (2019), <https://doi.org/10.1016/j.electacta.2019.134838>.
- [135] A. Krige, K. Ramser, M. Sjoblom, P. Christakopoulos, U. Rova, "A New Approach for evaluating electron transfer dynamics by using in situ resonance raman microscopy and chronoamperometry in conjunction with a dynamic model, *Appl. Environ. Microbiol.* 86 (20) (Oct 1 2020), <https://doi.org/10.1128/AEM.01535-20>.
- [136] P. Liu, P. Liang, Y. Jiang, W. Hao, B. Miao, D. Wang, X. Huang, "Stimulated electron transfer inside electroactive biofilm by magnetite for increased performance microbial fuel cell, *Appl. Energy* 216 (2018) 382–388, <https://doi.org/10.1016/j.apenergy.2018.01.073>.
- [137] D.R. Lovley, "Microbial fuel cells: novel microbial physiologies and engineering approaches, *Curr. Opin. Biotechnol.* 17 (3) (Jun 2006) 327–332, <https://doi.org/10.1016/j.copbio.2006.04.006>.
- [138] S. Parot, M.L. Delia, A. Bergel, "Forming electrochemically active biofilms from garden compost under chronoamperometry, *Bioresour. Technol.* 99 (11) (Jul 2008) 4809–4816, <https://doi.org/10.1016/j.biortech.2007.09.047>.
- [139] Y. Yi, T. Zhao, B. Xie, Y. Zang, H. Liu, "Dual detection of biochemical oxygen demand and nitrate in water based on bidirectional *Shewanella loihica* electron transfer, *Bioresour. Technol.* 309 (Aug 2020) 123402, <https://doi.org/10.1016/j.biortech.2020.123402>.
- [140] D.B. Matthews, "The Stern-Geary and related methods for determining corrosion rates", *Australian Journal of Chemistry* 28 (2) (1975) 243–251, <https://doi.org/10.1071/CH9750243>.
- [141] C. Andrade, C. Alonso, Test methods for on-site corrosion rate measurement of steel reinforcement in concrete by means of the polarization resistance method, *Mat. Struct.* 37 (2004) 623–643, <https://doi.org/10.1007/BF02483292>.
- [142] I. Epelboin, C. Gabrielli, M. Keddam, H. Takenouti, Alternating-current impedance measurements applied to corrosion studies and corrosion-rate determination, in *Electrochemical corrosion testing*, ASTM International (1981). <https://doi.org/10.1520/STP28031S>.
- [143] M.R. Di Wang, Sith Kumseranee, Suchada Punpruk, Tingyue Gu, "Mitigating microbiologically influenced corrosion of an oilfield biofilm consortium on carbon steel in enriched hydrotest fluid using 2,2-dibromo-3-nitropropionamide (DBNPA) enhanced by a 14-mer peptide, *J. Mater. Sci. Technol.* 57 (2020) 146–152, <https://doi.org/10.1016/j.jmst.2020.02.087>.
- [144] P. Cristiani, G. Perboni, Corrosion monitoring in microbial environments, in *Techniques for Corrosion Monitoring* L. Yang ed., (Second Edition), Woodhead Publishing Series in Metals and Surface Engineering, pp 335-377, 2021, ISBN: 9780081030035. <https://doi.org/10.1016/B978-0-08-103003-5.00015-1>.
- [145] I.B. Obot, I.B. Onyeachu, "Electrochemical frequency modulation (EFM) technique: Theory and recent practical applications in corrosion research, *J. Mol. Liq.* 249 (2018) 83–96, <https://doi.org/10.1016/j.molliq.2017.11.006>.
- [146] A. Gonzalez, M.L. Escudero, C. Andrade, Errors in the electrochemical evaluation of very small corrosion rates—I. Polarization resistance method applied to corrosion of steel in concrete, *Corros. Sci.* 25 (10) (1985) 917–930. [https://doi.org/10.1016/0010-938X\(85\)90021-6](https://doi.org/10.1016/0010-938X(85)90021-6).
- [147] P. Cristiani, G. Perboni, A. Debenedetti, "Effect of chlorination on the corrosion of Cu/Ni 70/30 condenser tubing, *Electrochim. Acta* 54 (1) (2008) 100–107, <https://doi.org/10.1016/j.electacta.2008.05.081>.
- [148] M. Mehanna, R. Basseguy, M.-L. Delia, A. Bergel, "Role of direct microbial electron transfer in corrosion of steels, *Electrochem. Commun.* 11 (3) (2009) 568–571, <https://doi.org/10.1016/j.elecom.2008.12.019>.
- [149] D. Wang, P. Kijlka, A.M. Saleh, S. Kumseranee, S. Punpruk, T. Gu, "Tafel scan schemes for microbiologically influenced corrosion of carbon steel and stainless steel", *J. Mater. Sci. Technol.* 130 (2022) 193–197.
- [150] M. Mehanna, R. Basseguy, M.-L. Delia, R. Gubner, N. Sathirachinda, A. Bergel, "Geobacter species enhances pit depth on 304L stainless steel in a medium lacking

- with electron donor, *Electrochem. Commun.* 11 (7) (2009) 1476–1481, <https://doi.org/10.1016/j.elecom.2009.05.035>.
- [151] M. Mehanna, R. Basséguy, M.-L. Délia, A. Bergel, "Geobacter sulfurreducens can protect 304L stainless steel against pitting in conditions of low electron acceptor concentrations, *Electrochem. Commun.* 12 (6) (2010) 724–728, <https://doi.org/10.1016/j.elecom.2010.03.017>.
- [152] S. Li, L. Li, Q. Qu, Y. Kang, B. Zhu, D. Yu, R. Huang, Extracellular electron transfer of *Bacillus cereus* biofilm and its effect on the corrosion behaviour of 316L stainless steel, *Colloids Surf. B Biointerfaces* 173 (2019) 139–147, <https://doi.org/10.1016/j.colsurfb.2018.09.059>.
- [153] D. Liang, W. He, C. Li, Y. Yu, Z. Zhang, N. Ren, Y. Feng, "Bidirectional electron transfer biofilm assisted complete bioelectrochemical denitrification process, *Chem. Eng. J.* 375 (2019), <https://doi.org/10.1016/j.cej.2019.121960>.
- [154] S. Parot, I. Vandecastelle, A. Courmet, M. Delia, P. Vandamme, M. Berge, C. Roques, A. Bergel, Catalysis of the electrochemical reduction of oxygen by bacteria isolated from electro-active biofilms formed in seawater, *Bioresour. Technol.* 102 (1) (2011) 304–311, <https://doi.org/10.1016/j.biortech.2010.06.157>.
- [155] M. Olliot, P. Chong, B. Erable, A. Bergel, "Influence of the electrode size on microbial anode performance, *Chem. Eng. J.* 327 (2017) 218–227, <https://doi.org/10.1016/j.cej.2017.06.044>.
- [156] D. Baron, E. LaBelle, D. Coursolle, J.A. Gralnick, D.R. Bond, "Electrochemical measurement of electron transfer kinetics by *Shewanella oneidensis* MR-1, *J. Biol. Chem.* 284 (42) (Oct 16 2009) 28865–28873, <https://doi.org/10.1074/jbc.M109.043455>.
- [157] P.F. Beese-Vasbender, S. Nayak, A. Erbe, M. Stratmann, K.J.J. Mayrhofer, "Electrochemical characterization of direct electron uptake in electrical microbially influenced corrosion of iron by the lithoautotrophic SRB *Desulfopila corrodens* strain IS4, *Electrochim. Acta* 167 (2015) 321–329, <https://doi.org/10.1016/j.electacta.2015.03.184>.
- [158] F. Guan, Z. Liu, X. Dong, X. Zhu, B.B. Zhang, J. Duan, N. Wang, Y. Gao, L. Yang, B. Hou, Synergistic effect of carbon starvation and exogenous redox mediators on corrosion of X70 pipeline steel induced by *Desulfovibrio singaporensis*, *Sci. Total Environ.* 788 (2021) 147573, <https://doi.org/10.1016/j.scitotenv.2021.147573>.
- [159] C.W. Marshall, H.D. May, "Electrochemical evidence of direct electrode reduction by a thermophilic Gram-positive bacterium, *Thermincola ferriacetica*, *Energy Environ. Sci.* 2 (6) (2009), <https://doi.org/10.1039/b823237g>.
- [160] P. Winaikij, P. Sreearunthai, K. Sombatmankhong, "Probing mechanisms for microbial extracellular electron transfer (EET) using electrochemical and microscopic characterisations, *Solid State Ion.* 320 (2018) 283–291, <https://doi.org/10.1016/j.ssi.2018.02.044>.
- [161] B. Zhang, H.Y. Cheng, A. Wang, "Extracellular electron transfer through visible light induced excited-state outer membrane C-type cytochromes of *Geobacter sulfurreducens*, *Bioelectrochemistry* 138 (Apr 2021) 107683, <https://doi.org/10.1016/j.bioelechem.2020.107683>.
- [162] J. Zhang, Q. Sun, H. Tang, Y. Qian, Y. Chen, X. Shan, X. Liu, H. Gu, "The direct electrochemistry of viable *Escherichia coli*, *J. Electroanal. Chem.* 895 (2021), <https://doi.org/10.1016/j.jelechem.2021.115426>.
- [163] E. Roubaud, R. Lacroix, S. Da Silva, J. Esvan, L. Etcheverry, A. Bergel, R. Basseguy, B. Erable, "Industrially scalable surface treatments to enhance the current density output from graphite bioanodes fueled by real domestic wastewater", *iScience* 24 (3) (2021) <https://doi.org/10.1016/j.isci.2021.102162>.
- [164] C. Gabrielli, M. Keddah, H. Takenouti, 7 - The Use of a.c. Techniques in the Study of Corrosion and Passivity," in *Treatise on Materials*, in: J.C. Scully (Ed.), Science and Technology 23, Elsevier, 1983, pp. 395–451, <https://doi.org/10.1016/B978-0-12-633670-2.50012-7>.
- [165] R. Chen, J. Hu, Y. Ma, W. Guo, H. Huang, J. Wei, S. Yin, Q. Yu, Characterization of the passive film formed on the reinforcement surface in alkali activated fly ash: surface analysis and electrochemical evaluation, *Corros. Sci.* 165 (2020), <https://doi.org/10.1016/j.corsci.2019.108393>.
- [166] B. Guitián, X.R. Nóvoa, B. Puga, "Electrochemical Impedance Spectroscopy as a tool for materials selection: water for haemodialysis, *Electrochim. Acta* 56 (23) (2011) 7772–7779, <https://doi.org/10.1016/j.electacta.2011.03.055>.
- [167] H. Mahmoud, M. Sánchez, M.C. Alonso, "Ageing of the spontaneous passive state of 2304 duplex stainless steel in high-alkaline conditions with the presence of chloride, *J. Solid State Electrochem.* 19 (10) (2015) 2961–2972, <https://doi.org/10.1007/s10008-015-2908-6>.
- [168] B. Munirathinam, R. Narayanan, L. Neelakantan, "Electrochemical and semiconducting properties of thin passive film formed on titanium in chloride medium at various pH conditions, *Thin Solid Films* 598 (2016) 260–270, <https://doi.org/10.1016/j.tsf.2015.12.025>.
- [169] M. Oje, A.A. Ogwu, S.U. Rahman, A.I. Oje, N. Tsendzughul, "Effect of temperature variation on the corrosion behaviour and semiconducting properties of the passive film formed on chromium oxide coatings exposed to saline solution, *Corros. Sci.* 154 (2019) 28–35, <https://doi.org/10.1016/j.corsci.2019.04.004>.
- [170] H. Zhang, C. Man, L. Wang, C. Dong, L. Wang, D. Kong, X. Wang, Different corrosion behaviors between  $\alpha$  and  $\beta$  phases of Ti6Al4V in fluoride-containing solutions: Influence of alloying element Al, *Corros. Sci.* 169 (2020), <https://doi.org/10.1016/j.corsci.2020.108605>.
- [171] E. Huttunen-Saarivirta, M. Bomberg, L. Carpen, "EIS study on aerobic corrosion of copper in ground water: influence of micro-organisms, *Electrochim. Acta* 240 (2017) 163–174, <https://doi.org/10.1016/j.electacta.2017.04.073>.
- [172] A. Naguib, F. Mansfeld, "Evaluation of microbially influenced corrosion inhibition (MICI) with EIS and ENA, *Electrochim. Acta* 47 (13) (2002) 2319–2333, [https://doi.org/10.1016/S0013-4686\(02\)00082-8](https://doi.org/10.1016/S0013-4686(02)00082-8).
- [173] M.E. Orazem, B. Tribollet, "An integrated approach to electrochemical impedance spectroscopy, *Electrochim. Acta* 53 (25) (2008) 7360–7366, <https://doi.org/10.1016/j.electacta.2007.10.075>.
- [174] Z. Stoynov, Differential impedance analysis: insight into the experimental data, *Polish Journal of Chemistry* 71 (1997) 1204–1210. <https://api.semanticscholar.org/CorpusID:102159719>.
- [175] Z.B. Stoynov, D.E. Vladikova, MEASUREMENT METHODS Electrochemical: Impedance Spectroscopy, J. Garche, Encyclopedia of Electrochemical Power Sources (2009) 632–642, <https://doi.org/10.1016/B978-0-44452745-5.00068-X>. Elsevier.
- [176] J.R. Macdonald, L. Potter, A flexible procedure for analyzing impedance spectroscopy results: Description and illustrations, *Solid State Ionics* 24 (1) (1987) 61–79, [https://doi.org/10.1016/0167-2738\(87\)90068-3](https://doi.org/10.1016/0167-2738(87)90068-3).
- [177] S. Werwinski, J.A. Wharton, M. Nie, K.R. Stokes, "Electrochemical sensing and characterization of aerobic marine bacterial biofilms on gold electrode surfaces, *ACS Appl. Mater. Interfaces* 13 (27) (2021) 31393–31405, <https://doi.org/10.1021/acsami.1c02669>.
- [178] S. Werwinski, J.A. Wharton, M. Nie, K.R. Stokes, "Monitoring aerobic marine bacterial biofilms on gold electrode surfaces and the influence of nitric oxide attachment control, *Anal. Chem.* 94 (36) (2022) 12323–12332, <https://doi.org/10.1021/acs.analchem.2c00934>.
- [179] I.B. Beech, J.A. Sunner, C.R. Arciola, P. Cristiani, "Microbially-influenced corrosion: damage to prostheses, delight for bacteria," (in eng), *Int J. Artif. Organs* 29 (4) (Apr 2006) 443–452, <https://doi.org/10.1177/039139880602900415>.
- [180] Z. He, F. Mansfeld, "Exploring the use of electrochemical impedance spectroscopy (EIS) in microbial fuel cell studies, *Energy Environ. Sci.* 2 (2) (2009) 215–219, <https://doi.org/10.1039/b814914c>.
- [181] F. Zhao, R.C. Slade, J.R. Varcoe, "Techniques for the study and development of microbial fuel cells: an electrochemical perspective, *Chem. Soc. Rev.* 38 (7) (Jul 2009) 1926–1939, <https://doi.org/10.1039/b819866g>.
- [182] Y. Zhao, E. Zhou, Y. Liu, S. Liao, Z. Li, D. Xu, T. Zhang, and T. Gu, "Comparison of different electrochemical techniques for continuous monitoring of the microbially influenced corrosion of 2205 duplex stainless steel by marine *Pseudomonas aeruginosa* biofilm, *Corros. Sci.* 126 (2017) 142–151, <https://doi.org/10.1016/j.corsci.2017.06.024>.
- [183] C.M. Abreu, R. Losada, X.R. Nóvoa, G. Pena, M.C. Pérez, "High frequency impedance spectroscopy study of passive films formed on AISI 316 stainless steel in alkaline medium, *J. Electroanal. Chem.* 572 (2) (2004) 335–345, <https://doi.org/10.1016/j.jelechem.2004.01.015>.
- [184] S. Chakri, I. Frateur, M.E. Orazem, E.M.M. Sutter, T.T.M. Tran, B. Tribollet, V. Vivier, Improved EIS Analysis of the Electrochemical Behaviour of Carbon Steel in Alkaline Solution, *Electrochimica, Acta* 246 (2017) 924–930, <https://doi.org/10.1016/j.electacta.2017.06.096>.
- [185] S. Chakri, A.N. Patel, I. Frateur, F. Kanoufi, E.M.M. Sutter, T.T.M. Tran, B. tribollet, V. Vivier, Imaging of a Thin Oxide Film Formation from the Combination of Surface Reflectivity and Electrochemical Methods," (in eng), *Anal. Chem.* 89 (10) (2017) 5303–5310, <https://doi.org/10.1021/acs.analchem.6b04921>.
- [186] A. Fattah-alhosseini, "Passivity of AISI 321 stainless steel in 0.5M H2SO4 solution studied by Mott-Schottky analysis in conjunction with the point defect model, *Arab. J. Chem.* 9 (2016) S1342–S1348, <https://doi.org/10.1016/j.arabjc.2012.02.015>.
- [187] M.J. Carmezim, M.F. Montemor, M.D. Cunha Belo, Capacitance behaviour of passive films on ferritic and austenitic stainless steel, *Corros. Sci.* 47 (2005) 581–591, <https://doi.org/10.1016/j.corsci.2004.07.002>.
- [188] V.M.P. Marcus, Electrochemical impedance spectroscopy: a tool for the investigation of passive layers and localized corrosion processes, *J. Electroanal. Chem.* 357 (1993) 191–207, <https://doi.org/10.21577/1984-6835.20200123>.
- [189] M. Eashwar, A. Lakshman Kumar, R. Hariharasathan, J. Kennedy, "The enrichment of surface passive film on stainless steel during biofilm development in coastal seawater, *Biofouling* 31 (6) (2015) 511–525, <https://doi.org/10.1080/08927014.2015.1062476>.
- [190] Z. Li, W. Chang, T. Cui, D. Xu, D. Zhang, Y. Lou, H. Qian, H. Song, A.M. Mol, F. Ceo, T. Gu, X. Li, "Adaptive bidirectional extracellular electron transfer during accelerated microbially influenced corrosion of stainless steel, *Commun. Mater.* 2 (1) (2021), <https://doi.org/10.1038/s43246-021-00173-8>.
- [191] Y. Lou, C. Dai, W. Chank, H. Qian, L. Huang, C. Du, D. Zhang "Microbiologically influenced corrosion of FeCoCrNiMo0.1 high-entropy alloys by marine *Pseudomonas aeruginosa*" *Corros. Sci.* 165202010.1016/j.corsci.2019.108390.
- [192] H. Qian, L. Ma, D. Zhang, Z. Li, L. Huang, Y. Lou, and C. Du, "Microbiologically influenced corrosion of 304 stainless steel by halophilic archaea *Natronorubrum tibetense*, *J. Mater. Sci. Technol.* 46 (2020) 12–20, <https://doi.org/10.1016/j.jmst.2019.04.047>.
- [193] L. Pons, M.-L. Délia, R. Basséguy, A. Bergel, "Effect of the semi-conductive properties of the passive layer on the current provided by stainless steel microbial cathodes, *Electrochim. Acta* 56 (6) (2011) 2682–2688, <https://doi.org/10.1016/j.electacta.2010.12.039>.
- [194] P. Slepiski, M.M. Solomon, S.A. Umoren. Application of Dynamic Electrochemical Impedance Spectroscopy Technique in Corrosion and Corrosion-Inhibition Studies," in *Corrosion Science Theoretical and Practical Applications*, CRS Press, 2024, pp. 519–540, <https://doi.org/10.1201/9781003328513-18>.
- [195] K. Darowicki, P. Ślepiski, M. Szociński, "Application of the dynamic EIS to investigation of transport within organic coatings, *Prog. Org. Coat.* 52 (4) (2005) 306–310, <https://doi.org/10.1016/j.porgcoat.2004.06.007>.

- [196] H. Gerengi, "The use of dynamic electrochemical impedance spectroscopy in corrosion inhibitor studies, *Prot. Met. Phys. Chem. Surf.* 54 (3) (2018) 536–540, <https://doi.org/10.1134/S2070205118030267>.
- [197] A. Rauf, W.F. Bogaerts, "Employing electrochemical frequency modulation for pitting corrosion, *Corros. Sci.* 52 (9) (2010) 2773–2785, <https://doi.org/10.1016/j.corsci.2010.04.016>.
- [198] R.W. Bosch, J. Hubrecht, W.F. Bogaerts, B.C. Syrett, "Electrochemical frequency modulation: a new electrochemical technique for online corrosion monitoring, *Corrosion* 57 (1) (2001) 60–70, <https://doi.org/10.5006/1.3290331>.
- [199] M. Moradi, J. Li, W. Liu, D. Xu, F. Wang, "Inhibitory effect of *Vibrio neocaledinococcus* sp. and *Pseudoalteromonas piscicida* dual-species biofilms on the corrosion of carbon steel, *Acta Metall. Sin. (Engl. Lett.)* 35 (4) (2021) 551–562, <https://doi.org/10.1007/s40195-021-01295-1>.
- [200] P. Beese, H. Venzlaff, J. Srinivasan, J. Garrelfs, M. Stratmann, K.J.J. Mayrhofer, "Monitoring of anaerobic microbially influenced corrosion via electrochemical frequency modulation, *Electrochim. Acta* 105 (2013) 239–247, <https://doi.org/10.1016/j.electacta.2013.04.144>.
- [201] R.S. Lillard, "A novel method for generating quantitative local electrochemical impedance spectroscopy, *J. Electrochem. Soc.* 139 (4) (1992) doi: DOI 10.1149/1.2069332.
- [202] O. Gharbi, K. Ngo, M. Turmine, V. Vivier, "Local electrochemical impedance spectroscopy: a window into heterogeneous interfaces, *Curr. Opin. Electrochem.* 20 (2020) 1–7, <https://doi.org/10.1016/j.coelec.2020.01.012>.
- [203] N. Jadhav, V.J. Gelling, "Review—the use of localized electrochemical techniques for corrosion studies, *J. Electrochem. Soc.* 166 (11) (2019) C3461–C3476, <https://doi.org/10.1149/2.0541911jes>.
- [204] A.J. Bard, M.V. Mirkin. *Scanning Electrochemical Microscopy*, 2nd edition, CRC Press, 2012, p. 670, <https://doi.org/10.1201/b11850>.
- [205] C. Batchelor-McAuley, E.J. Dickinson, N.V. Rees, K.E. Toghill, R.G. Compton, *New electrochemical methods*, *Anal. Chem.* 84 (2) (2012) 669–684, <https://doi.org/10.1021/ac2026767>.
- [206] H. Qian, D. Zhang, T. Cui, W. Chang, F. Cao, C. Du, X. Li, "Accelerating effect of catalase on microbiologically influenced corrosion of 304 stainless steel by the halophilic archaeon *Natronorubrum tibetense*", *Corros. Sci.* 178 (2021) <https://doi.org/10.1016/j.corsci.2020.109057>.
- [207] J. Zhang, T. Zhu, J. Lang, W. Fu, F. Li, "Recent advances of scanning electrochemical microscopy and scanning ion conductance microscopy for single-cell analysis, *Curr. Opin. Electrochem.* 22 (2020) 178–185, <https://doi.org/10.1016/j.coelec.2020.06.001>.
- [208] G. Caniglia, C. Kranz, "Scanning electrochemical microscopy and its potential for studying biofilms and antimicrobial coatings, *Anal. Bioanal. Chem.* 412 (24) (2020) 6133–6148, <https://doi.org/10.1007/s00216-020-02782-7>.
- [209] K.B. Holt, A.J. Bard, "Interaction of Silver(I) ions with the respiratory chain of *Escherichia coli*: an electrochemical and scanning electrochemical microscopy study of the antimicrobial mechanism of micromolar Ag<sup>+</sup>, *Biochemistry* 44 (39) (2005) 13214–13223, <https://doi.org/10.1021/bi0508542>.
- [210] K. Nagamine, T. Kaya, T. Yasukawa, H. Shiku, T. Matsue, "Application of microbial chip for amperometric detection of metabolic alteration in bacteria, *Sens. Actuators B: Chem.* 108 (1–2) (2005) 676–682, <https://doi.org/10.1016/j.snb.2004.10.050>.
- [211] N. Matsui, T. Kaya, K. Nagamine, T. Yasukawa, H. Shiku, T. Matsue, "Electrochemical mutagen screening using microbial chip, *Biosens. Bioelectron.* 21 (7) (Jan 15 2006) 1202–1209, <https://doi.org/10.1016/j.bios.2005.05.004>.
- [212] C. Cai, B. Liu, M.V. Mirkin, H.A. Frank, J.F. Rusling, Scanning electrochemical microscopy of living cells. 3. *Rhodobacter sphaeroides*, *Anal. Chem.* 74 (1) (2002) 114–119, <https://doi.org/10.1021/ac010945e>.
- [213] K. Nagamine, N. Matsui, T. Kaya, T. Yasukawa, H. Shiku, T. Nakayama, T. Nishino, Amperometric detection of the bacterial metabolic regulation with a microbial array chip, *Biosens. Bioelectron.* 21 (2005) 145–151, <https://doi.org/10.1016/j.bios.2004.08.039>.
- [214] L. Huang, Z. Li, Y. Lou, F. Cao, D. Zhang, X. Li, "Recent advances in scanning electrochemical microscopy for biological applications, *Materials* 11 (8) (Aug 9 2018), <https://doi.org/10.3390/ma11081389>.
- [215] W. Zhang, H. Wu, I.M. Hsing, "Real-time label-free monitoring of *Shewanella oneidensis* biofilm formation on electrode during bacterial electrogenesis using scanning electrochemical microscopy, *Electroanalysis* 27 (3) (2015) 648–655, <https://doi.org/10.1002/elan.201400578>.
- [216] W.C.L. Huang, D. Zhang, Y. Huang, Z. Li, Y. Lou, H. Qian, C. Jiang, X. Li, A. Mol, Acceleration of corrosion of 304 stainless steel by outward extracellular electron transfer of *Pseudomonas aeruginosa* biofilm, *Corros. Sci.* 199 (2022) 110159, <https://doi.org/10.1016/j.corsci.2022.110159>.
- [217] P.L. Frederix, P.D. Bosshart, T. Akiyama, M. Chami, M.R. Gullo, J.J. Blackstock, K. Dooleweerd, N.F. de Rooij, U. Staufer, and A. Engel, "Conductive supports for combined AFM-SECM on biological membranes, *Nanotechnology* 19 (38) (2008) 384004, <https://doi.org/10.1088/0957-4484/19/38/384004>.
- [218] Q.-H. Zhang, X.R. Li, P. Liu, X.Z. Meng, L.K. Wu, Z.Z. Luo, and F.H. Bao, "Quantitative study of the kinetics of hydrogen evolution reaction on aluminum surface and the influence of chloride ion, *Int. J. Hydrog. Energy* 46 (80) (2021) 39665–39674, <https://doi.org/10.1016/j.ijhydene.2021.09.189>.
- [220] G. Ghiara, R. Spotorno, S.P. Trasatti, P. Cristiani, "Effect of *Pseudomonas fluorescens* on the electrochemical behaviour of a single-phase Cu-Sn modern bronze, *Corros. Sci.* 139 (2018) 227–234, <https://doi.org/10.1016/j.corsci.2018.05.009>.
- [221] R. Basséguy, M.L. Delia, B. Erable, A. Bergel, Understanding biocorrosion, fundamentals and applications chapter 5 electroactive biofilms, *Eur. Fed. Corros. (EFC)* (2014) 107–143, <https://doi.org/10.1533/9781782421252.1.107>.
- [222] R.H. Gaines, Bacterial Activity as a Corrosive Influence in the Soil, *Ind. Eng. Chem.* 2 (4) (1910) 128–130, <https://doi.org/10.1021/ie50016a003>.
- [223] C.F. Dong, H. Sheng, Y.H. An, X.G. Li, K. Xiao, Y.F. Cheng, Corrosion of 7A04 aluminum alloy under defected epoxy coating studied by localized electrochemical impedance spectroscopy, *Progress in Organic Coatings* 67 (3) (2010) 269–273, <https://doi.org/10.1016/j.porgcoat.2009.11.004>.